University of Alberta

Long Period Gratings in Multimode Interference Devices

by

Christopher Paul Wong

A thesis submitted to the Faculty of Graduate Studies and Research in partial fulfillment of the requirements for the degree of *Master of Science*

Department of *Electrical and Computer Engineering*

Edmonton, Alberta

Fall 2006

Your file Votre référence
ISBN: 978-0-494-22409-0
Our file Notre référence
ISBN: 978-0-494-22409-0

Abstract

The mathematical theory of tilted long period gratings (LPGs) written on multimode interference (MMI) devices is presented in this thesis. Theoretically, long period gratings can be used to change the multimode imaging in a planar waveguide by coupling modes of light. Simulations and designs of these devices are accomplished using MATLAB.

Using long period gratings to couple core-modes to core-modes in order to modify multimode images is presented as a novel concept. This forward-looking concept can be used to create dynamic long period gratings in order to create dynamic optical power splitters or switches. These dynamic long period gratings can be accomplished by using technologies such as thermo-optic materials, electro-optic materials or liquid crystals.

Table of Contents

List of Tables

List of Figures

Appendix

List of Abbreviations

AON	All Optical Networks
C-band	Conventional Band
CMT	Coupled Mode Theory
DWDM	Dense Wavelength Division Multiplexing
EDFA	Erbium Doped Fiber Amplifier
FBG	Fiber Bragg Grating
FLPG	Fiber Long Period Grating
FTTH	Fiber to the Home
FWHM	Full-Width Half Maximum
Gb/s	Gigabits per second
ITU	International Telecommunications Union
L-band	Long Band
LPG	Long Period Grating
MEMS	Micro-Electro-Mechanical Systems
MMI	Multimode Interference
OEO	Optical-Electrical-Optical
PON	Passive Optical Networks
PC	Personal Computer
RPM	Rotations per minute
SiO_2	Silica
SMF	Single Mode Fiber
TIR	Total Internal Reflection
UV	Ultra-violet
WDM	Wavelength Division Multiplexing

[1] Introduction

1.1 An Introduction to Optical Communication

Despite the dot-com bust at the beginning of the millennium, the demand for digital-based services has not waned. The world hungers for higher and higher bandwidths of information resulting from the ubiquity of personal computers, personal data organizers, music and video devices, telephones and of course the Internet. That is, larger quantities of information at an ever increasing rate. At the heart of this digital network is optics. A laser pulses at billions of times a second, pumping bits of information through optical fibres to the continents of the world. The optical core of this network continues to evolve striving to attain faster, flexible, more robust and more cost effective ways of manipulating the optical domain.

Current Dense Wavelength Division Multiplexing (DWDM) systems are complex networks spanning hundreds of kilometres, composed of dozens of nodes and multiple rings. In order to transport data from one point to another, light of different wavelengths is multiplexed and sent down the same silica optical fibre. DWDM systems are based on the fact that the datastreams can be separated by selective filtering by wavelength. No two datastreams at the same wavelength can comprehensibly exist on the same length of fibre at any one time. Each wavelength is located in the low loss absorption region of silica fibre, either the C-band spanning from 1530nm to 1570nm or the L-band spanning from 1570nm to 1612nm. Specific wavelengths are assigned for wavelength division multiplexing (WDM) applications by the International Telecommunications Union (ITU) and this wavelength ensemble is called the ITU grid. The majority of telecommunications data is imparted to each wavelength via an externally modulated semiconductor laser composed of Indium Phosphide in a distributed feedback physical architecture. Each wavelength has a specifically designed starting point and ending point controlled by the optical filters. At present, industry standard is supporting 40Gb/s on one wavelength, though demonstrations far exceeding this data rate have been shown.

DWDM networks are moving towards all-optical networks (AONs) – that is networks with no, or few optical-electrical-optical (OEOs) conversions. Each OEO conversion is expensive, as it requires high-speed electronics, extra lasers, receivers and other expensive hardware. These electronics are a speed bottleneck as well, in that they have problems keeping up with the high optical data speeds in present day networks. One would then prefer to have data both communicated and manipulated in the optical domain with few, if any OEO conversions. A technology known as Integrated Optics is integral to the spread of all-optical networks.

1.2 Basics of Optical Waveguides

At the heart of optical communication is the concept of total internal reflection (TIR), first demonstrated by John Tyndall in 1854 [94]. Tyndall showed that if light is

coupled to a water medium surrounded by air, the light will travel along the curved path of water. When a lightwave propagating in a medium, for instance water, comes upon a medium with a lesser index of refraction, such as air, the light is bent such that the exit angle is greater than the incident angle. This exit angle will then approach 90° at a specific incident angle θ_c also known as the critical angle. The critical angle can be readily calculated from Snell's law [59]:

$$n_1 \sin(\theta_1) = n_2 \sin(\theta_2) \tag{1-1}$$

Here n_1 is the index of refraction of the first material, and n_2 is the index of refraction of the second material, in the TIR case $n_1 > n_2$. The angle of incidence in the first material is represented by θ_1 and the angle of refraction in the second material is represented by θ_2. By setting the refraction angle equal to 90°, the critical angle can be calculated, as shown in Figure 1-1.

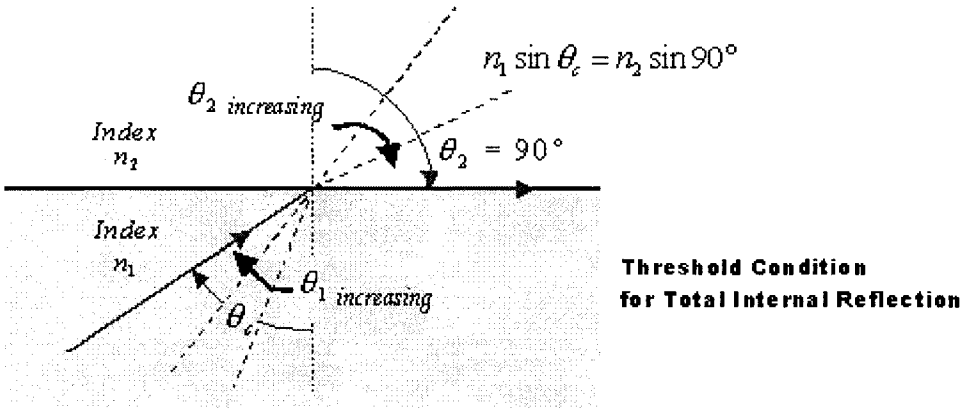

Figure 1-1: Snell's Law

If the angle of incidence is greater than this critical angle there will be total internal reflection – that is, light will not escape into the medium of lower refractive index as shown in Figure 1-2. If the angle of incidence is less than the critical angle, part of the incident light will be transmitted and part will be reflected. Therefore, it is crucial that the initial lightwave be launched at the proper angle such that energy is not radiated out. By this method one can confine a lightwave for hundreds of kilometres.

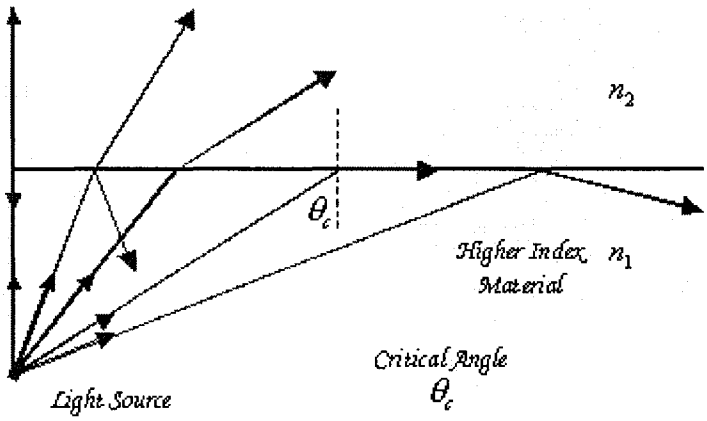

Figure 1-2: The Critical Angle for Total Internal Reflection

Standard singlemode fibre (SMF) has a 9 micron diameter core and a 125 micron diameter cladding with refractive indices of both of them around 1.5, with the core having a slightly higher index of refraction by virtue of germanium doping [62]. Due to the inherent optical properties of silica glass, only a small portion of the bandwidth of silica is used; only laser light between (roughly) 1490nm and 1612nm is used corresponding to the low attenuation window of silica (typically 0.2dB loss per kilometre). Fibre optic communication using silica fibre is advantageous over communication by electrical wiring, or free-space communication in that it has lower power dissipation, high bandwidth, is immune to electromagnetic interference, and operates at lower communication energy. Laser light undergoing total internal reflection is the basis of fibre optic communication. However, it must be noted that the simplicity of Snell's law and the concept of total internal reflection is a macroscopic view of light behaviour. In order for one to scrutinize the behaviour of light at a more fundamental level, the wave theory of light must be introduced and used.

1.3 Integrated Optics

Integrated optics is the technology of integrating various optical devices and components for the generation, focusing, splitting, combining, isolation, polarization, coupling, switching, modulation and detection of light - all on a single substrate or chip. The goal is to manipulate or create optical signals for telecommunications. The waveguides used to create integrated optics are planar optical waveguides, and fabrication is accomplished using thin film technology methods. For ease of processing and to prevent material incompatibilities, ideally the waveguides are fabricated using one base material, such as silica (SiO_2). The goal is to create miniaturized optical systems. The idea was first put forth in 1969 by Stewart E. Miller [124]. Miller proposed that optical components be monolithically integrated in materials such as silicon, as analogous optical versions of electronic integrated circuits. By integrating multiple devices on a single substrate one can conceivably create a faster more robust system.

Two such integrated optical components are the multimode interference splitter and the refractive index grating. Multimode interference (MMI) splitters are used to split a single signal into multiple signals that can then be routed elsewhere. The strength of this device lies in its simplicity and compact form. Refractive index gratings, such as the Bragg grating or the Long Period Grating (LPG) are used in a variety of ways. The strength of these devices lies in the ability to couple optical power from an initial optical mode into a second optical mode, thus manipulating light in the optical domain. Both of these devices, the MMI splitter and the refractive index grating will be briefly touched on in sections 1.4 and 1.5. Thorough mathematical interpretations will be presented in Chapters 2,3 and 4.

1.4 Multi-Mode Interference

The concept of multimode imaging was first put forth by John Talbot in 1836, but only since the early 1990's has the concept been studied for integrated optics. Key papers written by L. B. Soldano, E. C. M. Penning et. al. [7,11,8] analyzed the mathematics of the self-imaging phenomenon by calculating the coupling coefficients, and predicting where multiple images can be found. Another key paper by M. Bachmann et. al. [5] in 1994 took this theory even further to calculate the phase relations between the input and the outputs, and outputs relative to each other. Since the mid 1990's many groups have designed and fabricated multimode imaging devices, optimized for use by means of different material systems and geometries [16-25].

A standard MMI splitter is a planar waveguide in the geometry of a rectangle on the order of hundreds of microns. A multimode splitter is used to split up an input light signal into 2, 3, 4 or more multiple outputs – ideally with a minimum loss of power and a minimum amount of substrate surface area. Systems require splitting of incoming signals for such things as redundant protection, power monitoring, or signal splitting to different nodes. Designs typically result in equal power splitting of the incoming lightwave. The MMI waveguide is merely a planar rectangular waveguide fabricated using thin film technology composed of plastics, polymers or materials such as silicon. Therefore, the MMI is inherently a passive static device and as such, split ratios and multimode images cannot be easily changed. Firstly, light in the form of a monochromatic laser is coupled to the input waveguide; secondly, multimode interference occurs in a wide section; finally, if the coupler is designed properly, equal amounts of power are coupled to the output waveguides. This can be demonstrated in Figure 1-3 where one input is split into five outputs. The pictures and diagrams in this thesis are not to scale.

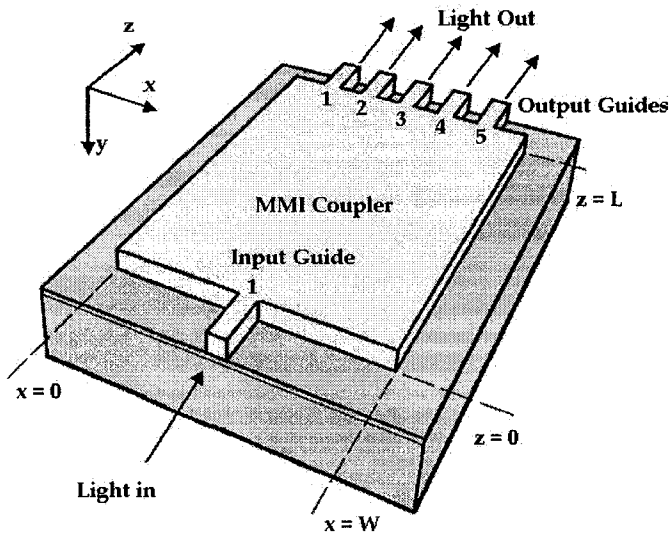

Figure 1-3: Schematic diagram of an MMI coupler

Imaging design depends on the material properties, geometry, placement of the input waveguides and the wavelength of the incoming lightwave. Examples of characteristics affecting the real device images are sidewall roughness, quality/impurity of the thin film waveguide, quality of the input image and precision of the waveguide geometry.

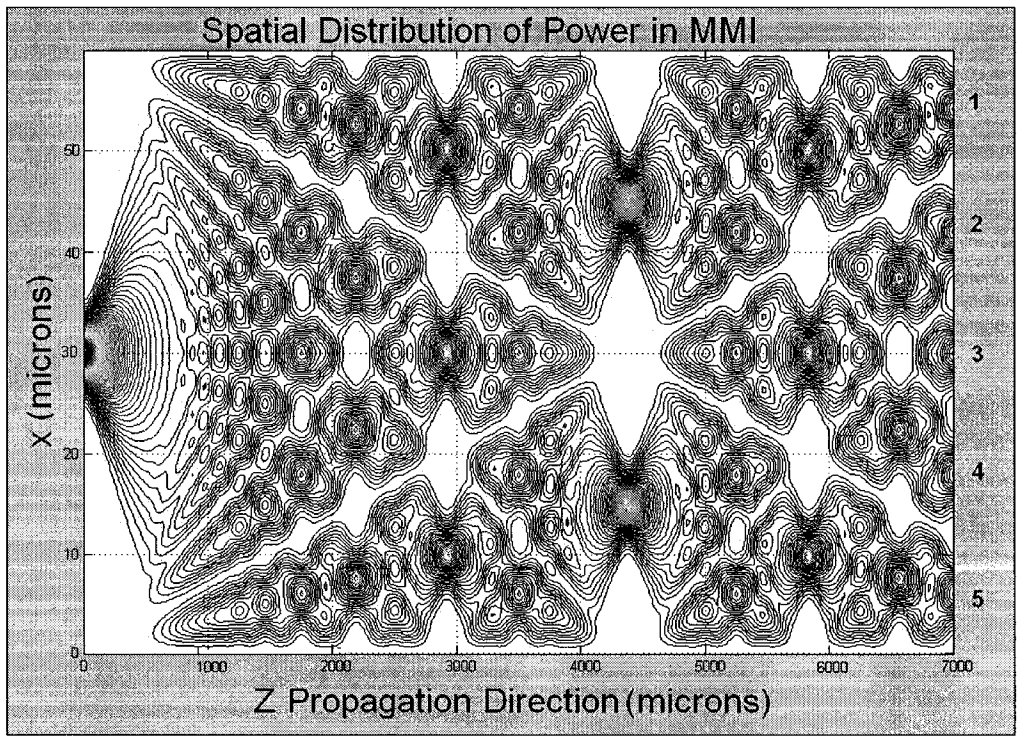

Figure 1-4: Simulation of a 1 x 5 Multimode splitter

Figure 1-4 depicts the MMI imaging within the waveguide with one central input and five outputs carrying equal amounts of power. Figure 1-5 shows the power distribution relative to the input laser Gaussian.

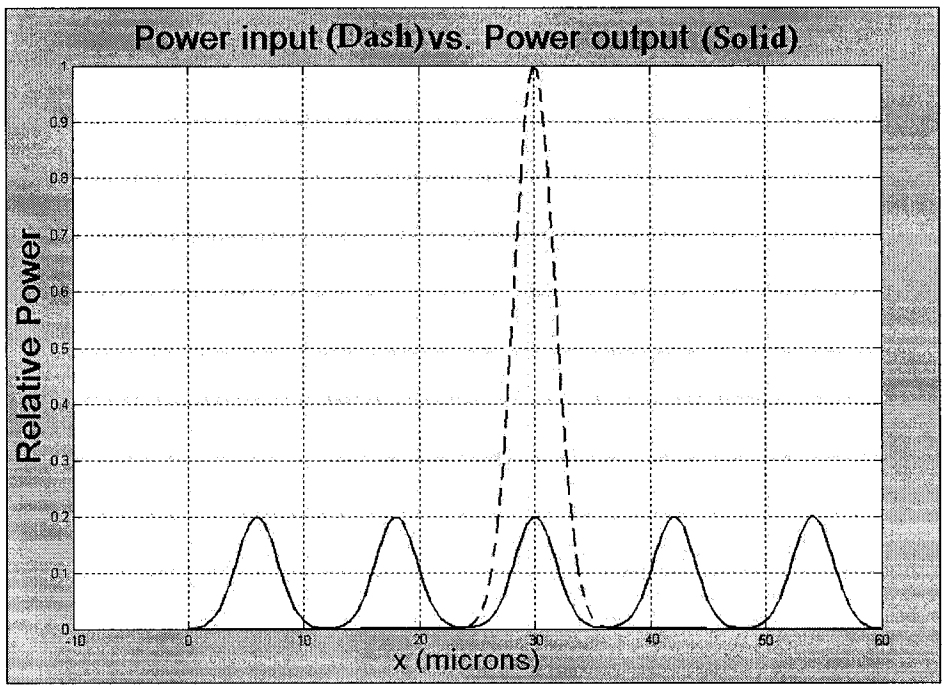

Figure 1-5: Input Power of the laser versus the Output Power out of a 1 x 5 splitter

A full mathematical treatment of the MMI as well as extending the theory for the purpose of this thesis can be found in Chapters 2, 3 and 4.

1.5 The Refractive Index Grating

A refractive index grating is basically a systematic patterning of the refractive index of the waveguide. These periodic perturbations, if properly designed, can have a cumulative manipulative effect on the lightwave in question. Gratings can be used for different types of light manipulation dependent on grating characteristics such as the grating strength and grating period. The refractive index of the waveguide can be changed in a multitude of ways such as systematic strain [55], temperature difference [26], electro-optically [27], using liquid crystals [28], acoustically [29] or more commonly by photosensitivity - exposing a material such as germanium doped silica to UV light [94].

A short period grating, or Bragg grating is named after Sir William Henry Bragg, who won the Nobel Prize in physics jointly with his son Lawrence in 1915 [94]. The Braggs studied the structure of crystals using X-rays. It is this that led to the development of a simple formula to explain reflection of X-ray light from crystals. In 1978, Dr. Kenneth Hill and his group discovered that when standard optical fibre is exposed to intense laser light the refractive index is altered [94]. By changing the

refractive index periodically a grating is made. Dr. Hill named this the Fibre Bragg Grating (FBG), as the same formula the Braggs derived identically explained the reflection of laser light from Hill's grating. Fibre Bragg gratings can also be used to reflect a specific wavelength of light back from whence it came, which has proven to be useful in telecommunication systems. This can be used as a selective filter – reflecting one wavelength but letting all other wavelength signals pass as illustrated in Figure 1-6 [10].

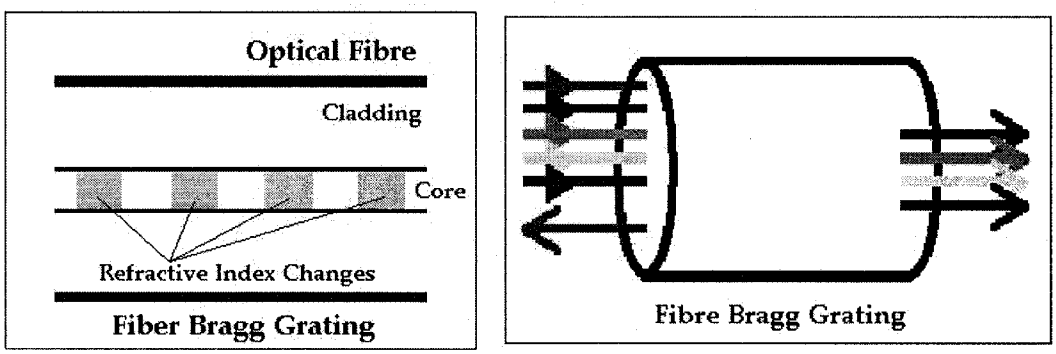

Figure 1-6: Conceptual look at Fibre Bragg Gratings as optical filters

If one knows which wavelength one would like to reflect, one can tailor the period of the grating and also the magnitude of the refractive index change in order to accomplish this. If the spacing of the index periods is equal to one half of the wavelength of the light then the waves will interfere constructively (the round trip of each reflected wave is one wavelength) and a large reflection will occur from the periodic array of refractive index changes. Optical signals whose wavelengths are not equal to one half the spacing will travel through the periodic array of refractive index changes unaffected as shown in Figure 1-7.

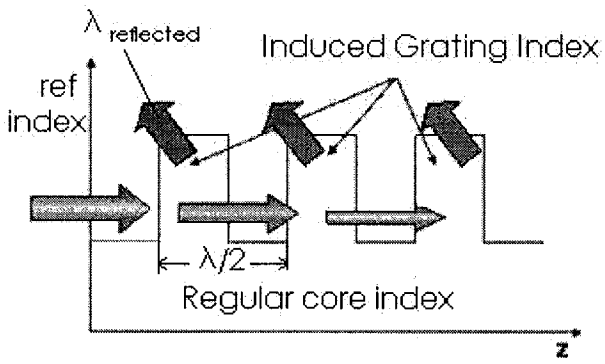

Figure 1-7: Conceptual look at reflection due to a Bragg grating

In essence the Bragg grating, in this single mode waveguide, transfers the power of the initial "mode" of light into another "mode" of light – identical in characteristic but in the opposite direction. All gratings can be modelled as 'mode couplers'.

Furthermore, a multimode fibre grating can be designed to couple one mode to another, either in a forward or backward direction. Likewise, a lightwave can also be coupled from a single mode fibre core to a multiplicity of the fibres' cladding modes. The type of grating used to accomplish this is known as a Long Period Grating (LPG) [55]. Long period gratings are similar to Bragg gratings but instead of reflecting the lightwave, it couples the lightwave into higher order forward propagating modes. As one shall see in Chapter 3 and Chapter 4, LPGs can also couple forward propagating core modes to other forward propagating core modes.

Fiber Long Period Gratings (FLPGs) are LPGs that are typically directly written into a standard telecommunications single mode fibre for Dense Wavelength Division Multiplexing [4] [36]. It is advantageous as it is basically an insitu device used to manipulate the telecommunication wavelengths already in the system. Certainly, grating theory can be used for many applications, but for a FLPG, one is dealing with standard single mode fibre made of silica. It is a cylindrical core surrounded by a cladding of a lower refractive index as shown in Figure 1-8. Light from a core mode to a cladding mode is coupled via a photoinduced refractive index grating as in Figure 1-9.

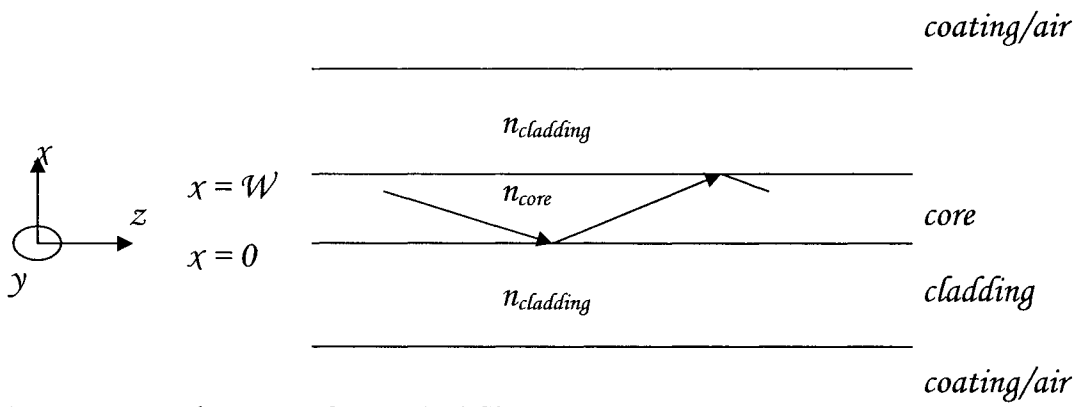

Figure 1-8: Schematic of an optical fibre

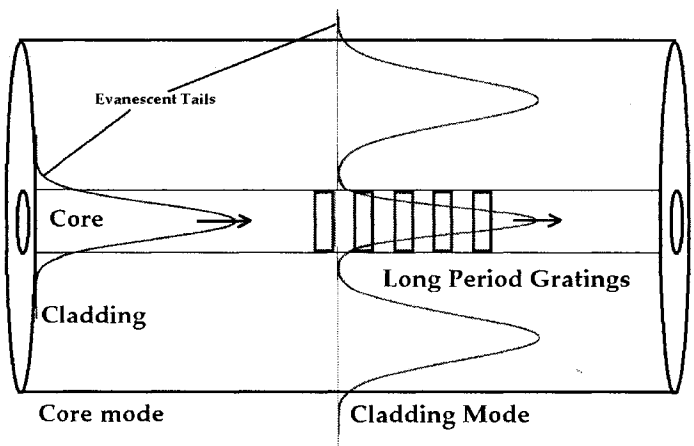

Figure 1-9: Fibre Long Period Grating – Coupling to higher order cladding modes

In a FLPG, the energy coupled to the cladding mode will be attenuated in the coated fibre part. This results in the resonance loss in the transmission spectrum leading to wide band filtering of resonant wavelengths. What results is power loss over a wideband spectrum within the core, effectively removing it from the telecommunications system as in Figure 1-10. This effect is used as a wideband filter for use in Erbium Doped Fibre Amplifiers (EDFA) for amplifier levelling [4,17,30], dispersion control [31, 32] or for fibre optic sensors [33,55].

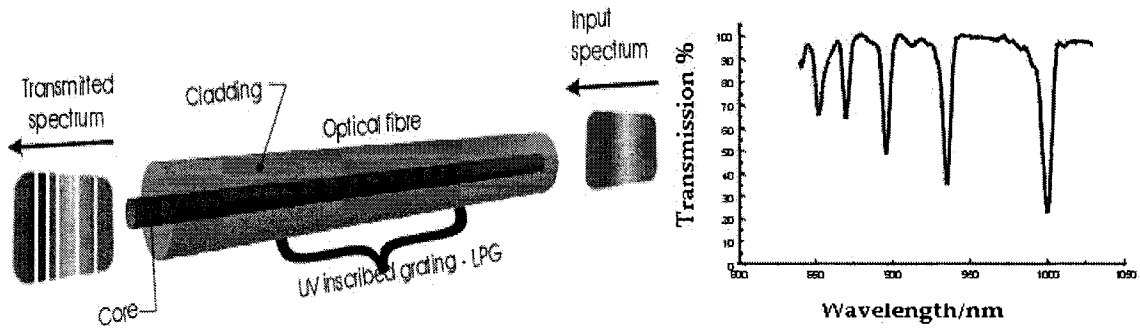

Figure 1-10: Schematic of a LPG and the selective filtering of a spectrum of radiation [96]

Both tilted gratings and long period gratings are mathematically explained and extended in Chapters 3 and 4. Furthermore, modes are thoroughly discussed in Chapters 2, 3 and 4.

1.6 Thesis Objective

This work seeks to combine the technologies of multimode splitters and gratings to manipulate lightwaves in new ways. Using a tilted LPG written on a planar optical multimode waveguide one can tailor the output image. In this case, a core mode is coupled to a higher order core mode. This coupling changes the imaging dynamics within the waveguide. Outputs can then be predicted via simulation. The power of this novel concept lies in the ability to do "image switching" using a dynamic grating. While the grating is 'off' the MMI exhibits its natural characteristics and imaging. Once the grating is turned 'on', that is a refractive index change is induced, the MMI images change. This dynamic grating can be potentially implemented in numerous ways. These technologies are discussed in the Chapter 6. The fabrication of a dynamic grating is beyond the scope of this thesis. Here we examine multimode imaging with and without a grating written on the waveguide in order to show proof of concept. The effect of a dynamic grating can be extrapolated from these simulations. In particular, we present the mathematical theory necessary to analyze such a device. A program written in MATLAB applies the mathematical theory and enables a platform for simulation and design.

Applications of such a device are in power monitoring, protection switching or signal splitting to different devices. While this technology is limited by the switching speed and switching method, the concept is potentially important in future applications.

1.7 Thesis Organization

The organization of this thesis is as follows. Chapter 2 presents a necessary full mathematical treatment of the MMI, starting with the concept of optical modes, and followed by formulas for the complete MMI imaging within a waveguide, including phase relations. Chapter 3 presents a necessary full treatment of general coupled mode theory (CMT) [63]. Chapter 4 takes the mathematics derived in both Chapters 2 and 3 to provide a full mathematical treatment of tilted long period gratings written on multimode waveguides and the effects on the imaging and outputs. Chapter 5 provides details on the MATLAB simulation and design. A subset of favourable designs is also presented in this chapter. Chapter 6 includes dynamic grating solutions such as thermo-optic, electro-optic and liquid crystal gratings. Finally Chapter 7 provides the summary of this thesis with discussion on future devices and potential uses. Appendices are provided and include mathematical concepts not included in the thesis body, designs, and details of the MATLAB program.

[2] Multimode Imaging (MMI) Waveguides

2.1 Introduction

The human eye, like many optical sensors, can only see the intensity and color of light. Yet in order to analyze light in integrated optics, this is not sufficient. One must appreciate that light exists as modes and that intensity is dependent on these modes. Each mode is a spatial distribution of light energy. What one 'sees' is the culmination of all these modes interfering with one another. Mathematically, each mode is a solution to the wave equation given the physical aspects of the problem. This chapter includes optical waveguide theory, and the mathematical treatment of the slab waveguide; all in the context of planar integrated optical waveguides. The theory of multimode imaging is derived with the help of these concepts. A full mathematical treatment is presented in order to prevent any ambiguity.

2.2 Optical Waveguide Theory

2.2.1 Calculating the effective refractive index

Integrated optical waveguides are fabricated using thin film methods. Materials are deposited on a substrate stacked on top of each other. An example of this is the Ridge Guide or Rib Guide depicted in Figure 2-1.

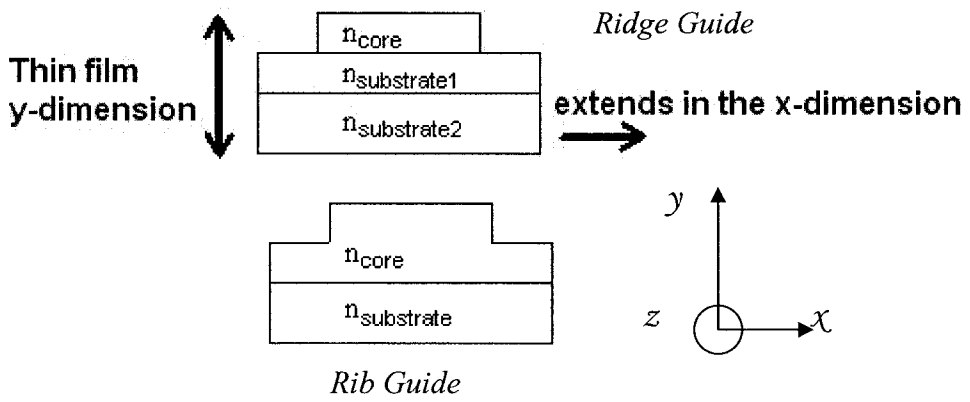

Figure 2-1: Typical integrated optics waveguides

Ideally the dimensions of the waveguide are such that the only one mode exists in the thin y-dimension. In order to describe the guided modes in x and z, one must calculate the effect refractive index taking into account the one mode confined in the y-dimension (Figure 2-2).

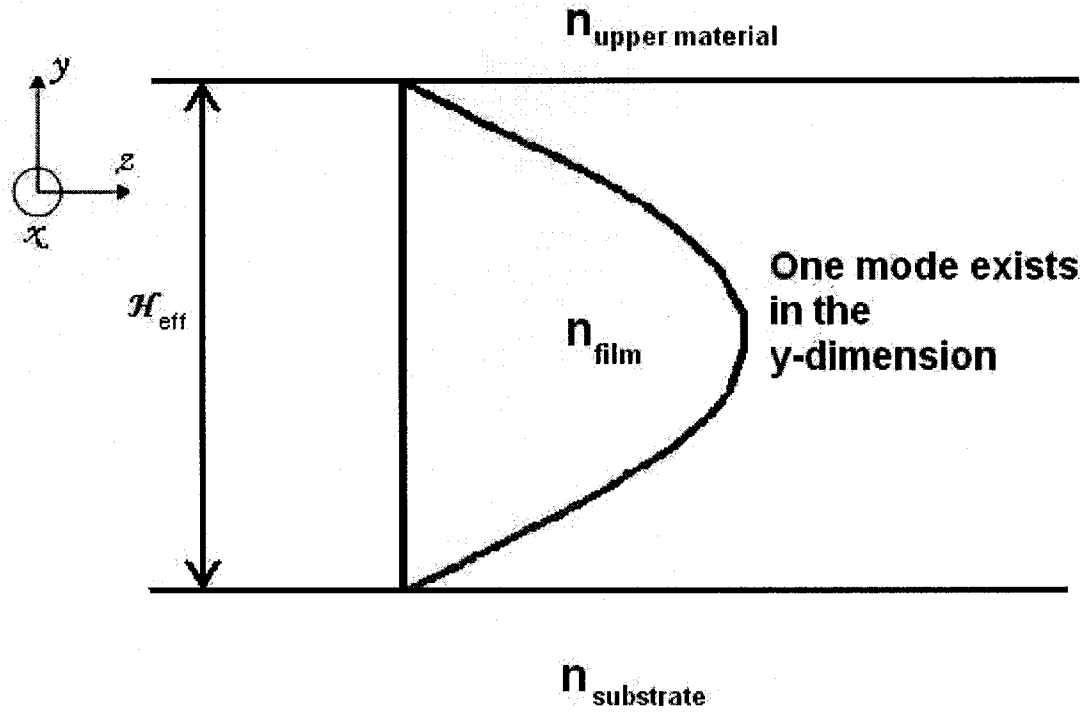

Figure 2-2: Depiction of the one mode that exists in the y-dimension, H_{eff} = effective height.

Using Maxwell's equations and knowing the material system, one is able to construct the wave equation. Here, we are assuming a simple isotropic material commonly used in integrated optics such as a polymer. It is safe to assume that the fields involved will be harmonically varying at some single angular frequency ω. One is working with monochromatic light i.e. a laser. Therefore, it is convenient to eliminate any time dependence consideration from the wave equation [63]. The time independent wave equation is:

$$\vec{\nabla}^2\vec{\mathrm{E}}(x,y,z) = -k^2 n^2 \vec{\mathrm{E}}(x,y,z) \qquad (2\text{-}1)$$

where $k = \frac{\omega}{c} = \frac{2\pi}{\lambda}$ is the planewave propagation constant and n is the refractive index of the material, ω is the angular frequency of the wave, c is the speed of light in a vacuum, and λ is the free-space wavelength. The electric field is represented by $\vec{\mathrm{E}}$. One is dealing with plane waves, which are solutions to this wave equation given this geometry [63].

Traveling plane waves can be modeled as:

$$\vec{E}(x,y,z,t) = \vec{\mathrm{E}}(x,y,z)e^{j\omega t} \qquad (2\text{-}2)$$

The one mode in the y-dimension can be modelled as a sine wave:

$$\sin\left(\frac{\pi y}{H_{eff}}\right) \tag{2-3}$$

where H_{eff} is the effective height of the waveguide taking into account the penetration depths into the upper material and substrate. The one mode in the y-dimension is strictly not a sine wave; however, it is a good enough approximation. The modelling of guided modes as sine waves will be discussed in Section 2.3.1.

One can approximate solutions to the time independent wave equation as

$$\vec{\mathrm{E}}(x,y,z) = \mathrm{E}(x)\sin(Qy)e^{-j\beta z} \tag{2-4}$$

where $Q = \frac{\pi}{H_{eff}}$. Inputting this solution into the time independent wave equation in Equation 2-1 one has:

$$\left(\frac{d^2}{dx^2}+\frac{d^2}{dy^2}+\frac{d^2}{dz^2}\right)\left(\mathrm{E}(x)\sin(Qy)e^{-j\beta z}\right)+k^2 n_{film}^2\left(\mathrm{E}(x)\sin(Qy)e^{-j\beta z}\right)=0 \tag{2-5}$$

which is equal to:

$$\frac{d^2\mathrm{E}(x)}{dx^2}+\left[k^2 n_{film}^2 - Q^2 - \beta^2\right]\mathrm{E}(x) = \frac{d^2\mathrm{E}(x)}{dx^2}+\left[k^2 n_{eff}^2 - \beta^2\right]\mathrm{E}(x)=0 \tag{2-6}$$

where the effective refractive index is:

$$n_{eff}^2 = n_{film}^2 - \frac{Q^2}{k_0^2} \tag{2-7}$$

From this point onwards, whenever the term $\frac{d^2}{dy^2}$ appears, it will be replaced by the term($-Q^2$). This allows one to describe the electric field of guided modes propagating in the z-direction in a material with an effective refractive index, n_{eff}, as

$$\vec{\mathrm{E}}(x,z) = \mathrm{E}(x)e^{-j\beta z} \tag{2-8}$$

2.2.2 Modes within a slab waveguide

All the refractive indices depicted in Figure 2-3 are effective refractive indices; the core with refractive index n_{CORE} is surrounded on both sides (in the x direction) by

a cladding of lower refractive index equal to $n_{CLADDING}$. Light propagates in the z -direction and is confined in the x-direction by virtue of total internal reflection.

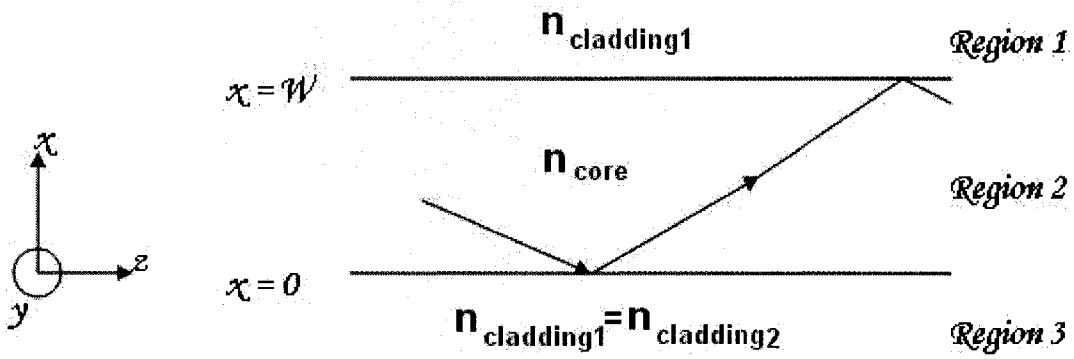

Figure 2-3: The slab waveguide

A symmetric slab waveguide differs from free space in that the waveguide (Figure 2-1) assumes that the cladding ($n_{CLADDING}$) layer extends to infinity in the x dimension and that both the core (n_{CORE}) and cladding extends to ± infinity in the y and z plane.

The wave equation must be written for the three separate regions along the x coordinate, the upper cladding $n_{CLADDING1}$, the core n_{CORE} and the lower cladding $n_{CLADDING2}$ [63].

$$\frac{\partial^2 \mathrm{E}(x)}{\partial x^2} + (k^2 n_{CLADDING\,1}^2 - \beta^2)\mathrm{E}(x) = 0 \qquad \text{REGION 1 (TOP)} \qquad (2\text{-}9)$$

$$\frac{\partial^2 \mathrm{E}(x)}{\partial x^2} + (k^2 n_{CORE}^2 - \beta^2)\mathrm{E}(x) = 0 \qquad \text{REGION 2 (MIDDLE)} \qquad (2\text{-}10)$$

$$\frac{\partial^2 \mathrm{E}(x)}{\partial x^2} + (k^2 n_{CLADDING\,2}^2 - \beta^2)\mathrm{E}(x) = 0 \qquad \text{REGION 3 (BOTTOM)} \qquad (2\text{-}11)$$

One can derive the discrete modes within the core by solving these equations. For guided modes there will be sinusoidal-like propagation within the region of n_{co} and exponential-decay propagation in the regions of $n_{cl\,1}$ and $n_{cl\,2}$, the upper and lower cladding respectively.

For the geometry in Figure 2-3, the solutions to Equations 2-9 to 2-11 are $\mathrm{E}(x)$ for the case of guided modes. :

$$\mathrm{E}(x)=\begin{cases} C'\{\cos[\kappa_f W-\arctan(\gamma_a/\kappa_f)]\exp[-\gamma_c(x-W)]\} & \text{for } W<x<\infty \\ C'\{\cos[\kappa_f x-\arctan(\gamma_a/\kappa_f)]\} & \text{for } 0\le x\le W \\ C'\{\cos[\arctan(\gamma_a/\kappa_f)]\exp[\gamma_a x]\} & \text{for } -\infty<x<0 \end{cases}$$

(2-12a,2-12b,2-12c)

where

$$\gamma_c=(\beta^2-n_{cl1}^2k^2)^{1/2} \tag{2-13}$$

$$\kappa_f=(n_{co}^2k^2-\beta^2)^{1/2} \tag{2-14}$$

$$\gamma_a=(\beta^2-n_{cl2}^2k^2)^{1/2} \tag{2-15}$$

Equations 2-12 through 2-15 use notation according to Pollock [68] and Lee [3]; however, if the dimensions of the waveguide were not labelled as in Figure 2-1, Equation 2-12 would be represented differently, though mathematically equivalent [53] [68].

Referring to Equation 2-12, C' is an arbitrary constant that can be normalized such that $\mathrm{E}(x)$ represents a power flow of one Watt per unit width [53]. For each mode ν, C' can be calculated as:

$$C_\nu'=2\kappa_{f\nu}\left[\frac{\omega\mu}{|\beta_\nu|(W+1/\gamma_{c\nu}+1/\gamma_{a\nu})(\kappa_{f\nu}^2+\gamma_{c\nu}^2)}\right]^{1/2} \tag{2-16}$$

Where $\nu=1,2,3,4...N$ is the mode number, which is finite for guided modes. It is worth noting that in literature the term '$\nu-1$' is known as the mode 'order' and can be represented by ζ. The mode number ν is mainly used in this thesis unless otherwise stated.

The electric field distribution in Equation 2-12 is only for guided modes as shown in Figure 2-4 [68]. If the width of the slab waveguide is wide enough, multiple modes can exist simultaneously.

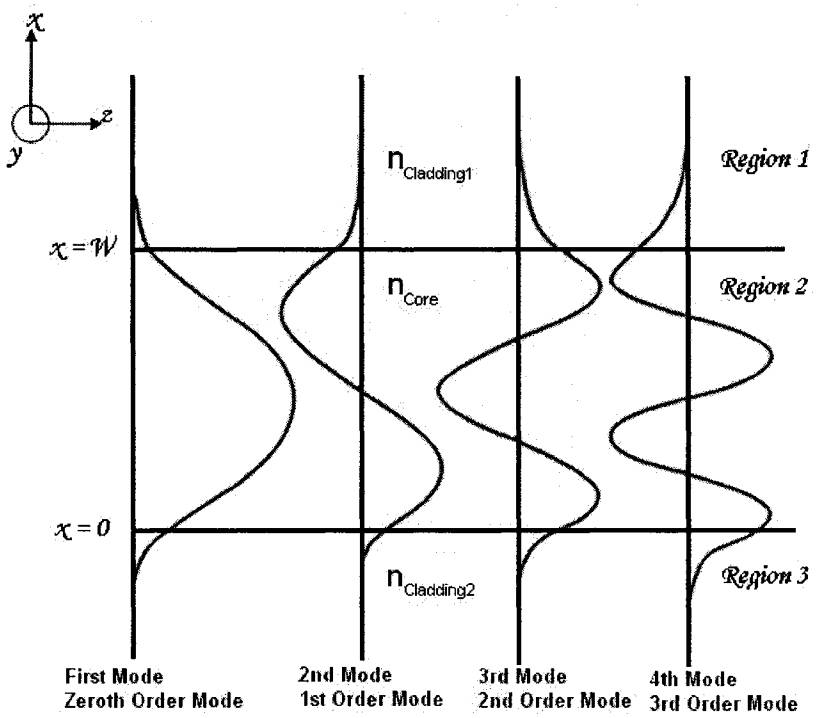

Figure 2-4: Electric field distribution of guided modes in a slab waveguide

By taking into account the boundary conditions at the core-cladding interfaces, one can solve the transcendental equation that yields the discrete solutions to the modes. The discrete solutions correspond to discrete values of β [53]: There are a finite number of solutions, and therefore a finite number of guided modes that can propagate. The boundary conditions are that the electric field be continuous at the border such that $E_{CORE}(x) = E_{CLADDING}(x)$ and $\frac{dE_{CORE}(x)}{dx} = \frac{dE_{CLADDING}}{dx}$. The transcendental equation is [53]:

$$\tan(\kappa_f W) = \frac{\gamma_a + \gamma_c}{\kappa_f (1 - \gamma_c \gamma_a / \kappa_f^2)} \tag{2-17}$$

The transcendental equation can be graphed as in Figure 2-5. In this simple example, the intersections of the two graphs lead to guided wave solutions. If one measures the value of κ_{f_ν} for these crossings (the graph's x-axis), one can solve $\gamma_{c\nu}$, $\gamma_{a\nu}$ and β_ν; where $\nu = 1,2,3,4...N$ which is finite for guided modes. There are 6 guided wave solutions in this example, with parameters λ =650nm, n_{CORE} =1.59, $n_{CLADDING1} = n_{CLADDING2}$=1.58, W=10 microns. This is not a practical waveguide for the applications discussed in this thesis but illustrates how one can solve for the variables in Equations 2-12 through 2-15.

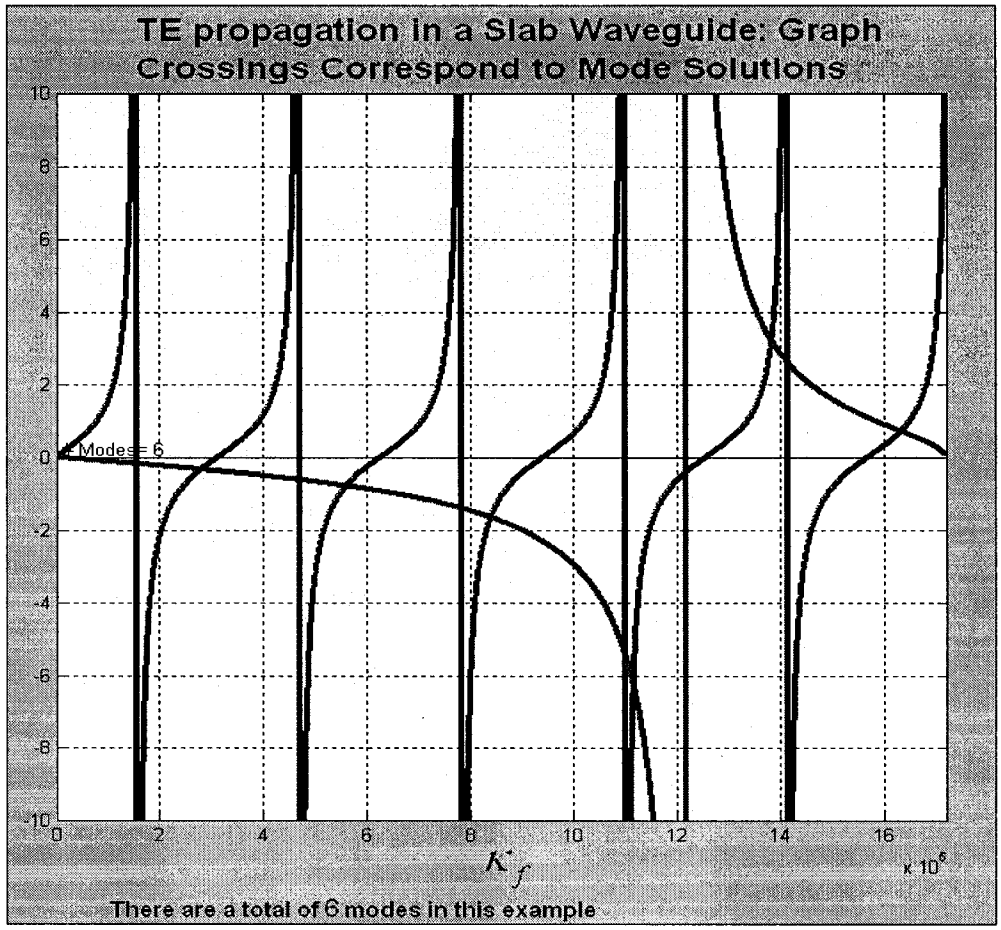

Figure 2-5: Graph of the transcendental equation, Equation 2-17
λ=650nm, n_{CORE}=1.59, $n_{CLADDING1}=n_{CLADDING2}$=1.58, W=10 microns

Given the material system and geometry one can find the number of guided modes and their corresponding propagation constants β_v using Equation 2-17. Note that $1/\gamma_c$ is the penetration depth into the top cladding and $1/\gamma_a$ is the penetration depth into the bottom cladding [53]. These should be equal for a symmetrical slab waveguide. Also note that the effective width of a mode can be calculated by adding $1/\gamma_c, 1/\gamma_a$ and W. However, this width changes from mode to mode and is thus not constant.

This section contains equations for solving what modes can exist within the waveguide it does not give what modes do exist with any significant power. The input lightwave characteristics and the waveguide characteristics determine the relative power within the modes. Once the relative power in each mode is known, one can calculate the optical power at any point within the device. For example Figure 2-6 depicts a laser modeled as a Gaussian input coupled to a large MMI waveguide via an input waveguide. A multimode image will exist within the large MMI section. Multimode Imaging is discussed in the next section.

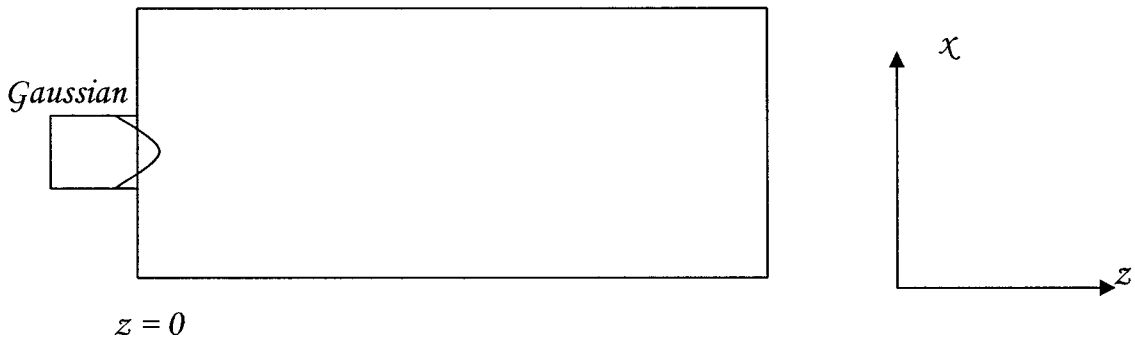

Figure 2-6: Multimode interference waveguide section

2.3 Multimode Imaging

2.3.1 Sinusoidal approximation of the guided modes

It has been established that multiple modes can exist within the large MMI section, with each mode propagating with a different propagation constant β. The different modes go through a periodic phase change $e^{-j\beta_\nu z}$, where ν is the mode number.

In order to simplify the calculations for multimode images, it is convenient to model the modes in the waveguide as perfect sinusoids and estimate a constant effective width.

Constant Effective Width Estimate [7]:

$$W_{eff} = W + \left(\frac{\lambda}{\pi}\right)\left(n_{co}^2 - n_{cl}^2\right)^{-1/2} \qquad (2\text{-}18)$$

This effective constant width differs from the real effective width $(1/\gamma_c + 1/\gamma_a + W)$ in that both γ_c and γ_a are dependent on the mode order, while W_{eff} above is not. The effective width in Equation 2-18 corresponds to the effective width of the lowest order mode.

The constant effective width is important in order to simplify the mathematics in subsequent chapters. The modes will be described as sinusoids with a constant effective width, rather than having to deal with the cumbersome equations presented in Equation 2-12.

The difference between the physical width and the effective width is:

$$dW = W_{eff} - W \tag{2-19}$$

The modes (depicted in Figure 2-7 b) can be modeled as [7]:

$$\mathrm{E}_{\nu}(x) = \sqrt{\frac{2}{W_{eff}}} \sin\left[\frac{\pi\nu(x+dW/2)}{W_{eff}}\right] \quad \text{for the range} -\frac{dW}{2} \le x \le W + \frac{dW}{2} \tag{2-20}$$

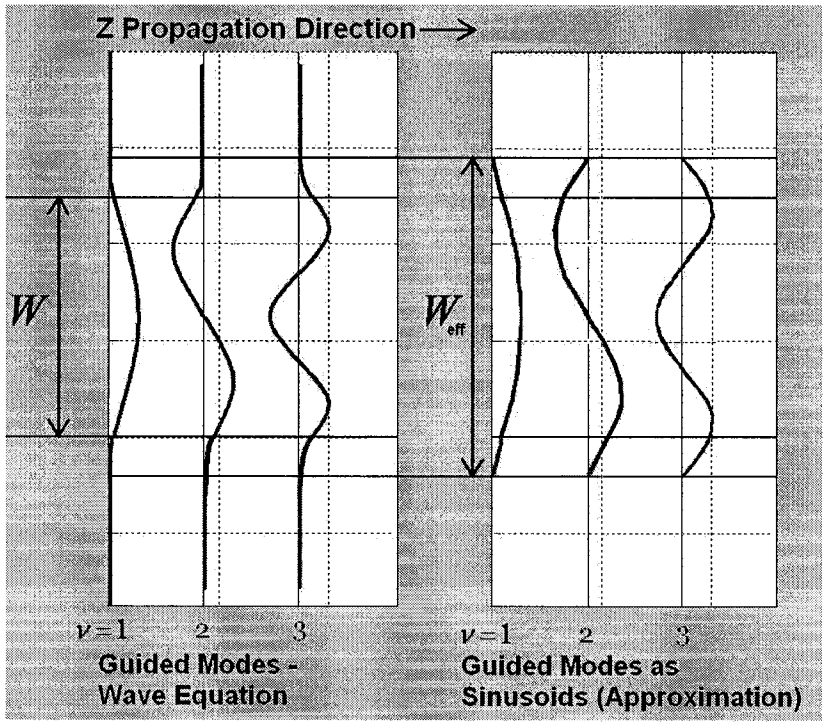

Figure 2-7: Modes modeled by sinusoids

Equation 2-20 models the electric field distribution of the modes as a sine wave, which has magnitude zero at the boundaries. Therefore, it does not accurately model the exponential decay (field penetration) into the cladding layer. Nonetheless, it is often a good enough estimate.

Each mode is independent and orthogonal of each other. For a uniform dielectric material each mode propagates independent of all others and each mode has no effect on the propagation of the others.

For a complete electrical field depiction of any mode, including the electric field amplitudes at z = 0, where the input waveguide reaches the MMI section [7]:

$$G_{\nu}^{z=0}(x) = a_{\nu}\mathrm{E}_{\nu}^{z=0}(x) = a_{\nu}\sqrt{\frac{2}{W_{eff}}} \sin\left[\frac{\pi\nu(x+dW/2)}{W_{eff}}\right] \tag{2-21}$$

Here a_{ν} is the amplitude of the electric field.

Multiple modes can exist within the MMI section but how much power is distributed to each mode? In order to calculate this, information is needed on the input beam coming in from the input waveguide. Using the effective width as the integral boundaries, one must perform an overlap integral with the input field (e.g. a Gaussian) and the possible modes that can exist. To find the amplitudes of the electric field at z = 0, the following Fourier series coefficient must be calculated for every mode [7]:

$$a_\nu = \frac{2}{W_{eff}} \int_{W_{eff}} f(x) \mathrm{E}_\nu^*(x) dx \tag{2-22}$$

where $f(x)$ is the input field from a laser source and $2/W_{eff}$ is a normalization factor. This is the calculation of the amplitude of the electric field for each mode and must be performed when there is a significant perturbation in the refractive index of the waveguide. Obviously the first instance of this calculation is at z = 0, when the slim input waveguide connects to the wide multimode section of the waveguide - a drastic perturbation. It is worth noting that a_ν is only the amplitude of the electric field and carries no information of the spatial distribution.

It is convenient to model the input beam as a Gaussian beam. Thus in Equation 2-22, $f(x)$ is the input Gaussian field modeled as:

$$f(x) = \exp\left[-\frac{1}{2}\left(\frac{x - x_0}{\sigma_x}\right)^2\right] \tag{2-23}$$

Where x_0 is the displacement in the x direction and σ_x is the one half of the full-width half maximum (FWHM) of the Gaussian beam.

As each mode propagates along z through the MMI section an accumulated phase must be mathematically considered for each mode. Each mode propagates with a different propagation constant β_ν as defined by the transcendental equation, Equation 2-17. Therefore, at any point greater than z = 0, the electric field of the lightwave for each mode is [7]:

$$G_\nu(x,z) = a_\nu \mathrm{E}_\nu(x,z) = a_\nu \sqrt{\frac{2}{W_{eff}}} \sin\left[\frac{\pi\nu(x + dW/2)}{W_{eff}}\right] \exp(-j\beta_\nu z) \tag{2-24}$$

Equation 2-24 is the formula for the electric field of each independent orthogonal mode. The information contained in the equation is the amplitude of the electric field a_ν, the sinusoidal spatial distribution of the electric field and the phase accumulation given by the exponential term. In order to calculate the electric field at each point in the x-z plane one must sum the components of each mode at that point.

The total electric field at any point in the x-z plane is [7]:

$$f_{out}(x,z) = \sum_{\nu=1}^{N} a_\nu \mathrm{E}_\nu \exp(-j\beta_\nu z) \tag{2-25}$$

At the input of the MMI section where z = 0 the electric field will be:

$$f_{in}(x,0) = \sum_{\nu=1}^{N} a_\nu \vec{\mathrm{E}}_\nu \tag{2-26}$$

The intensity at any x-z point is the magnitude of the square of the electric field at that x-z point:

$$I(x,z) = \left|f_{out}(x,z)\right|^2 = \left|\sum_{\nu=1}^{N} a_\nu \mathrm{E}_\nu \exp(-j\beta_\nu z)\right|^2 \tag{2-27}$$

and therefore the Total power can be calculated by integrating over the entire x dimension of the waveguide:

$$P_{tot}(x,z) = \int_{\frac{-dW}{2}}^{W+\frac{dW}{2}} I(x,z)dx \tag{2-28}$$

Assuming that the waveguide is lossless and assuming the scatter and radiation mode coupling are negligible, the total power should be identically equal to the power of the input Gaussian pulse:

$$P_{Gaussian,in} = \int_{-dW/2}^{W+dW/2} \left|f_{Gaussian}(x)\right|^2 dx = \int_{-dW/2}^{W+dW/2} \left|\exp\left[-\frac{1}{2}\left(\frac{x-x_0}{\sigma_x}\right)^2\right]\right|^2 dx \tag{2-29}$$

Equation 2-27 for $I(x,z)$ lets one map out the power distribution within the waveguide. However, it is not intrinsically clear that multimode images occur with a predictable pattern such as one would need to design and fabricate a splitter. The key to understanding this lies in the propagation constants of each individual mode. As stated earlier, all modes are orthogonal to one another. So long as no perturbations in the material are experienced by the modes, each mode will propagate, changing only their phase relationship and not the power they carry. In order to glean information from the power distribution inside the MMI one must first find the electric field magnitude at each x-z point in the waveguide. The modes move through the waveguide independently and their sum, the total electric field at any point, can be large or small due to constructive or destructive interference. Mathematically, this is due to

the addition of the complex numbers representing both the phase and magnitude of each individual mode. Only the output power image at the end of the MMI waveguide is useful, as this is where the output waveguides lie.

2.3.2 General interference: Predicting the self-imaging location

Using the information presented in Section 2.3.1, one is able to calculate the modes of a waveguide, calculate the phase of each mode, and calculate the power distribution within the multimode interference device. However, how does one predict where self-images or multiple-images occur?

In order to predict the field distribution inside an MMI section, further steps must be taken. The goal is to predict where self-imaging exists, then extend this theory to predict where multiple images exist. The first case is called General Interference, which is independent of the modal excitation [7]. The analysis of General interference, presented here, as well as Paired interference and Symmetric interference, presented in the next section, is taken from Reference 7, by Soldano et. al.

It is useful to recall the lateral wave number represented in Equation 2-14

$$\kappa_f = (n_2^2 k^2 - \beta^2)^{1/2}$$

and recall the constant effective width represented in Equation 2-18

$$W_{eff} = W + \left(\frac{\lambda}{\pi}\right)\left(n_c^2 - n_{cl}^2\right)^{-1/2}.$$

As an approximate solution for κ_f, instead of solving the transcendental equation use

[7]: $$\kappa_f = \frac{\nu\pi}{W_{eff}}. \qquad (2\text{-}30)$$

The mode number ranges from $\nu = 1..N$.

Rearranging Equation 2-14 for the propagation constant one has

$$\beta_\nu = (n_{co}^2 k^2 - {\kappa_{f\nu}}^2)^{1/2}. \qquad (2\text{-}31)$$

Using the first two terms of the Binomial Expansion, in optics known as the paraxial approximation, Equation 2-31 can be approximated as

$$\beta_\nu = kn_{co} - \frac{1}{2}\frac{1}{kn_{co}}\kappa_{f\nu}^2. \qquad (2\text{-}32)$$

Using the definition of the wavenumber $$k = \frac{\omega}{c} = \frac{2\pi}{\lambda} \qquad (2\text{-}33)$$

and using Equation 2-30, the propagation constant β_ν in Equation 2-32 becomes

$$\beta_\nu = kn_{co} - \frac{\lambda}{4n_{co}} \frac{\nu^2 \pi}{W_{eff}^2}. \tag{2-34}$$

Images of the input field within the MMI will self-replicate when the phases of the mode "beat" together. That is when the modes carrying the most power come in phase at a specific value of z along the propagation axis and interfere constructively. It is therefore useful to define L_π as the beat length (in the z –direction) of the two lowest order modes [7].

Beat Length is defined as

$$L_\pi = \frac{\pi}{\beta_1 - \beta_2} \approx \frac{4n_{co}W_{eff}^2}{3\lambda}. \tag{2-35}$$

The propagation constants spacing can be approximated as [7]

$$\beta_1 - \beta_\nu = \frac{(\nu - 1)(\nu + 1)\pi}{3L_\pi}. \tag{2-36}$$

The electric field at any point x, z can be described as in Equation 2-25

$$f_{out}(x,z) = \sum_{\nu=1}^{N} a_\nu \mathrm{E}_\nu \exp(-j\beta_\nu z). \tag{2-37}$$

By factoring out the phase of the fundamental mode in Equation 2-37, we obtain:

$$f_{out}(x,z) = \exp(-j\beta_1 z)\sum_{\nu=1}^{N} a_\nu \mathrm{E}_\nu \exp\left[j(\beta_1 - \beta_\nu)z\right]. \tag{2-38}$$

Using Equation 2-36 one finally arrives at the formula for $f_{out}(x,z)$ that can give information where to find self-images

$$f_{out}(x,z) = \exp(-j\beta_1 z)\sum_{\nu=1}^{N} a_\nu \mathrm{E}_\nu \exp\left\{j\left[\frac{(\nu - 1)(\nu + 1)\pi}{3L_\pi}\right]z\right\}. \tag{2-39}$$

The total electric field at the input of the MMI section, z=0 is called $f_{in}(x,z)$

$$f_{in}(x, z = 0) = \sum_{\nu=1}^{N} a_\nu \mathrm{E}_\nu. \tag{2-40}$$

By inspecting Equation 2-39 and comparing it to Equation 2-40, the input image at z = 0 can only be self replicated if this condition holds [7]:

$$\exp\left\{ j\left[\frac{(\nu-1)(\nu+1)\pi}{3L_\pi} \right] z \right\} = \begin{cases} 1 & or \\ (-1)^{\nu-1} \end{cases}. \qquad (2\text{-}41)$$

The first condition means that the phase changes of the modes along L (in the z –direction) must differ by integer multiples of 2π. The second case means that the phase changes must be alternatively even and odd multiples of π. In this case, all guided modes interfere with the same relative phases [7]. The conditions of Equation 2-41 will be fulfilled when:

$$z = M(3L_\pi) \qquad (2\text{-}42)$$

where $M = 0,1,2,...$

Equation 2-42 allows one to predict where self images form and is the important result for the case of General Interference [7]. It gives the distance along z where self-images will be produced. Furthermore, since M is zero or a positive integer it denotes the periodic nature of the imaging along z. This means if a waveguide existed that was lossless and infinite in length, the same images will repeat as one views the multimode section along z, as M goes from zero to infinity.

For multiple images, $z = \frac{M}{N}(3L_\pi)$. (2-43)

Where N is an integer with no common divisor with M and refers to the number of images along the x-axis for the given length in z.

An example of General Interference is provided in Figure 2-8, 2-9 and 2-10. They are calculated for n_{effco} =1.563, W_{eff} =45 microns, z =13000 microns, λ=650.3e-9 and TE polarization is used and the input waveguide is placed at $W_{eff}/6$. The distribution of power in each mode is shown in Figure 2-8, the multimode image is depicted in Figure 2-9 and the output power image is depicted in Figure 2-10.

The first example called General Interference is presented here. The examples for Paired interference and Symmetric interference is presented in the next section and take the same values for n_{effco}, W_{eff}, and λ as the example for General Interference. All three examples are of 1x3 splitters, and the only thing that changes is the z-length. This z-length of the MMI is different in all cases due to the different mode excitations based on the placement of the input waveguide.

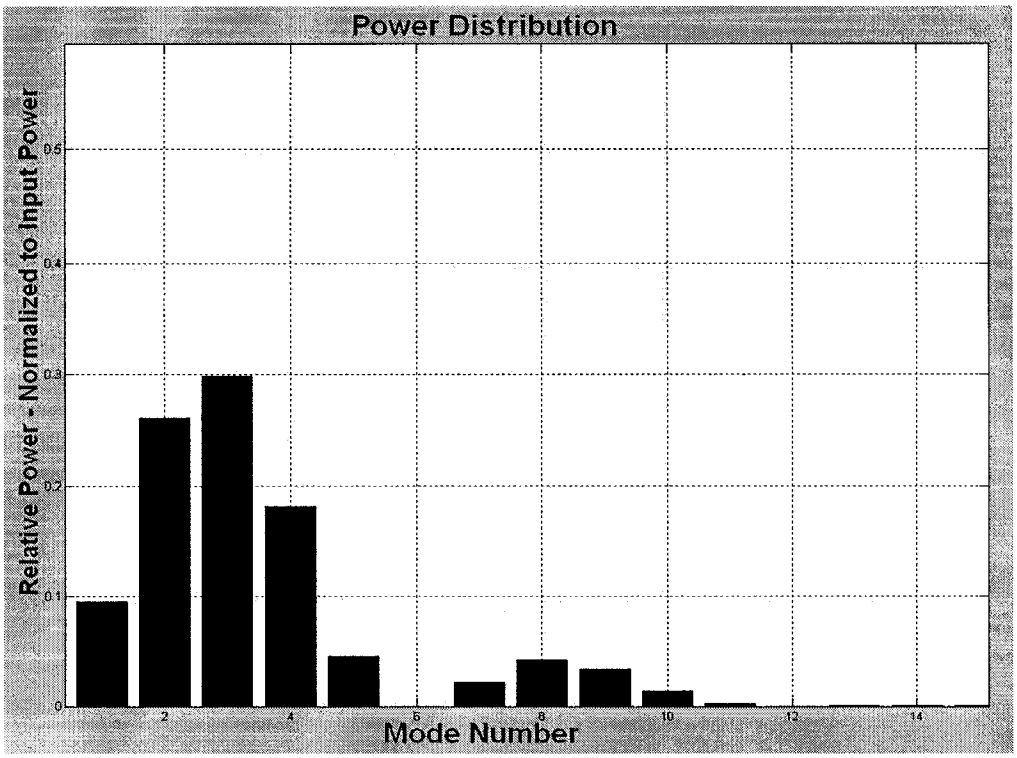

Figure 2-8: Distribution of power in each mode for the example of a 1x3 splitter using General Interference. n_{effco}=1.563, W_{eff}=45 microns, z =13000 microns, λ=650.3e-9 and TE polarization

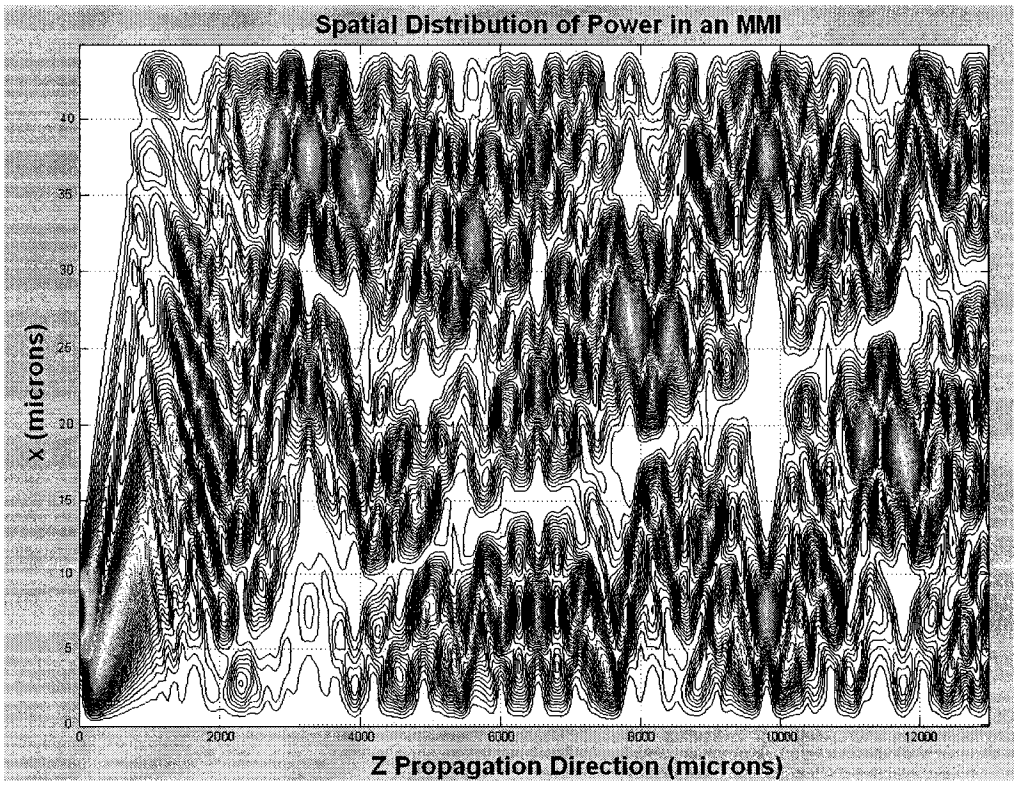

Figure 2-9: Multi-Mode Image for the 1x3 splitter example for General Interference

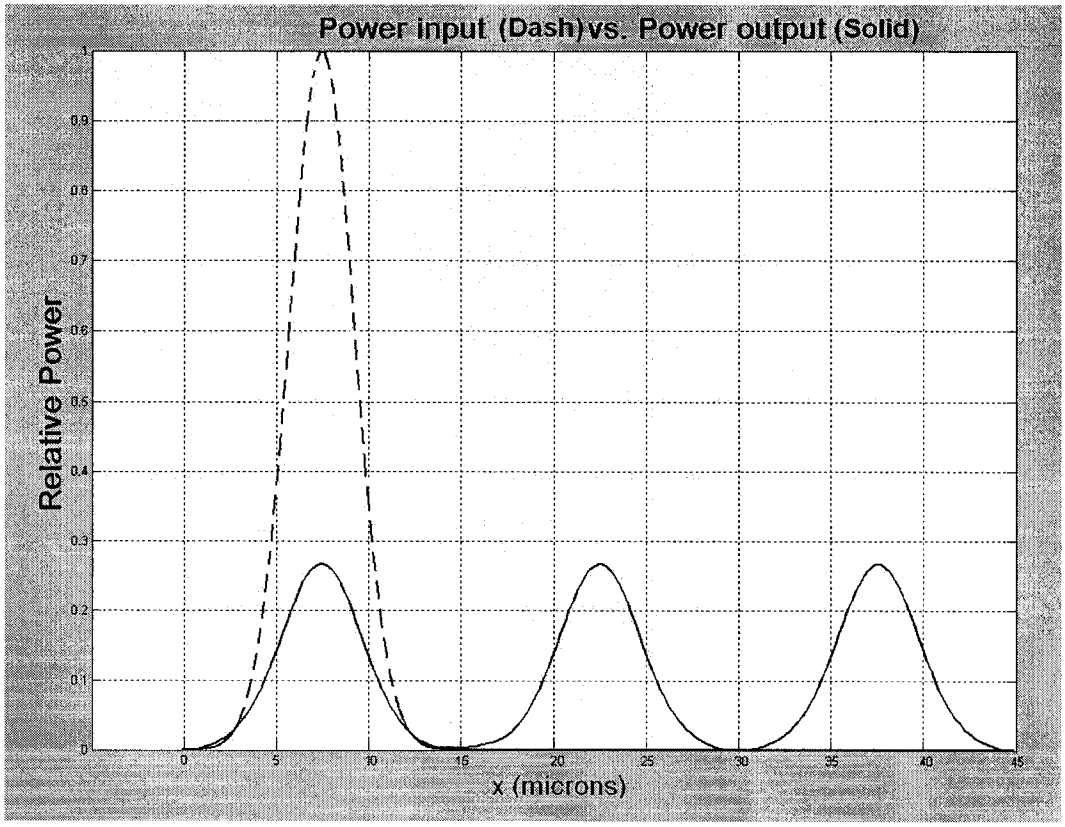

Figure 2-10: Output Image for the 1x3 splitter example for General Interference

2.3.3 Restricted interference: Predicting the self-imaging and multiple-imaging locations

In order to get efficient predictable splitting it is beneficial to place the input waveguides at specific values along the x-axis. Restricted interference is when self-images are obtained by exciting a limited number of modes [7]. There are two cases where selective excitation of modes is beneficial, Paired Interference and Symmetric Interference.

1. 'Paired Interference'

In this case the input field is located at either $\frac{1}{3}W_{eff}$ or $\frac{2}{3}W_{eff}$. At these positions the $\nu = 3^{rd}$, 6^{th}, 9^{th}, 12^{th}...number modes will have zero power coupled to them as the spatial overlap integrals (Equation 2-22) will integrate to zero [7]. Under these circumstances the N-fold images will be formed at distances:

$$z = \frac{M}{N} L_{\pi} \tag{2-44}$$

Where $M \geq 0$ and $N \geq 1$ are integers having no common divisor.

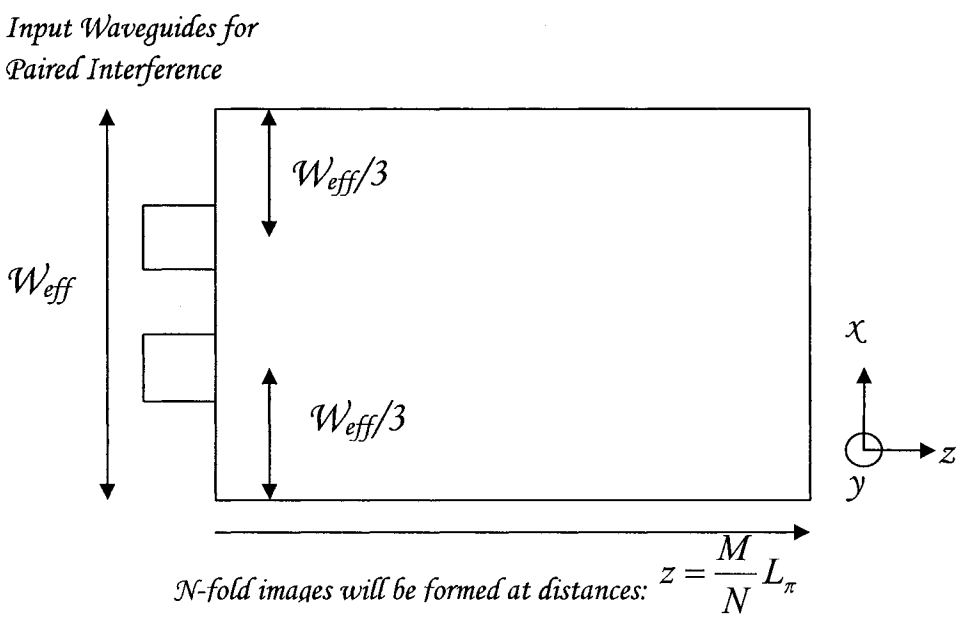

Figure 2-11: Multimode splitter using Paired Interference by placing input waveguides at either $\frac{1}{3}W_{eff}$ or $\frac{2}{3}W_{eff}$

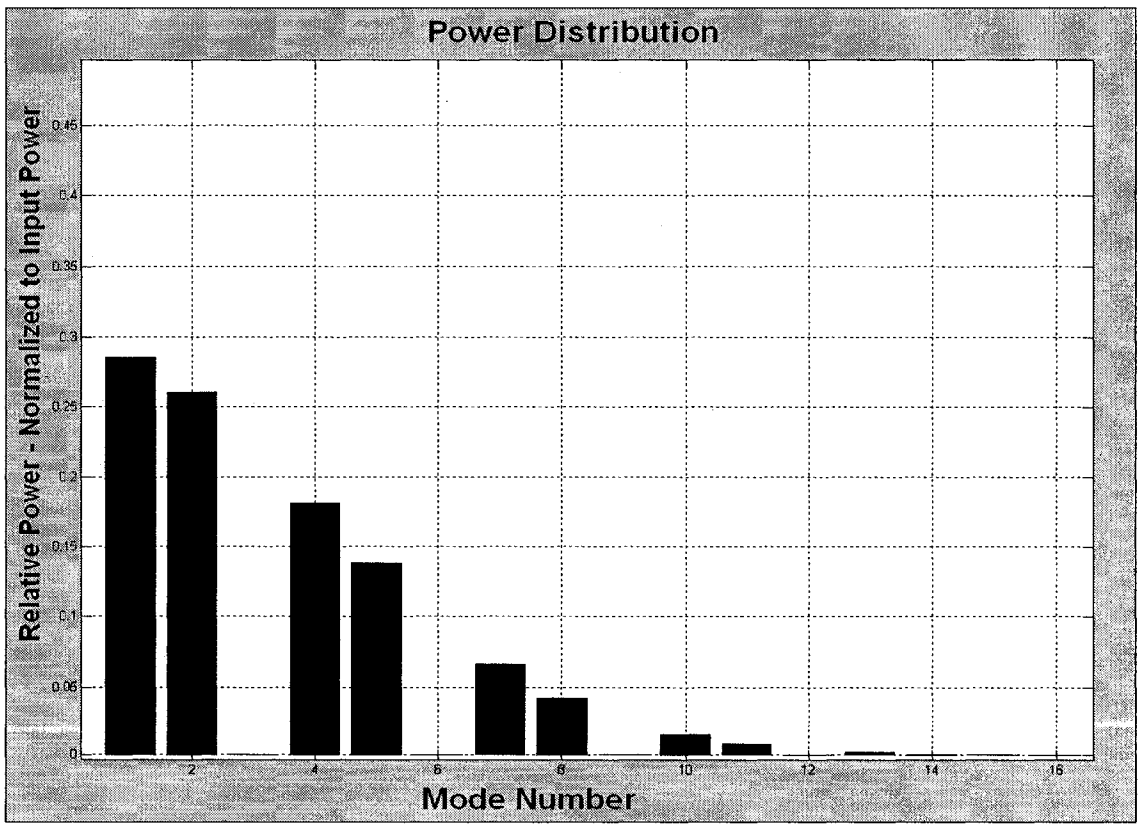

Figure 2-12: Distribution of power in each mode for the example of a 1x3 splitter using Paired Interference. n_{effco} =1.563 W_{eff} =45 microns z=4333 microns λ=650.3nm TE polarization

Figure 2-11 is an example of Paired Interference, where n_{effco}=1.563 W_{eff}=45 microns z=4333 microns λ=650.3nm TE polarization is used. Notice that $\nu = 3^{rd}$, 6^{th}, 9^{th}, 12^{th}... numbered modes do not have any power coupled to them from the Gaussian input. Also notice that this circumstance is called "Paired Interference" because of the paired nature of modes that carry power. For example Mode numbers 1,2 and 4,5 and 7,8 etc.

Figure 2-13 is the multimode interference pattern in the waveguide for a 'Paired Interference' example. Note the input is at $\frac{1}{3}W_{eff}$ in the x dimension. Equation 2-44 governs the values of z where multiple images will be seen.

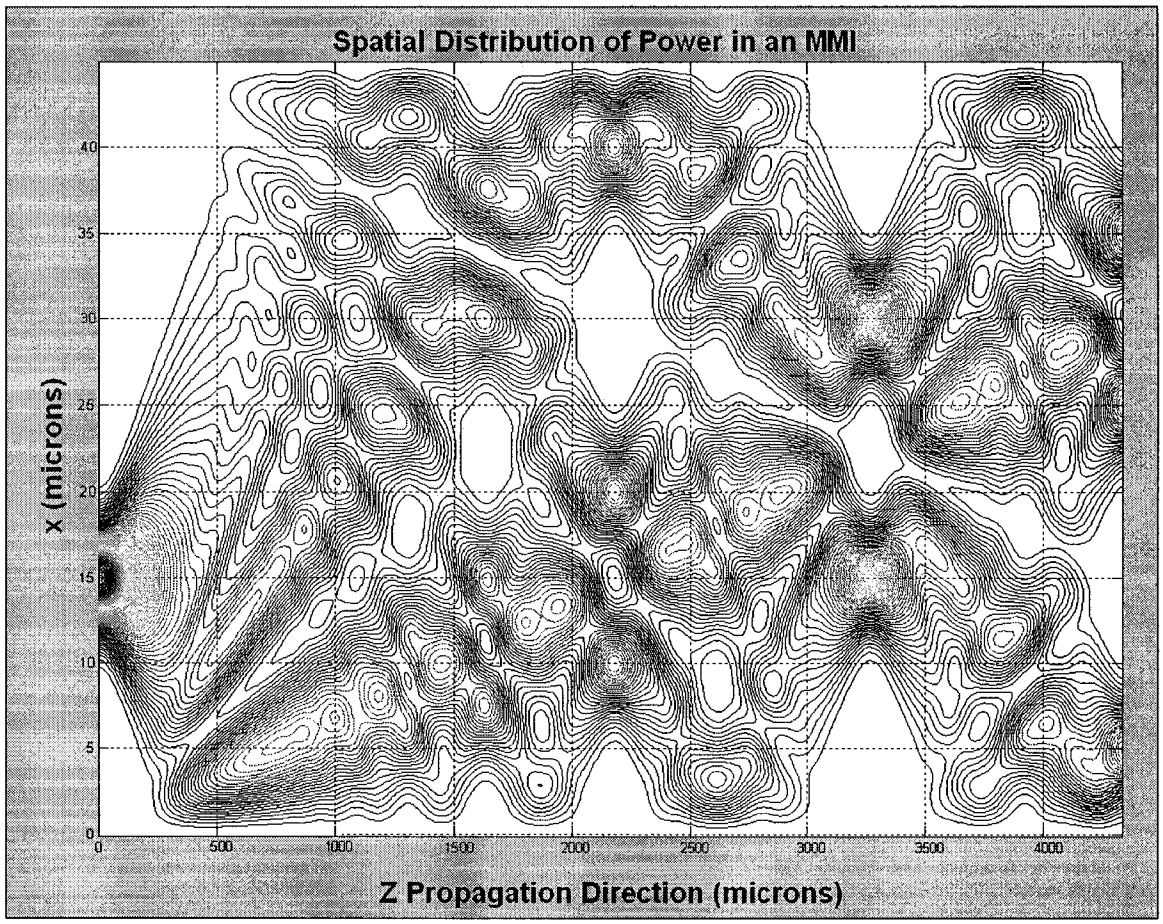

Figure 2-13: Multi-Mode Image for the 1x3 splitter example for Paired Interference n_{effco}=1.563 W_{eff}=45 microns z=4333 microns λ=650.3nm TE polarization

2. 'Symmetric Interference'

This is the second case where selective excitation of modes is beneficial. In this case the input field is located at $\frac{1}{2}W_{eff}$, that is the center of the waveguide. At these positions the $\nu=2^{nd}$, 4^{th}, 6^{th}, 8^{th}... modes will have zero power coupled to them as the spatial overlap integrals (Equation 2-22) will integrate to zero because the modes have odd symmetry[7]. Under these circumstances the images N-fold images will be formed at distances:

$$z=\frac{M}{N}\left(\frac{3L_{\pi}}{4}\right) \tag{2-45}$$

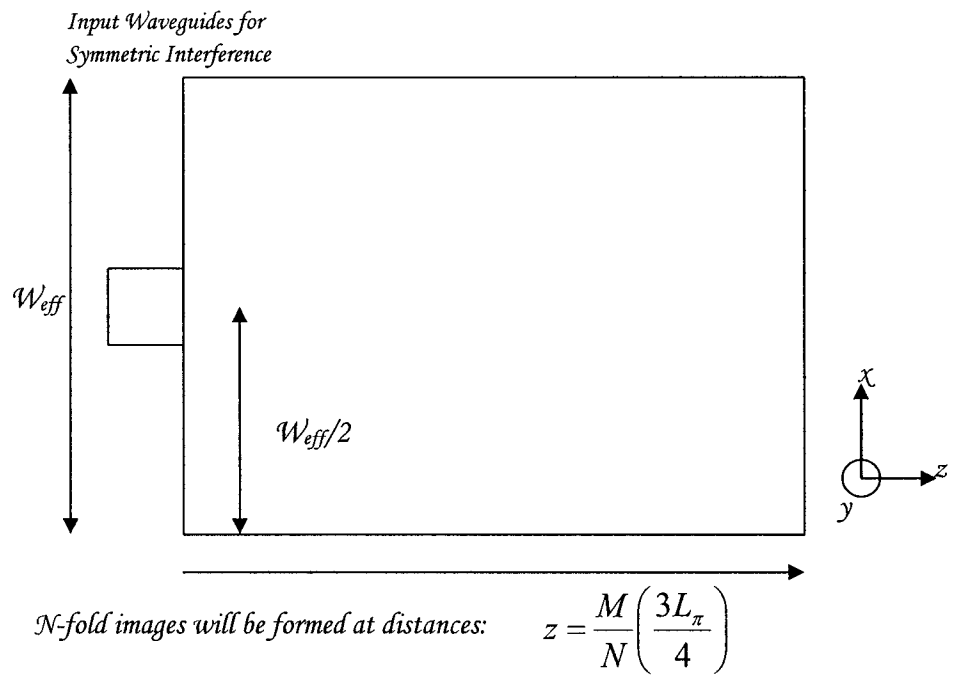

Figure 2-14: Symmetric Interference by placing input waveguides at $\frac{1}{2}W_{eff}$

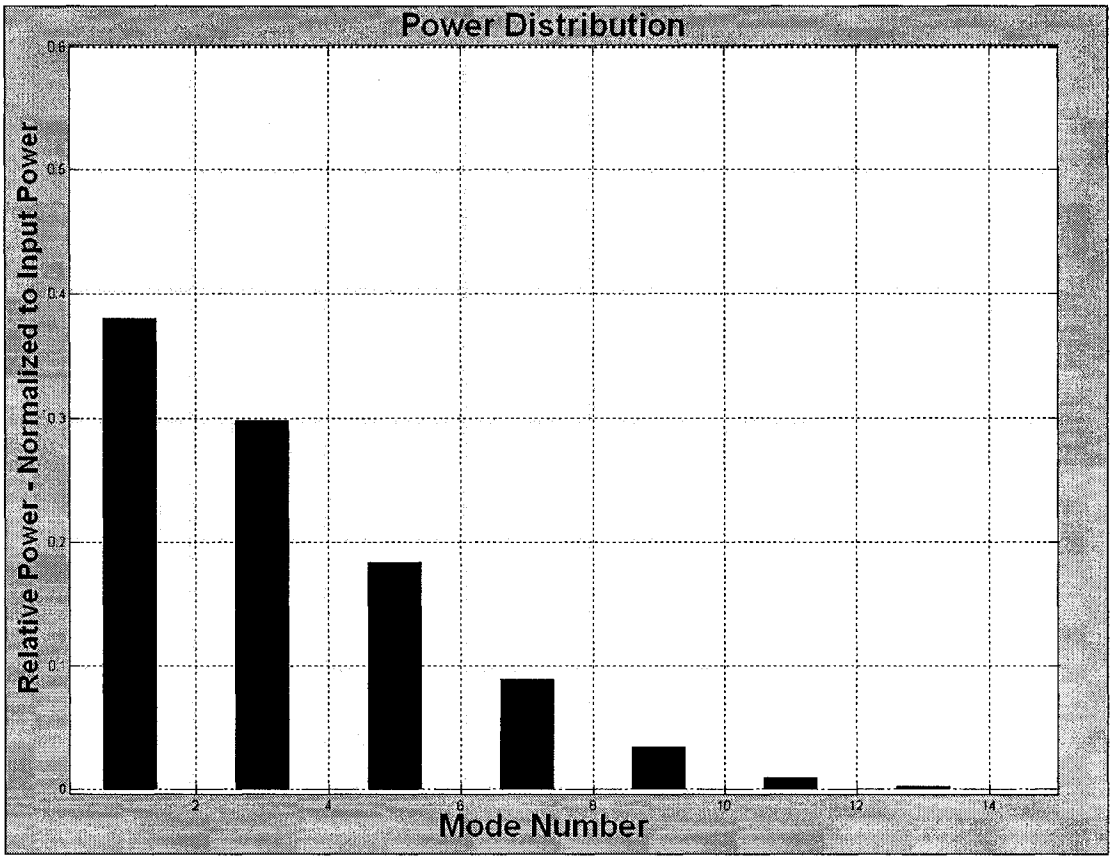

Figure 2-15: Distribution of power in each mode for the example of a 1x3 splitter using Symmetric Interference. n_{effco} =1.563 W_{eff} =45 microns z=3250 microns λ=650.3nm TE polarization

Figure 2-15 and 2-16 depict an arbitrary example of Symmetric Interference where n_{effco}=1.563 W_{eff}=45 microns z=3250 microns λ=650.3nm and TE polarization is used. Notice that $\nu=2^{nd}, 4^{th}, 6^{th}, 8^{th}\ldots$ modes do not have any power coupled to them from the Gaussian input.

Figure 2-16 is the multimode interference pattern in the waveguide for a 'Symmetric Interference' example. Note the input is at $\frac{1}{2}W_{eff}$ in the x dimension. Equation 2-43 governs the values of z where multiple images will be seen.

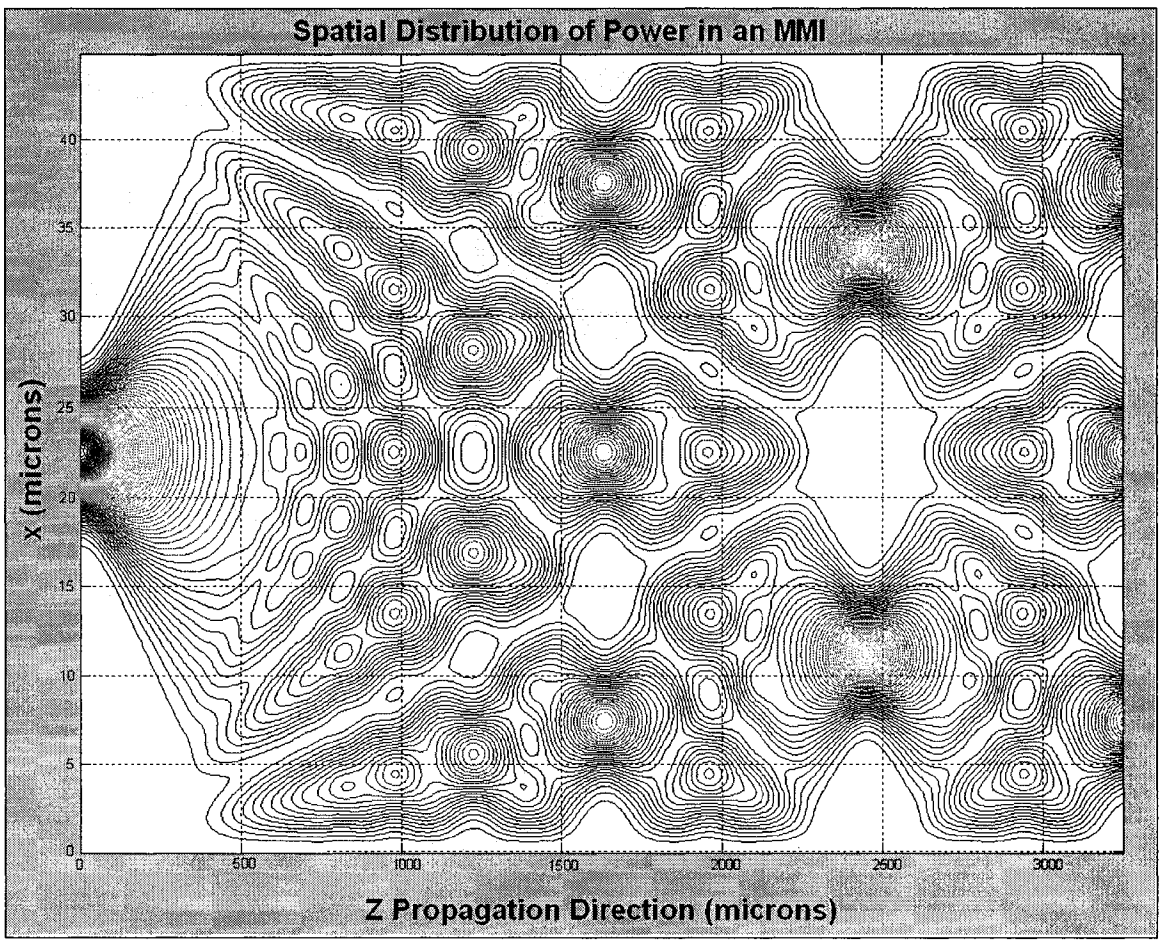

Figure 2-16: Multi-Mode Image for the 1x3 splitter example using Symmetric Interference. n_{effco} =1.563 W_{eff} =45 microns z=3250 microns λ =650.3nm TE polarization

For both the Paired Interference and Symmetric Interference cases, the overall length of the waveguide can be reduced. So long as the output waveguides are placed where the images are, you can create simple, efficient short lightwave power splitters. Note that for the same number of desired images, Equation 2-44 for paired interference and Equation 2-45 for symmetric interference provide shorter waveguide solutions than that of Equation 2-43 for general interference.

2.3.4 Predicting the relative phases of the multimode images

The three Equations 2-43, 2-44 and 2-45 for the general, paired and symmetric interference, respectively, provide information where self-images or multi-images appear in the z direction. However, they do not provide information on the image position in the x–direction and phases of the output images. These two pieces of information are important. One needs to know where multi-images appear in order to design output waveguides to capture the optical outputs. Furthermore, phase information of the output images is important for such devices as Generalized

Mach-Zehnder Interferometers that use the difference in the output phases for such things as optical switching [70].

Recalling the basic equation for finding the optical image at any point in the x-z plane, Equation 2-25 $f_{out}(x,z)=\sum_{\nu=1}^{N} a_\nu \mathrm{E}_\nu \exp(-j\beta_\nu z)$.

Equation 2-25 in its current form does not give information of the x-axis placement of a multimode image nor the phase. The goal is to take Equation 2-25 and produce an equation that generates this information readily. The results outlined here are derived from Bachmann et. al [5]. The main results are presented here, rather than the full derivation.

Bachmann et. al. prove that Equation 2-25 is equal to:

$$f_{out}(x,z)=\frac{1}{C}\sum_{q=1}^{N-1} f_{in}(x-x_q)\exp(j\varphi_q)$$

where $\Phi_{\zeta,q}=-\pi(\zeta+1)\frac{x_q}{W_{eff}}+\varphi_q$ (2-46)

$$x_q=(2q-N)\frac{M}{N}W_{eff} \quad (2\text{-}47)$$

$$\varphi_q=q(N-q)\frac{M}{N}\pi \quad (2\text{-}48)$$

$$C=\exp(j\beta_0 L_N^M)\sum_{q=0}^{N-1}\exp\left[-j\pi\frac{x_q}{W_{eff}}+j\varphi_q\right] \quad (2\text{-}49)$$

at values lengths along z equal calculated by Equation 2-43:

$$z=L_N^M=\frac{M}{N}3L_\pi=\frac{M}{N}\frac{3\pi}{\Delta\beta_{01}} \quad \text{(Equation 2-43 repeated)}$$

For a given z value (Equation 2-43) one shall find N images at coordinates x_q along the x-axis (Equation 2-47) and with phases φ_q (Equation 2-48) relative to the input Gaussian beam. Here C is a complex normalization constant [5]. Also q denotes the output image number. For example if the device is a 1 x 4 equal power splitter, q ranges from output 1 to output 4. The term ζ is the mode order and is equal to $(\nu-1)$, where ν is the mode number. These positions and phases are dependent on the geometry of the MMI section, the material system, the input waveguide placement, and characteristics of the input Gaussian pulse.

2.4 Chapter 2 Summary

Chapter 2 focused directly on the multimode splitter and multimode imaging. Though the derivation is not shown, wave theory is derived from Maxwell's equations. Chapter 2 uses wave theory to analyze confined modes in a planar optical waveguide restricted in the y-axis, where one mode exists and also the x-axis where multiple modes exist, such that multimode interference can occur. The constructive and destructive interference of all modes within the planar optical waveguide can be predicted. Graphs for a fully simulated view of the internal power distribution can be calculated. Furthermore, one can predict where the multimode output images occur in the z-x axis and also the phase of each individual maximum. Using this knowledge a simulation can be constructed for simple rectangular planar multimode splitters for use in integrated optics. This basic MMI theory will be extended in Chapter 4 to include Long Period Grating theory. However, Coupled Mode Theory (CMT) must first be presented in Chapter 3.

[3] Refractive Index Perturbations and Coupled Mode Theory

3.1 Introduction

In the previous chapter it was assumed that the MMI waveguide is of a uniform material without perturbations. How would the multimode images change, however, if a refractive index perturbation existed within the MMI section? A common method to analyze mode coupling due to these refractive index perturbations is Coupled Mode Theory (CMT). Another common method is to calculate mode coupling using entirely numerical methods. Here, CMT will be used to derive equations for periodic perturbations in the MMI section of a waveguide. The modes are physical solutions to the wave equation based on materials, lightwave characteristics and waveguide dimensions. As stated earlier, so long as there is not a perturbation in the refractive index of the material, the only thing that changes for each mode is the phase factor $\exp(-j\beta_\nu z)$. However, once a perturbation in the waveguide is in place both the phase and the power in each mode can change. Yet how does one model this perturbation effect? Furthermore, how can one design these perturbation effects to be beneficial in integrated optics to manipulate the light in the waveguide? In order to answer these questions, one needs to derive the General Coupled Mode Equations.

Coupled Mode Equations are a set of equations that calculate the new electric field magnitude and phase of the affected modes. Each mode that exists within a waveguide can be perturbed simultaneously. However, for special designs such as long period gratings, only a few modes are strongly affected [64]. In fact, a well-designed grating will usually be designed to couple two modes. In Chapter 4, CMT specific to LPGs written on multimode interference waveguides will be discussed.

3.2 Derivation of the General Coupled Mode Equations

For a planar waveguide of a given dimension and material system there are approximate modes, represented by the electric field in Equation 2-24 and repeated here, including the amplitudes

$$G_\nu(x,z) = a_\nu \mathrm{E}_\nu(x,z) = a_\nu \sqrt{\frac{2}{W_{eff}}} \sin\left[\frac{\pi\nu(x+dW/2)}{W_{eff}}\right] \exp(-j\beta_\nu z).$$

(Equation 2-24 –repeated)

Where $\mathrm{E}_\nu(x,z)$ are solutions to the wave equation, where y-dependency is eliminated due to the effective refractive index argument presented in section 2.2.1, here the wave equation is

$$\left(\frac{\partial^2}{\partial x^2}+\frac{\partial^2}{\partial z^2}\right)\vec{\mathrm{E}}(x,z)+k^2 n_{eff}^2\vec{\mathrm{E}}(x,z)=0. \tag{3-1}$$

Typically in many integrated optical devices the refractive index variations are not individually strong. That is the perturbed refractive index is still very close in value to the unperturbed value. Thus one may take the unperturbed value of the refractive index as the background refractive index and then model a perturbation equation around this. A model of a perturbation in the dielectric permittivity is equivalent to modeling a perturbation in the refractive index [3]. The relation is $n=\sqrt{\varepsilon_r}$, where ε_r is the relative permittivity (relative to ε_0) of the material.

Dielectric Permittivity Perturbation can be modeled as

$$\begin{aligned}\varepsilon'(x,y,z)&=\varepsilon(x,y)+\Delta\varepsilon(x,y,z) \\ &=background+perturbation.\end{aligned} \tag{3-2}$$

Propagation of the lightwave is purely in the z-direction. The general wave equation for guided modes has general solutions

$$\mathrm{E}_\nu(x,z)=\mathrm{E}_\nu(x)\exp(-j\beta_\nu z). \tag{3-3}$$

The electric field distribution is $\mathrm{E}_\nu(x)$ and the phase is $\exp(-j\beta_\nu z)$; which is dependent on the propagation constant of the mode, β_ν, and the position along the z-axis.

Perturbations in the waveguide are such things as changing waveguide dimensions or changing the dielectric constants of the materials. So long as there are no waveguide perturbations, each mode is completely independent from one another. The optical power distribution in an MMI can be calculated by taking the square of the sum of all modal electric fields and is represented by Equation 2-27 in Chapter 2.

Any deviation away from the background refractive index perturbs the modes and couples energy between them. The electric field of any mode after a perturbation can be described as a superposition of the original modes. Therefore, general solutions to the wave equation in the presence of the perturbation can be represented as [68]

$$E_{Perturbed}(x,z)=\sum_{\nu=1}^{N}[A_\nu(z)\mathrm{E}_\nu(x)\exp(-j\beta_\nu z)+B_\nu(z)\mathrm{E}_\nu(x)\exp(+j\beta_\nu z)]. \tag{3-4}$$

The value $A_\nu(z)$ represents the amplitude of the forward traveling wave, while $B_\nu(z)$ represents the amplitude of the backward traveling wave in the –z direction. Note that $A_\nu(z)$ is the 'New' value of the electric field amplitude due to the perturbation, is dependent on z, and is analogous to the original electric field amplitude a_ν in Equation

2-22 such that $A_\nu(z=0) = a_\nu(z=0)$. Recall that before any perturbation, the amplitudes of the respective electric fields $a_1, a_2 \ldots$are not functions of z.

If one is dealing with only forward modes coupling to other forward modes, then Equation 3-4 simplifies to

$$E_{Perturbed}(x,z) = \sum_{\nu=1}^{N}[A_\nu(z)\mathrm{E}_\nu(x)\exp(-j\beta_\nu z)]. \tag{3-5}$$

For simplicity, Equation 3-5 will be used, ignoring backward traveling waves, which are typical of short period or Bragg gratings. It is also worth noting that coupling to radiation modes is also omitted from Equations 3-4 and 3-5; one shall assume here that it is negligible. Only perturbations that couple forward propagating modes are considered.

Firstly, insert the unperturbed waveguide solutions, Equation 3-3 into the wave equation, Equation 3-1. These equations will be used for simplification in forthcoming equations. Modes number from 1 to N, and therefore one will have N equations as

Mode 1:

$$\frac{\partial^2 \mathrm{E}_1(x)}{\partial x^2} + (k_0^2 n_{eff1}^2 - \beta_1^2)\mathrm{E}_1(x) = 0 \tag{3-6}$$

Mode 2:

$$\frac{\partial^2 \mathrm{E}_2(x)}{\partial x^2} + (k_0^2 n_{eff2}^2 - \beta_2^2)\mathrm{E}_2(x) = 0 \tag{3-7}$$

*

* likewise for Modes 3 through N.

Equation 3-6 is the result of inputting the *Mode* 1 solution, into the wave equation and Equation 3-7 is the result of inputting the *Mode* 2 solution into the wave equation. Almost identical equations are provided for Modes 3 through N.

The general solutions after the perturbation is applied, as shown in Equation 3-5, must also be substituted into the wave equation. One must also take into account the dielectric permittivity perturbation in Equation 3-2; the substitution is

$$\left[\frac{\partial^2}{\partial x^2} + \frac{\partial^2}{\partial z^2}\right]\left[\sum_{\nu=1}^{N}[A_\nu(z)\mathrm{E}_\nu(x)\exp(-j\beta_\nu z)]\right]$$
$$+(\omega^2\mu_0\varepsilon + \omega^2\mu_0\Delta\varepsilon)\left[\sum_{\nu=1}^{N}[A_\nu(z)\mathrm{E}_\nu(x)\exp(-j\beta_\nu z)]\right] = 0$$

and taking derivatives of the terms in the brackets one has

$$\sum_{\nu=1}^{N}\left(\exp(-j\beta_\nu z)\left[\begin{array}{l} A_\nu(z)\dfrac{\partial^2 \mathrm{E}_\nu(x)}{\partial x^2}+\left(\dfrac{d^2A_\nu(z)}{dz^2}-2j\beta_\nu\dfrac{dA_\nu(z)}{dz}-A_\nu(z)\beta_\nu^2\right)\mathrm{E}_\nu(x) \\ +\omega^2\mu_0\varepsilon A_\nu(z)\mathrm{E}_\nu(x)+\omega^2\mu_0\Delta\varepsilon A_\nu(z)\mathrm{E}_\nu(x)\end{array}\right]\right)=0. \tag{3-8}$$

Equation 3-8 requires further simplification. Using the equations such as Equations 3-6 and 3-7, several terms in Equation 3-8 may be cancelled as they add up to zero. What remains from Equation 3-7 is

$$\sum_{\nu=1}^{N}\left[\left(\frac{d^2A_\nu(z)}{dz^2}-2j\beta_\nu\frac{dA_\nu(z)}{dz}+\omega^2\mu_0\Delta\varepsilon A_\nu(z)\right)\mathrm{E}_\nu(x)\exp(-j\beta_\nu z)\right]=0. \tag{3-9}$$

In a typical derivation of the coupled mode equations one uses the parabolic approximation [see examples in references 3, 10, 38, 55, 63, 68]. It is stated as follows

$$\left|\frac{d^2}{dz^2}A_\nu\right| << \left|\beta_\nu\frac{d}{dz}A_\nu\right|. \tag{3-10}$$

This approximation assumes that the dielectric perturbations are weak and that the mode amplitudes vary slowly over the course of the waveguide; or likewise A_ν must vary negligibly over one wavelength.

To obtain the Coupled Mode Equations, use the parabolic approximation, then divide by $\exp(-j\beta_\nu z)$ and finally multiply by the complex conjugate of $\mathrm{E}_\nu(x)$ and integrate over the cross section [63]. For a given number of modes $\nu=1..N$, one will have N coupled mode equations with N elements each.

The coupled mode equations will calculate the change in the energy and phase of each mode due to the perturbation. Each element of the equation will represent the coupling between mode ν-th and the μ-th mode. The results of the manipulation discussed above is

$$-2j\beta_\nu\frac{dA_\nu(z)}{dz}\int_{W_{eff}}\mathrm{E}_\nu(x)\mathrm{E}_\nu^*(x)dx+\omega^2\mu_0A_\nu(z)\int_{W_{eff}}\Delta\varepsilon(x,z)\mathrm{E}_\nu(x)\mathrm{E}_\nu^*(x)dx+$$

$$\sum_{\nu=1}^{N}\left(\begin{array}{l}-2j\beta_\mu\dfrac{dA_\mu(z)}{dz}\exp\left[-j(\beta_\mu-\beta_\nu)z\right]\displaystyle\int_{W_{eff}}\mathrm{E}_\mu(x)\mathrm{E}_\nu^*(x)dx+ \\ \omega^2\mu_0A_\mu(z)\exp\left[-j(\beta_\mu-\beta_\nu)z\right]\displaystyle\int_{W_{eff}}\Delta\varepsilon(x,y,z)\mathrm{E}_\mu(x)\mathrm{E}_\nu^*(x)dx\end{array}\right)=0 \tag{3-11}$$

The integrals in Equation 3-11 are spatial overlap integrals of the mode profiles that can exist in the x or y–direction of the waveguide. Equation 3-11 can be simplified, as the second term in the above equation is negligible for small perturbations $\Delta\varepsilon(x,y,z)$. Also, the third term is equal to zero due to mode orthogonality.

The fourth term is known as the coupling coefficient $\kappa_{\nu\mu}$, equal to

$$\kappa_{\nu\mu} = \int_{W_{eff}} \Delta\varepsilon(x,z)\mathrm{E}_{\mu}(x)\mathrm{E}_{\nu}^{*}(x)dx . \tag{3-12}$$

A slight perturbation $\Delta\varepsilon(x,y,z)$ can make this integral a significant value.

Equation 3-11 can be simplified as

$$\frac{dA_{\nu}(z)}{dz} = \frac{\sum_{\nu=1}^{N}\left(\omega^{2}\mu_{0}A_{\mu}(z)\exp\left[-j\left(\beta_{\nu}-\beta_{\mu}\right)z\right]\kappa_{\nu\mu}\right)}{2j\beta_{\nu}\int_{W_{eff}}\mathrm{E}_{\nu}(x)\mathrm{E}_{\nu}^{*}(x)dx} . \tag{3-13}$$

If the wavefunctions of the modes are normalized to a power of 1W, the orthonormalization of the modes can be written as [63]

$$\iint_{\infty}\mathrm{E}_{l}\mathrm{E}_{m}dxdy = \frac{2\omega\mu}{|\beta_{m}|}\delta_{lm} \tag{3-14}$$

where δ_{lm} is the Kronecker delta function defined by $\delta_{lm}\begin{cases}0 & \text{for}\begin{cases}l\neq m\\ l=m\end{cases}\\ 1\end{cases}$ and l and m are arbitrary mode numbers. When $l=m=1$, the term $\int_{W_{eff}}\mathrm{E}_{\nu}(x)\mathrm{E}_{\nu}^{*}(x)dx$ in Equation 3-13 becomes

$$\int_{W_{eff}}\mathrm{E}_{\nu}(x)\mathrm{E}_{\nu}^{*}(x)dx = \frac{2\omega\mu_{0}}{|\beta_{\nu}|} . \tag{3-15}$$

Therefore, setting a convention such that $\nu<\mu$, $|\beta_{\nu}|>|\beta_{\mu}|$, where ν is the lower order mode. Since we are dealing with forward propagating modes $\frac{|\beta_{\nu}|}{\beta_{\nu}}=1$. Equation 3-15 then becomes

$$\frac{dA_{\nu}(z)}{dz} = \frac{-j\omega}{4}\sum_{\mu}\kappa_{\nu\mu}A_{\mu}(z)\exp\left[j\left(\beta_{\nu}-\beta_{\mu}\right)z\right]. \tag{3-16}$$

This is the general coupled mode equation for the effect of the perturbation.

The coupling coefficient $\kappa_{\nu\mu}$ for mode numbers ν and μ are affected by the spatial overlap of the two electric field distributions. It is also affected by the value of the dielectric permittivity perturbation, $\Delta\varepsilon(x,y,z)$. In Equation 3-16, ν and μ are mode numbers and take on a positive integer value.

3.3 Chapter 3 Summary

Chapter 3 focused exclusively on the mathematical theory necessary to model the effect of a perturbation on forward propagating modes. This can be modeled using Coupled Mode Theory derived from Maxwell's wave equation and solutions to this wave equation. The theory presented in Chapter 3 is essential to understanding the mathematics underlying the topic of this thesis. Using tilted long period gratings to tailor multi-mode images in planar optical waveguides will be discussed in the next chapter.

[4] Using Coupled Mode Theory to analyze Tilted Long Period Gratings to Tailor Multimode images

4.1 Introduction

The previous two chapters examined multimode interference in planar optical waveguides and coupled mode theory. Here, in Chapter 4, an analysis of long period gratings written onto multimode planar optical waveguides is presented. These long period gratings also need to be tilted to introduce an x (or y) dependency for mode coupling. This results in a change of the output image from the multimode section of the waveguide. The goal, for example, might be to have a 1 x 4 splitter, having 25% of the optical power at each of the four outputs, changed, by virtue of a dynamic grating, to a 1 x 2 splitter having 50% of the optical power at only two outputs. This is a powerful device, as instead of having the inherent properties of a static 1 x 4 splitter, one can create a dynamic splitter by activating a dynamic grating. The theory developed here is a novel concept. The tilted long period grating couples core modes to other core modes in the multimode waveguide. Usually orthogonal modes, modeled by sine waves, cannot be coupled as their overlap integrals equal zero over the waveguide dimension. However, as one shall see, that is where the x (or y) dependency of the refractive index perturbation becomes important. Chapter 4 builds significantly on the previous two chapters and references to these chapters are used.

4.2 Analysis of the Coupled Mode Equations Part I: Perturbations with x or y-dependency

As stated in Chapter 2, thin film planar waveguides are often designed and fabricated such that only one mode exists in the y-dimension. Using a effective refractive index, modal interference in a rectangular waveguide can be looked at in the x-z plane. This modal interference begets optical maxima and minima in the form of multimode images. The electric fields contained within Equation 3-12 are still of the form

$$\mathrm{E}_{\nu}(x,z) = \sqrt{\frac{2}{W_{eff}}}\sin\left[\frac{\pi\nu(x+dW/2)}{W_{eff}}\right]\exp(-j\beta_{\nu}z). \qquad (4\text{-}1)$$

The goal is to couple core modes into other core modes. All modes within the rectangular waveguide can be classified as core modes. If one models the modes along the x-axis, they resemble sinusoidal modes. If one wishes to couple one mode to another there must be a non-zero spatial overlap between the two modes. That means the overlap integral over the dimension of the waveguide must be non-zero. If $\Delta\varepsilon(x,y,z)$ in the coupling coefficient has no x or y dependency, that is, the perturbation is perpendicular to the axis of propagation z, then $\Delta\varepsilon(x,y,z) \rightarrow \Delta\varepsilon(z)$. Taking Equation 4-1 into account, for this case, the coupling coefficient is

$$\kappa_{\nu\mu} = \Delta\varepsilon(z)\exp(-j\beta_\nu z)\exp(-j\beta_\mu z)\frac{2}{W_{eff}}\int_{Weff}\sin\left[\frac{\pi\nu x}{W_{eff}}\right]\sin^*\left[\frac{\pi\mu x}{W_{eff}}\right]dx\,. \tag{4-2}$$

Here the overlap integral $\int_{Weff}\sin\left[\frac{\pi\nu x}{W_{eff}}\right]\sin^*\left[\frac{\pi\mu x}{W_{eff}}\right]dx$ will always integrate to zero. This means that sinusoidal modes cannot couple to each other using perturbations that are only written perpendicular to the propagation axis. Thus, one needs to use a perturbation with an x or y-dependency.

4.3 Analysis of the Coupled Mode Equations Part II: Defining a Useful Refractive Index Perturbation

Dielectric waveguides are typically characterized by the refractive index rather than the permittivity. The permittivity perturbation as appearing in Equation 3-2 in Chapter 3 becomes

$$\Delta\varepsilon(x,y,z) = \varepsilon_0\left[n^2_{perturbed}(x,y,z) - n^2_{background}(x,y,z)\right]. \tag{4-3}$$

As an approximation, Equation 4-3 can be written as [3]

$$\Delta\varepsilon(x,y,z) \approx 2\varepsilon_0 n(x,y,z)\Delta n(x,y,z)\,. \tag{4-4}$$

In Equation 4-4 the background refractive index of the material is $n(x,y,z)$ and the refractive index perturbation is $\Delta n(x,y,z)$.

The key to making the coupling coefficients non-zero, and thus inducing core mode to core mode coupling lies in designing the dielectric permittivity perturbation, $\Delta\varepsilon(x,y,z)$. If $\Delta\varepsilon(x,y,z)$ has any x or y-dependency the coupling coefficient, $\kappa_{\nu\mu}$ will be non-zero. Potentially advantageous mode coupling can be accomplished using a wide variety of exotic perturbations in x, y and z. The goal of this chapter, however, is to analyze a perturbation that is simple, produces a non-zero coupling coefficient and also allows strong core mode to core mode coupling over the length of the waveguide. The last point must take into account the full coupled mode equations and requires 'phase matching' using periodic perturbations. Many refractive index structures may satisfy these requirements, though the simplest is the tilted long period grating.

The long period grating was briefly touched upon in Chapter 1. The relatively long periodicity of the periodic perturbation is necessary to phase match the modes. This will become apparent later; however, one must first introduce the geometry of the tilted long period grating.

In order to examine the tilted long period grating, an axis system needs to be defined as in Figure 4-1. For simplicity, tilted gratings in the x-z plane are analyzed. Tilted gratings in the y-z plane would follow the same analysis. Note that in Figure 4-1, θ is defined as the tilt angle away from the x-axis. Also Λ_g is the period of the long period grating, and Λ is the period of the LPG along the z-axis as in Figure 4-1. If the angle θ approaches 90° the period of the long period grating Λ_g can be relatively short, but the z-axis component of the period, Λ, can be significantly longer.

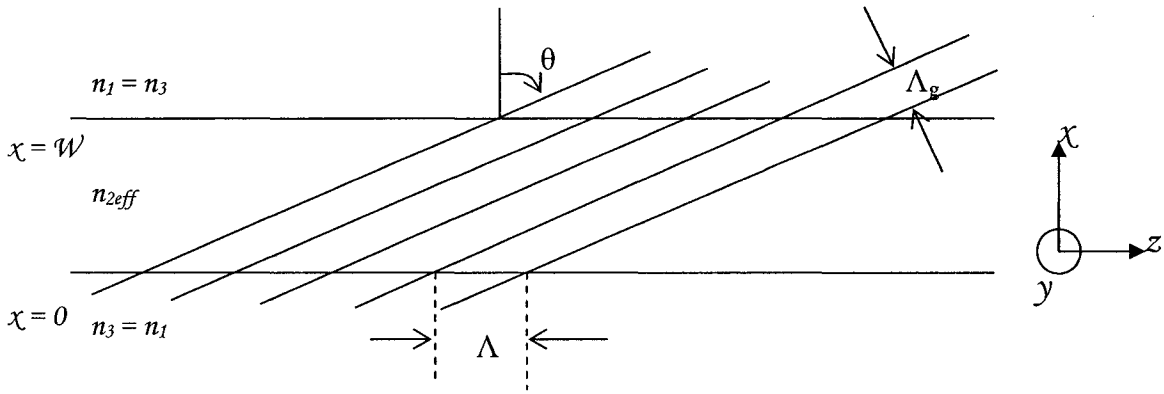

Figure 4-1: Schematic of a Tilted Long Period Grating

For a complete characterization of the tilted long period grating, the amplitude and shape of the refractive index needs to be addressed. As previously stated, one can change the refractive index in numerous ways, such as pressure, heat, surface corrugations or permanently photoinducing the material. Here, surface corrugations are modeled since this would probably be the easiest way to fabricate the LPGs.

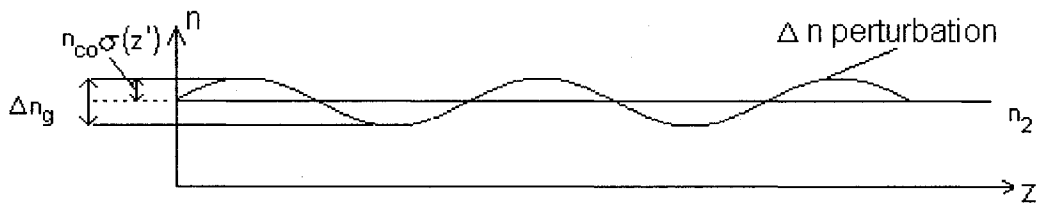

Figure 4-2: Schematic of the refractive index perturbation characteristics

In Figure 4-2, $n_{co}\sigma(z')$ denotes the peak magnitude of the refractive index change due to surface corrugation, the variable $\sigma(z')$ is a fraction multiple of this peak, and Δn_g is the peak-to-peak effect. The refractive index denoted by n_{co} is the background effective refractive index.

The tilted grating in Figure 4-1 and 4-2 can be modeled as a sine/cosine modulation of the refractive index. In order to model the tilted grating mathematically, the equation for the refractive index change is [3]

$$\Delta n(x,z,\theta) = n_{co}\sigma\left[1+\cos(2K_g z')\right]. \tag{4-5}$$

Where the variables used are defined in the paper by K. S. Lee [3] as:

$$z' = z\cos\theta - x\sin\theta \tag{4-6}$$

$$K_g = \frac{\pi}{\Lambda_g} \tag{4-7}$$

$$n_{co}\sigma = \frac{\Delta n_g}{2} \tag{4-8}$$

$$\Lambda_g = \Lambda\cos\theta \tag{4-9}$$

As will be seen in the following section, one should design the value Λ, the z component of the grating periodicity, such that it 'phase matches' the two modes one is trying to couple. It must satisfy the following equation,

$$\Lambda = \frac{2\pi}{\beta_\nu - \beta_\mu}. \tag{4-10}$$

Equation 4-10 is exactly analogous to Bragg Grating theory as described in section 1.5 and shown in Appendix III.

So long as one knows the propagation constants within a waveguide, the periodicity of the grating can be calculated for maximum mode coupling. The periodicity, Λ , is inversely proportional to the difference in propagation constant $\beta_\nu - \beta_\mu$. Since the ν -th mode and μ -th mode are both forward propagating modes, their differences are relatively small, making it necessary to have a long period grating.

Now calculate the new coupling coefficients given a tilted long period grating. Substitute Equations 4-6 through 4-9 into Equation 4-4, to give the equation for the dielectric permittivity using a tilted grating [3],

$$\Delta\varepsilon \approx 2\varepsilon_0 n(x,y)\frac{\Delta n_g}{2}\left[1+\cos\left(2K_g[z\cos\theta - x\sin\theta]\right)\right]. \tag{4-11}$$

Substitute Equation 4-11 into the equation for the coupling coefficient $\kappa_{\nu\mu}$, one has the general form of coupling coefficient for a tilted grating using. The electric field has only an x-dependence, E(x) as shown in Chapter 2. The coupling coefficient is

$$\kappa_{\nu\mu} = \frac{2}{W_{eff}} \int_{W_{eff}} 2\varepsilon_0 n(x,y) \frac{\Delta n_g}{2} \left[1 + \cos\left[2K_g(z\cos\theta - x\sin\theta)\right]\right] \mathrm{E}_\mu(x)\mathrm{E}_\nu^*(x)dx. \quad (4\text{-}12)$$

Using the identity, $\cos\xi = \frac{1}{2}\left[e^{j\xi} + e^{-j\xi}\right]$ (4-13)

Equation 4-12 is now equal to

$$\begin{aligned}
\kappa_{\nu\mu} &= 2\varepsilon_0 n(x,y) \frac{\Delta n_g}{2} \frac{2}{W_{eff}} \int_{W_{eff}} \mathrm{E}_\mu(x)\mathrm{E}_\nu^*(x)dx \\
&+ 2\varepsilon_0 n(x,y) \frac{\Delta n_g}{2} \frac{1}{2} \exp(+j2K_g z\cos\theta) \frac{2}{W_{eff}} \int_{W_{eff}} \exp(-j2K_g x\sin\theta)\mathrm{E}_\mu(x)\mathrm{E}_\nu^*(x)dx \\
&+ 2\varepsilon_0 n(x,y) \frac{\Delta n_g}{2} \frac{1}{2} \exp(-j2K_g z\cos\theta) \frac{2}{W_{eff}} \int_{Weff} \exp(+j2K_g x\sin\theta)\mathrm{E}_\mu(x)\mathrm{E}_\nu^*(x)dx
\end{aligned} \quad (4\text{-}14)$$

Equation 4-14 is a long, complicated equation that represents only the coupling coefficient of the coupled wave equations for a tilted grating. The next step is deriving the full coupled mode equations using tilted long period gratings. This provides a mathematical basis to calculate the effects of tilted long period grating on the magnitude and phase of the existing modes within an MMI waveguide and thus the new imaging properties. Substituting Equation 4-14 into Equation 3-16 for the coupled mode equations:

$$\frac{dA_\nu(z)}{dz} = \frac{-j\omega}{4} \frac{2}{W_{eff}} \sum_\mu \left[
\begin{aligned}
&A_\mu(z) 2\varepsilon_0 n(x,y) \frac{\Delta n_g}{2} e^{j(\beta_\nu - \beta_\mu)z} \int_{Weff} \mathrm{E}_\mu(x)\mathrm{E}_\nu^*(x)dx \\
&+ A_\mu(z) 2\varepsilon_0 n(x,y) \frac{\Delta n_g}{2} \frac{1}{2} e^{j(\beta_\nu - \beta_\mu + 2K_g\cos\theta)z} \int_{Weff} e^{-j2K_g x\sin\theta} \mathrm{E}_\mu(x)\mathrm{E}_\nu^*(x)dx \\
&+ A_\mu(z) 2\varepsilon_0 n(x,y) \frac{\Delta n_g}{2} \frac{1}{2} e^{j(\beta_\nu - \beta_\mu - 2K_g\cos\theta)z} \int_{Weff} e^{+j2K_g x\sin\theta} \mathrm{E}_\mu(x)\mathrm{E}_\nu^*(x)dx
\end{aligned}
\right] \quad (4\text{-}15)$$

Equation 4-15 is the coupled mode equations for a tilted grating in the x-z plane. Due to mode orthogonality, the first term in Equation 4-15 will be equal to zero and can be ignored.

By looking at Equation 4-15 carefully, one can see the variables that affect the coupled mode equations. The coupled mode equations are significantly affected by the term in Equation 4-12,

$$\cos\left(2K_g[z\cos\theta - x\sin\theta]\right) = \frac{1}{2}\left[e^{j2K_g z\cos\theta}e^{-j2K_g x\sin\theta} + e^{-j2K_g z\cos\theta}e^{+j2K_g x\sin\theta}\right].$$

For the tilted long period grating one has two variables, the tilt angle θ and the grating frequency/ periodicity $K_g = \frac{\pi}{\Lambda_g}$. The factors $\exp(-j2K_g x\sin\theta)$ and $\exp(+j2K_g x\sin\theta)$ are x dependent and must be included in the integral in Equation 4-15. This factor leads to a non-zero value for the integral.

The factors $\exp(j2K_g z\cos\theta)$ and $\exp(-j2K_g z\cos\theta)$ are not x or y dependent and thus do no affect the overlap integral. However, they do affect whether or not the terms of the summation in Equation 4-15 are significant or not. If there is an exponential of the form $\exp(jMz)$ or $\exp(-jMz)$, where $M \neq 0$, then it is a rapidly oscillating term in z. A rapidly oscillating terms' contribution to mode coupling is insignificant over a distance that is much longer than the period of the index change or the perturbation. The only way to make either Term 2 or Term 3 in Equation 4-15 significant and therefore make the term of the coupling coefficient a non-negligible number is if one of these two conditions holds

$$\beta_\nu - \beta_\mu + 2K_g\cos\theta \approx 0 \qquad (4\text{-}16a)$$

or

$$\beta_\nu - \beta_\mu - 2K_g\cos\theta \approx 0. \qquad (4\text{-}16b)$$

However, it should be noted that if one chooses the tilt angle θ and the grating frequency/periodicity to make one term of the couple mode equation significant by matching two specific modes ν and μ, all other terms in the coupling coefficient become negligible by the rapid oscillation argument. Therefore, <u>one</u> tilted long period grating can only be designed to 'phase match' <u>two modes and two modes only</u>.

If one uses the number ν to be the lower order coupled mode and μ the higher order coupled mode such that $\beta_\nu > \beta_\mu$, then one must design for the phase matching in Equation 4-16b.

Gratings must be designed with two modes in mind, the initial mode, and the second mode that one wishes to couple power to. Therefore, one must also decide the specific two modes to couple, and solve the propagation constants of these two modes. The two modes one chooses to design a grating for are denoted p and q in the equations below. The variables p and q are analogous to ν and μ but are called p and q to distinguish them as 'chosen' modes.

Using the result from Equation 4-16 only two coupled mode equations exhibit non-negligible terms. The coupled mode equations in Equation 4-15 can be reduced to

$$\frac{dA_p(z)}{dz} = \frac{-j\omega}{4}\frac{2}{W_{eff}}\left[2\varepsilon_0 n_{CORE}\frac{\Delta n_g}{2}\frac{1}{2}A_q(z)e^{j(\beta_p-\beta_q-2K_g\cos\theta)z}\int_{Weff} e^{+j2K_g x\sin\theta}\mathrm{E}_q(x)\mathrm{E}_p^*(x)dx\right] \tag{4-17a}$$

for the first 'chosen' mode and

$$\frac{dA_q(z)}{dz} = \frac{-j\omega}{4}\frac{2}{W_{eff}}\left[2\varepsilon_0 n_{CORE}\frac{\Delta n_g}{2}\frac{1}{2}A_p(z)e^{j(\beta_p-\beta_q+2K_g\cos\theta)z}\int_{Weff} e^{-j2K_g x\sin\theta}\mathrm{E}_q(x)\mathrm{E}_p^*(x)dx\right] \tag{4-17b}$$

for the second 'chosen' mode.

Using p and q as the mode number, if one wanted to designed a tilted long period grating to couple Mode #1 and Mode #5, then p=1, q=5. Here $p<q$ and both p and q are used to identify the specific mode numbers used in the designs.

The significant coupled mode equations for a tilted long period grating on a planar multimode waveguide are

$$\frac{dA_p(z)}{dz} = \frac{-j\omega}{4}\frac{2}{W_{eff}}\left[2\varepsilon_0 n_{CORE}\frac{\Delta n_g}{2}\frac{1}{2}A_q(z)e^{j(\beta_p-\beta_q-2K_g\cos\theta)z}\int_{-dW/2}^{W+dW/2} e^{+j2K_g x\sin\theta}\mathrm{E}_q(x)\mathrm{E}_p^*(x)dx\right] \tag{4-18a}$$

$$\frac{dA_q(z)}{dz} = \frac{-j\omega}{4}\frac{2}{W_{eff}}\left[2\varepsilon_0 n_{CORE}\frac{\Delta n_g}{2}\frac{1}{2}A_p(z)e^{j(\beta_p-\beta_q+2K_g\cos\theta)z}\int_{-dW/2}^{W+dW/2} e^{-j2K_g x\sin\theta}\mathrm{E}_q(x)\mathrm{E}_p^*(x)dx\right] \tag{4-18b}$$

For a complete analysis of the interaction of modes, one must do the full calculation of Equation 4-15 including all fast oscillating terms. This is difficult, however, as one would end up with N simultaneous differential equations of N elements each, where N is the number of modes. Equations 4-18a and 4-18b are simpler coupled mode equations. In order to solve the simultaneous differential equations an algorithm such as the Runge-Kutta Method must be employed as will be discussed in the next Chapter. The values contained in Equation 4-18 can be complex numbers and therefore the modes will change phase and amplitude.

The phase matching condition in Equation 4-16b has two variables, the tilt angle and grating periodicity. One must set these variables to both phase match the modes and also have the integral be a significant value. An optimum value of the tilt angle for coupling between two modes is provided in Reference 3 and is repeated here [3],

$$\theta_{OptimumTilt} = \tan^{-1}\left[\frac{\left(n_2^2 - n_{eff(\mu)}^2\right)^{1/2}}{n_{eff(\nu)} - n_{eff(\mu)}}\right] \tag{4-19}$$

$$\text{where } n_{eff(\nu)} = \frac{\beta_\nu \lambda}{2\pi} \tag{4-20}$$

$$\text{and } n_{eff(\mu)} = \frac{\beta_\mu \lambda}{2\pi}. \tag{4-21}$$

The coupled mode equations, Equations 4-18a and 4-18b beget complex numbers, and therefore, both the phase and the magnitude of the modes may change due to the tilted long period grating. Ideally, all other modes other than p and q will be unaffected by the tilted long period grating, analogous to certain wavelengths passing through a Bragg grating filter undisturbed. This can be illustrated in Figures 4-3 through 4-5.

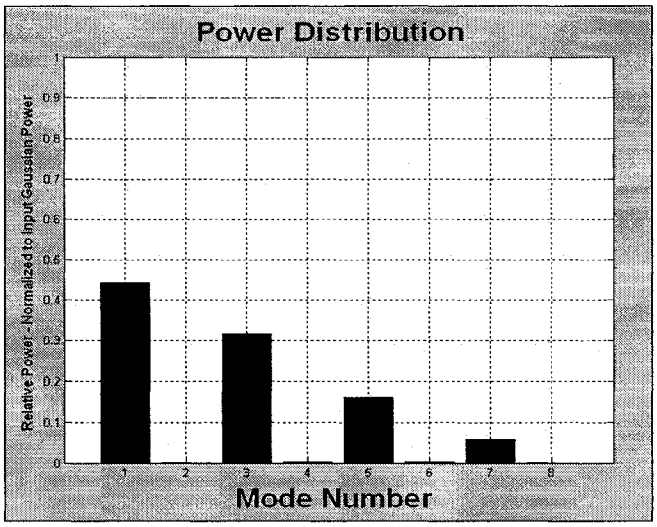

Figure 4-3: Power distribution in a symmetric interference MMI

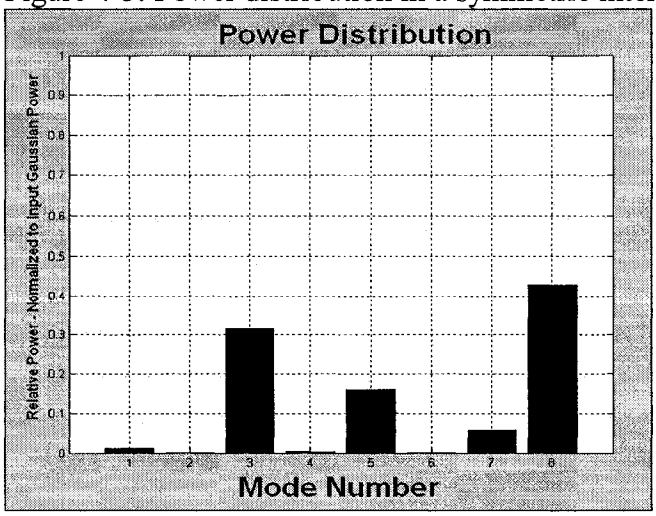

Figure 4-4: Power distribution after a tilted LPG couples Mode #1 to Mode #8

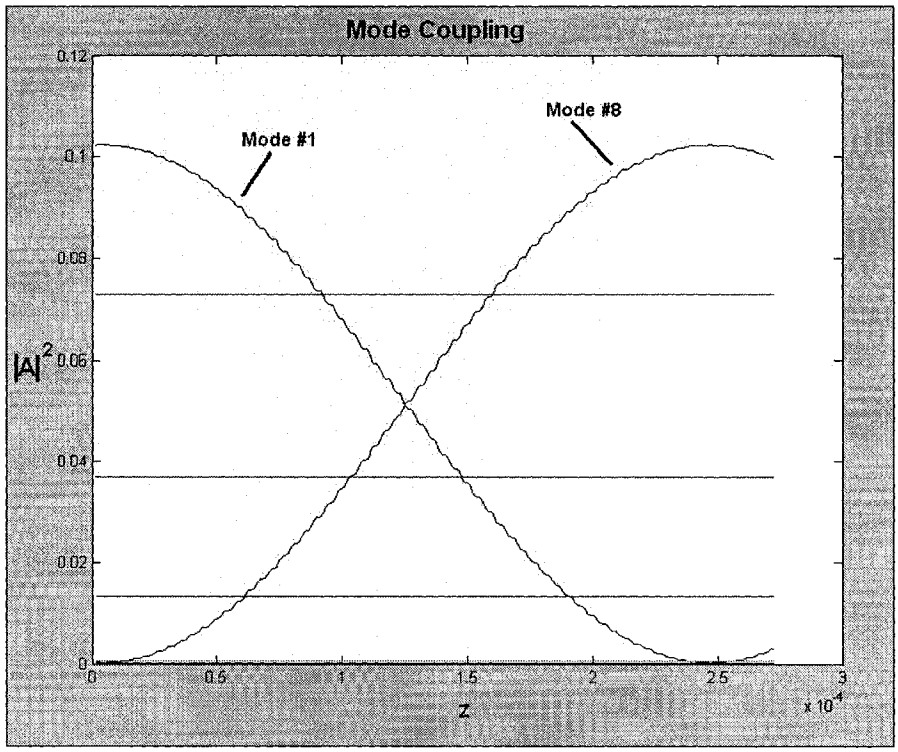

Figure 4-5: Square of electric field amplitude to illustrate mode coupling

Note that all other modes other than Mode #1 and Mode #8 do not change power. Figure 4-3 shows the original power distribution in modes for a symmetric MMI where n_{effco}=1.563, n_{effcl}=1.30, W_{eff}=8 microns, z=700 microns, λ=1550 nm, Δn=0.01, 50 grating periods. Figure 4-4 depicts the power distribution after coupling Mode #1 to Mode #8. The power in Mode #1 is now low and the power in Mode #8 is high. The square of the electric field amplitude is illustrated in Figure 4-5 to show the exchange of power.

4.4 Chapter 4 Summary

In this chapter, the tilted long period grating was modelled. In order to couple core modes to core modes, the perturbation must have an x or y dependency. The coupling coefficients and coupled mode equations using a tilted long period grating were derived. The tilt angle and periodicity of the tilted long period gratings are key variables in these equations. Note that in order to see the effect of any refractive index perturbation structure, the full form of the coupled mode equation must be used. In order to find the optical power at any x, z point one must take the square of the magnitude of the sum of the electric fields of all modes at that point. Since at least two modes can potentially have a new magnitude and phase, the summation of modes will be different, and predictability of where optical maxima and minima in the waveguide does not hold. As one shall see in the next chapter, in lieu of this unpredictability, simulations can be used for thorough design.

[5] Simulation and Device Design

5.1 Introduction

The coupled mode equations for tilted long period gratings and the coupling coefficients derived in Chapter 4 provide the basis for a simulation. This simulation is able to calculate the new electric field magnitude and phase of the affected modes and sum up the electric fields at all x and z points along the waveguide in order to graph the power distribution within the MMI. By this method one need only choose the geometry of the MMI, the characteristics of the material system and laser, and the geometry and intensity of the tilted long period grating as the inputs. The output will be the intensity plot within the MMI and the final output power distribution. The latter is important so one can design the output waveguides at the proper places in the x-axis.

5.2 Structure of the Simulation

5.2.1 Designer Decisions

The simulation discussed here was written in MATLAB. The first step to the simulation is to choose a wavelength to work with and to input the dimensions and material system, for example, as depicted in Figure 5-1.

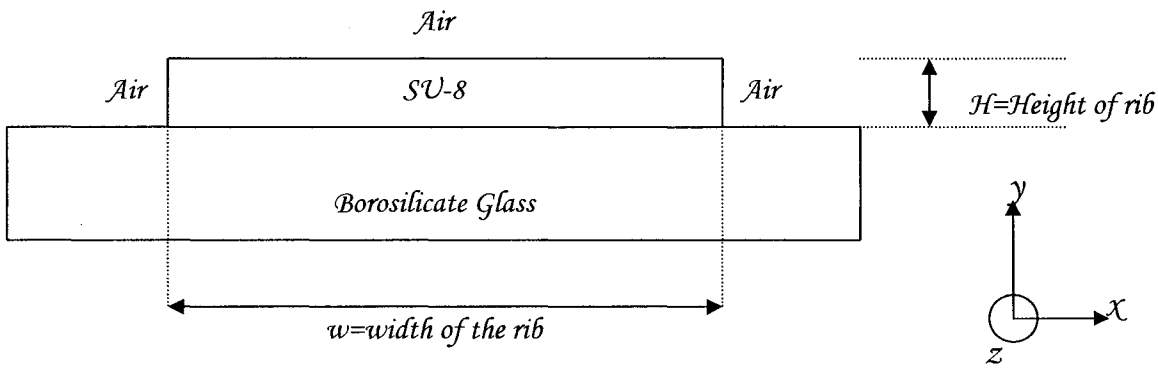

Figure 5-1: Schematic of a rib waveguide

The refractive indices of the SU-8, Borosilicate glass and air are entered, as the dimensions for the rib waveguide. The refractive indices are wavelength dependent and are shown in Figure 5-2 for SU-8 and Figure 5-3 for borosilicate glass.

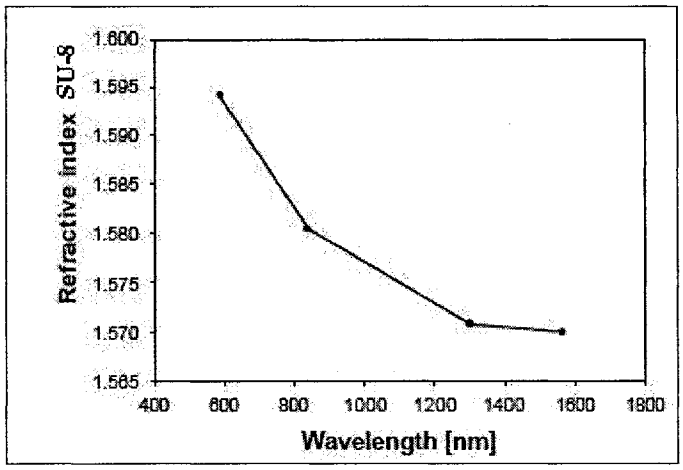

Figure 5-2: Refractive index of SU-8 versus wavelength [96]

Refractive Index of Low- Expansion Borosilicate Glass

Wavelength (nm)	Refractive Index, n	Fraunhofer Designation	Source	Spectral Region
486.1	1.479	F	H_2 arc	Blue
514.5	1.477		Ar laser	Green
546.1	1.476	e	Hg arc	Green
587.6	1.474	d	Na arc	Yellow
643.8	1.472	C'	Cd arc	Red

Figure 5-3: Refractive index of Borosilicate Glass [97]

The width of the MMI waveguide in the x-direction influences the number of lateral modes that can exist. The wider the dimension, the more modes can exist and the better the image quality. However, since the length is dependent on the width, if one has a wide waveguide one will also have a long waveguide, which is usually not advantageous.

Once the effective refractive index of the rib is found, the mode solutions that exist in the multimode section of the waveguide are calculated as in section 2.2.1. These are the modes that can exist; however, these modes might not carry any power. This is because one must calculate the overlap integral of these modes with the input Gaussian lightwave, as shown in Equation 2-22 in Chapter 2. In order to characterize the effect of the input Gaussian, one must choose the type of splitter interference – general, paired or symmetric as described in section 2.3.2 and section 2.3.3. This decision affects where to design the input waveguides. For paired interference, inputs must be designed at $W_{eff}/3$ or $2W_{eff}/3$ and for symmetric interference, the input must be placed at the center point along x.

The width of each input waveguide will affect the imaging as well. The wider the input waveguide, the wider the full-width half-maximum of the Gaussian input. The spatial shape of the input Gaussian waveguide affects the amount of coupling to each mode in the thick multimode region. Once the placement of the input waveguides is determined, one must choose the number of output images. Is this design to be a 1x2 splitter, 1x3 splitter, 1x4 splitter or higher? One can estimate the length of the multimode section in the z-dimension using Equation 2-43 for general interference, Equation 2-44 for paired interference or Equation 2-45 for symmetric interference in Chapter 2.

In order to construct the full modal treatment of the multimode waveguide, one must also calculate the following variables: the propagation constants β_ν, effective indices per mode $n_{eff(\nu)}$, the penetration depths $1/\gamma_c, 1/\gamma_a$, and the total number of modes ν. These variables, along with variables such as effective width W_{eff}, are easy to calculate extending from the transcendental mode equation, Equation 2-17. One then needs to model the input Gaussian as in Equation 2-23 and each mode as a sinusoid as in Equation 2-20. The overlap integral can then be calculated as in Equation 2-22 and the full representation of each mode, including the electric field magnitude, spatial distribution and phase shift due to propagation can be calculated as in Equation 2-24.

It is relatively easy from this point to view the optical power distribution within the MMI. One need only sum up all the modes at all x and z points in order to get the electric field magnitude as in Equation 2-25. Then calculate the power distribution from Equation 2-27 and compare the output image to the predicted output. However, in order to calculate the effect of a tilted long period grating, further modeling must be done.

The design of an MMI waveguide with a tilted long period grating is an iterative process. One is trying to find the right grating characteristics in order to change a naturally existing splitter into a waveguide with different but useful imaging qualities. In order to construct a simulation for this process, the user must first choose two modes, which will dictate grating characteristics. Equation 4-10 in Chapter 4 gives the grating periodicity along the z-axis from the propagation constants of the two modes. Equation 4-22 in Chapter 4 gives the optimum tilt angle for the long period grating knowing the effective refractive indices for each choice of mode. The designer next needs to input the grating profile characteristics from Equation 4-4 in Chapter 4 where a sinusoidal like profile is assumed written on the surface of the grating. Alternatively, one can use a Fourier series to represent a different profile characteristic like a square profile. For example, a refractive index model of a tilted grating using the optimum angle and a Fourier series square profile,

$$\Delta n(x,z,\theta) = n_2\sigma\frac{4}{\pi}\sum_{\tau=1,3,5\ldots}^{\infty}\frac{1}{\tau}\sin\left[\tau * 2K_g\left(z\cos\left(\theta_{OptimumTilt}\right) - x\sin\left(\theta_{OptimumTilt}\right)\right)\right]. \tag{5-1}$$

Furthermore, one must design where to place the grating along the MMI structure. This can affect the imaging properties as well. In Figure 5-4 below, sector 1 is a normal MMI section where modes do not couple but only accumulate a phase. Sector 2 is where coupling occurs. It is represented as a rectangle, but is the length of the grating section from the start of the first angled grating to the end of the last angled grating. Sector 3 is again a normal MMI section where the modes merely accumulate a phase.

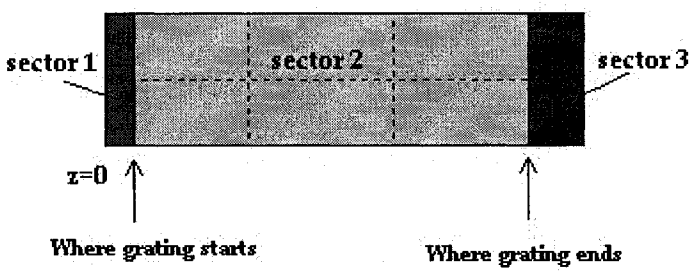

Figure 5-4: Placement of the grating section along the z-axis

One must now calculate the coupling coefficients and construct the coupled mode equations. This process is detailed in Chapter 4. In order to do a full proper treatment of the coupled mode equations one will have N number modes and N number of differential equations. Since with proper design, only two modes should couple, as an estimate, in order to save computing time, only the two differential equations that correspond with the two chosen modes can be solved. These equations are simultaneous differential equations and are solved numerically using Runge-Kutta iterations. Once the iterations have been done, one should have the electric field magnitude and phase of each mode in the x and z coordinates. Therefore, paralleling the normal MMI case it is easy to view the optical power distribution within the MMI. One need only sum up all the electric fields of the modes at all x and z points, Equation 2-25, then calculate the power distribution from Equation 2-27. A flow chart of the necessary steps in order to build this simulation is shown in Appendix II.

5.2.2 Runge-Kutta Iterations

The Runge-Kutta Method is used to solve a system of first order differential equations simultaneously. There are different orders of the Runge-Kutta method, which lead to different truncation errors in the calculations [69]. The higher the order, the more computing power but the advantage is a corresponding lower error. Essentially, a step-size is defined and a recalculation of all the variables is made per step. There is also a method known as the Runge-Kutta-Fehlberg Method, which is also known as the fifth-order Runge-Kutta method and uses an adjustable step size [69]. Designs using a fourth-order Runge-Kutta method were used. This was due to the desire to have new calculations for the optical modes at known values along the z-axis. This is desirable for accurate graphing in MATLAB.

The full description of the coupled mode equations as defined in Chapter 4 is repeated here,

$$\frac{dA_\nu(z)}{dz} = \frac{-j\omega}{4}\sum_\mu \kappa_{\nu\mu} A_\mu(z)\exp\left[j(\beta_\nu - \beta_\mu)z\right] \qquad \text{(3-16 -Repeated)}$$

where $\kappa_{\nu\mu}$ is known as the Coupling Coefficient and is defined as

$$\kappa_{\nu\mu} = \int_{W_{eff}} \Delta\varepsilon(x,z)\mathrm{E}_\mu(x)\mathrm{E}_\nu^*(x)dx\,. \qquad \text{(3-12 -Repeated)}$$

For an example of how the fourth-order Runge-Kutta treats these differential equations, let the number of modes that can exist in the waveguide be equal to 3. This is chosen so as not to have a large number of equations in this example, however it is not a realistic number for multimode interference devices. In the equations above, ν ranges from Modes 1 to 3 and μ ranges from Modes 1 to 3.

The simultaneous differential equations are thus

$$\frac{dA_1(z)}{dz} = \frac{-j\omega}{4}\left\{\begin{array}{l}\kappa_{11}A_1(z)\exp\left[j(\beta_1-\beta_1)z\right]+\kappa_{12}A_2(z)\exp\left[j(\beta_1-\beta_2)z\right]\\ +\kappa_{13}A_3(z)\exp\left[j(\beta_1-\beta_3)z\right]\end{array}\right\} \qquad \text{(5-2)}$$

$$\frac{dA_2(z)}{dz} = \frac{-j\omega}{4}\left\{\begin{array}{l}\kappa_{21}A_1(z)\exp\left[j(\beta_2-\beta_1)z\right]+\kappa_{22}A_2(z)\exp\left[j(\beta_2-\beta_2)z\right]\\ +\kappa_{23}A_3(z)\exp\left[j(\beta_2-\beta_3)z\right]\end{array}\right\} \qquad \text{(5-3)}$$

$$\frac{dA_3(z)}{dz} = \frac{-j\omega}{4}\left\{\begin{array}{l}\kappa_{31}A_1(z)\exp\left[j(\beta_3-\beta_1)z\right]+\kappa_{32}A_2(z)\exp\left[j(\beta_3-\beta_2)z\right]\\ +\kappa_{33}A_3(z)\exp\left[j(\beta_3-\beta_3)z\right]\end{array}\right\}. \qquad \text{(5-4)}$$

If the number of modes that can exist in the x-direction of the multimode waveguide ranges from 1..N, then one must construct N first order differential equations and each equation will have N number of terms.

The information one is trying to obtain by solving this system of differential equations is: new values of $A_1, A_2, \ldots A_N$ at the step intervals $z_1, z_2, \ldots z_N$ where $z_{g+1} - z_g$ is defined as a constant step size $h = dz$. The length of the entire waveguide in the z direction can be called Z_{Length}. The user must define the number of 'cuts' along the Z_{Length} in order to attain a desired resolution for the design. The longer the device length or the higher the desired resolution, the more cuts along z are needed and the longer the computational time as a new set of N simultaneous differential equations

with N elements each needs to be solved. To calculate the value of $h = dz$, choose the number of cuts, m, along Z_{Length}, then

$$h = \frac{Z_{length}}{m}. \tag{5-5}$$

The fourth-order Runge Kutta method is executed via these five equations [69]:

$$q^1 = f(z^k, A^k) \tag{5-6a}$$
$$q^2 = f(z^k + h/2, A^k + hq^1/2) \tag{5-6b}$$
$$q^3 = f(z^k + h/2, A^k + hq^2/2) \tag{5-6c}$$
$$q^4 = f(z^k + h, A^k + hq^3) \tag{5-6d}$$
$$\mathrm{A}^{k+1} = \mathrm{A}^k + \frac{h}{6}(q^1 + 2q^2 + 2q^3 + q^4) \tag{5-6e}$$

where the superscript k is used to denote the k-th discrete z-step z^k and $\frac{dA}{dz} = f(z, A)$. By using this method, one obtains points in x and z and the magnitude and phase of each mode's electric field in order to graph a full coupled mode treatment of every mode in the x, z plane of the waveguide.

5.3 Device Designs

Device designs were carried out using the MATLAB simulation built upon the mathematics in the previous chapters. This simulation is versatile and can be used to simulate devices that have different material systems other than SU-8.

5.3.1 Necessary inputs and important outputs

Table 5-1: Necessary inputs for Tilted LPG MMI simulation

Variable Inputs	Description	Value Used
λ	Laser Wavelength	Red Laser $\lambda = 650.2nm$
t_g	Width of the waveguide in the x direction	Varies
H	Height of the waveguide in the y direction	SU-8 polymer spins down to 3 microns
n_{core}	Refractive index of the core material at λ	$n_{SU-8} = 1.590@650nm$
n_{up}	Refractive index of the material above the core material at λ	$n_{up} = n_{air} = 1.00$
n_{down}	Refractive index of the material below the core material at λ	$n_{down} = n_{BorosilicateGlass} = 1.472@\sim 650nm$
z_{Length}	The length of the device in z	Varies – can be predicted given a waveguide geometry, material and desired signal splitter number
σ_x	Gaussian Half Width	Should be dependent on the input waveguide size. Taken to be ~ 2.5-4 microns
x_0	Gaussian Displacement in the x direction	Placement of the input waveguide – for Symmetric, Paired or General Interference. Usually used Symmetric Interference, therefore $x_0 = W_{eff}/2$
NUM_{x_divs}	Number of 'cuts' along x for imaging	Varies depending on waveguide width
NUM_{z_divs}	Number of 'cuts' along z for imaging	Varies depending on waveguide length
$1stMODE$	Choose a Mode to couple power from	Integer ranging from 1st order mode to Nth

		order mode
2ndMODE	Choose a Mode to couple power to	Integer ranging from 1st order mode to Nth order mode
Δn_g	Peak-to-Peak Index of Modulation away from the background waveguide refractive index	Can vary depending on intensity of corrugation, or if simulating thermo/electro-optic or liquid crystal ~ 0.002 estimate
NUM _PERIODS	Number of grating periods	Varies
GRATING _PROFILE	This can be a cosine, sine, square or other – must be described as an equation (i.e. Square – Fourier series)	Varies. Example: Fourier Series of a normal square wave is $f(x)=\frac{4}{\pi}\sum_{n=1,3,5,\ldots}^{\infty}\frac{1}{n}\sin\left(\frac{n\pi x}{L}\right)$
Optimum _Tilt _Angle	Choose to use an Optimum Tilt Angle?	Equation 4-19: $\theta_{OptimumTil}=\tan^{-1}\left[\frac{\left(n_2^2-n_{eff(\mu)}^2\right)^{1/2}}{n_{eff(\nu)}-n_{eff(\mu)}}\right]$
Where _Grating _Starts	Choose where along the z-axis the grating is written	Varies

Table 5-2: Important outputs from the Tilted LPG MMI simulation

Outputs	**Description**
β_ν	Propagation Constant for each mode
v_p	Phase Velocity for each mode
$n_{eff\nu}$	Effective index that each mode sees
$1/\gamma_{c\nu}$ $1/\gamma_{a\nu}$	Penetration Depths
Total Number of Modes	Ranges from 1...N
W_{eff}	Effective Width
Calculation of Optimum Tilt Angle	Calculated from Equation 4-19 in Chapter 4
Grating length and where grating ends in z axis	Dependent on where the grating starts, angle and number of periods
Graph: Magnitude of E-field of each mode at the start of the waveguide	Graph of the coupling between the input Gaussian and the excitation of the existing modes – to confirm Symmetric of Paired interference

Graph: Mode coupling	This graphs the change in E-field amplitude of each mode over the course of the grating
Graph: Input E-field versus Output E-field after perturbation	This graphs the input Gaussian and then output image, which the designer hopes to be an advantageous splitter
Graph: Full contour plot	This graphs the power distribution in the x-z plane of the waveguide, one can see the change in the power distribution compared to a normal MMI splitter without perturbation

5.3.2 Designs

A full description of all designs can be found in the Appendix I. However, three of the designs are discussed here. Design #1 is that of a 1 x 2 splitter measuring 30 μm in width and 3150μm in length. The image depicted in Figure 5-5 is a depiction of the actual power distribution inside the MMI waveguide. The next figure, Figure 5-6, shows the results of designing a tilted long period grating to couple mode #1 to mode #10 and therefore transfers power between the two. More specifically, this grating has a period of 173.1μm along the z axis, has 12 periods, is placed at z = 0 and has a tilt angle of 88.00°. Figure 5-7 depicts the input Gaussian image versus the output image of the 1 x 2 splitter after propagation through the wide MMI section. As one can see there is 1 Gaussian in and 2 Gaussians out. One must design proper output waveguides in order to capture this optical power to fabricate useful splitters. Figure 5-8 depicts the same Gaussian input, but now shows the output image after propagation through the tilted long period grating perturbation. As one can see, no longer is the output image a 1 x 2 splitter. Instead there is a peak at the center of the waveguide, so it changes the 1 x 2 splitter into a through waveguide without splitting, albeit with a loss of power.

The second design is a 1 x 5 splitter measuring 45 μm in width by 5900μm in length. Again, Figure 5-9 is a depiction of the power distribution in this normal MMI without perturbation. Figure 5-10 depicts the power distribution with a perturbation. Figure 5-11 shows the one input Gaussian and the five equal power outputs at the far end of the MMI. Figure 5-12 depicts the MMI waveguide with the tilted long period grating perturbation. Note that instead of a 1 x 5 splitter there is now a peak at the center of the waveguide, so it changes the 1 x 5 splitter into a through waveguide without splitting, again, with a loss of power. The tilted long period grating is designed to couple mode #5 to mode #13 and therefore transfers power between the two. More specifically this grating has a period of 272.2μm along the z axis, has 10 periods, is placed at z = 0 and has a tilt angle of 88.54°.

The third design is a 1 x 3 splitter measuring 45 μm in width by 3325μm in length. Details of both the MMI power distribution and the Gaussian input versus output images are depicted in Figures 6-13 through 6-16. The tilted long period grating is designed to couple mode #3 to mode #15 and therefore transfers power between the two. More specifically this grating has a period of 181.43μm along the z axis, has 10 periods, is placed at z = 0 and has a tilt angle of 88.10°.

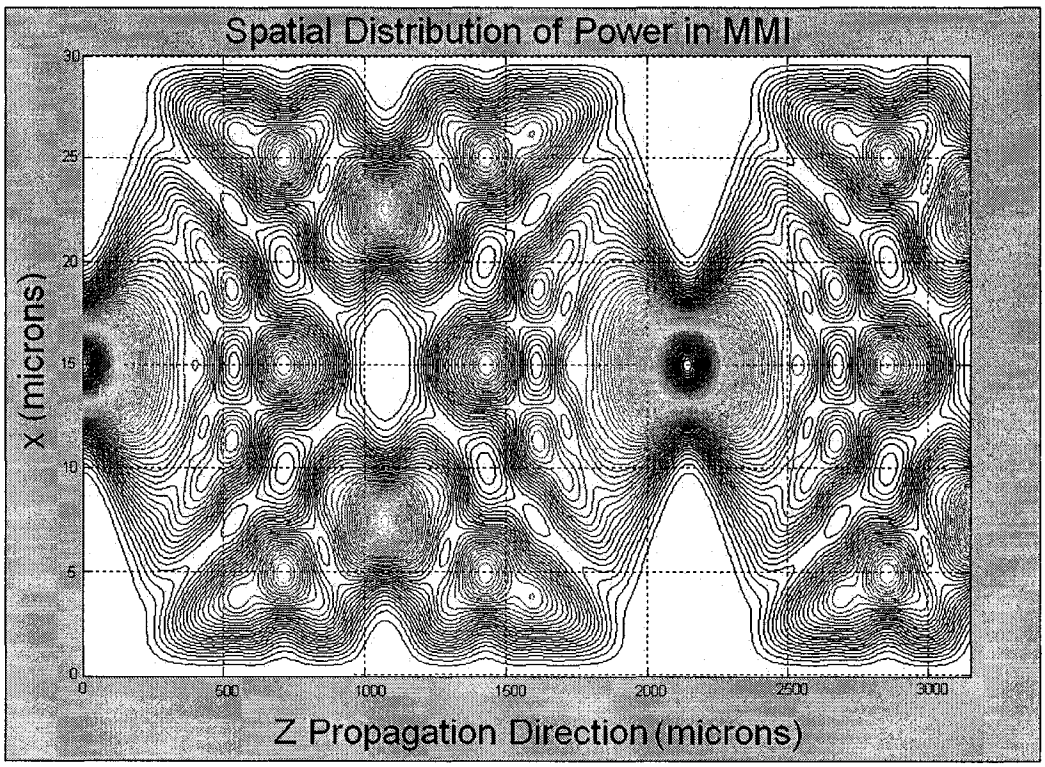

Figure 5-5: Design1 - MMI Image of a 1x2 splitter measuring 30 μm Width x 3150μm Length

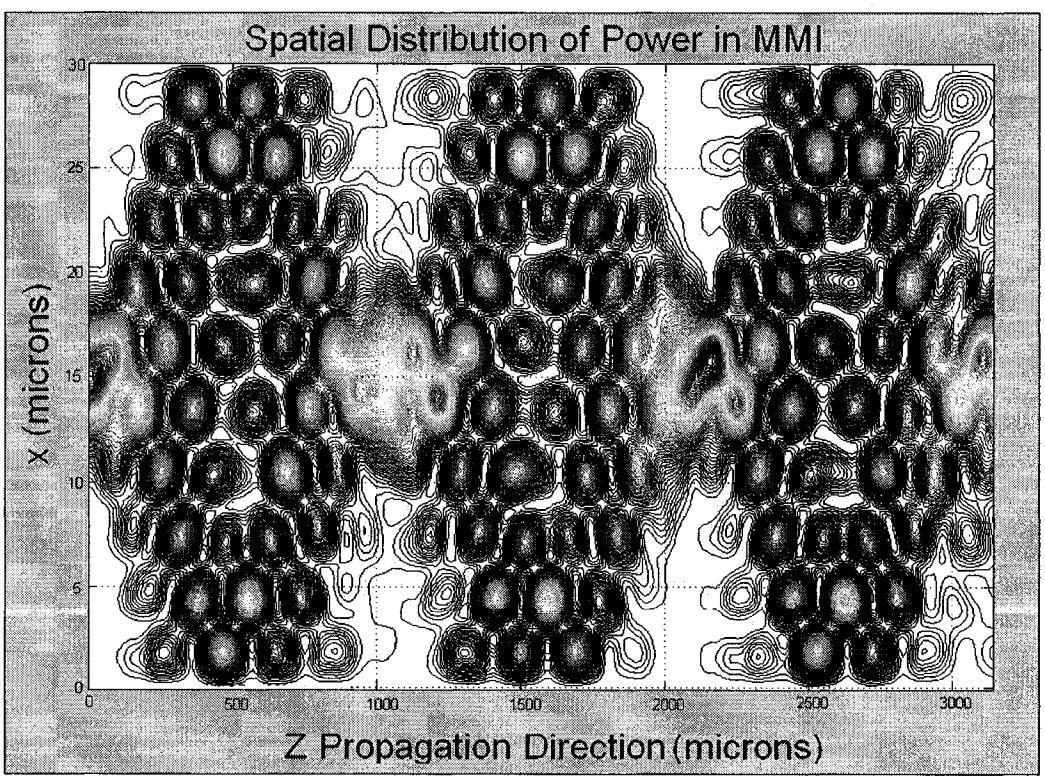

Figure 5-6: Design1 - Result of coupling mode #1 and mode #10 using a Tilted LPG over 12 periods

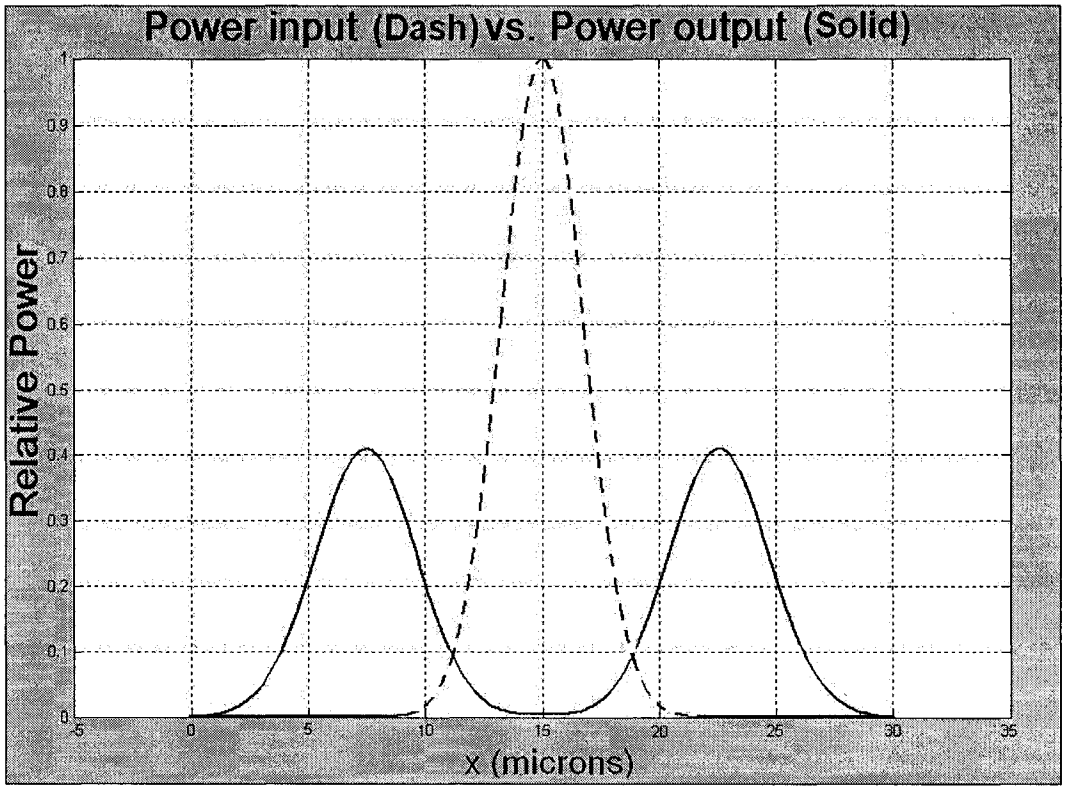

Figure 5-7: Design1 - Input Gaussian image versus MMI output image of a 1x2 splitter measuring 30 μm Width x 3150μm Length

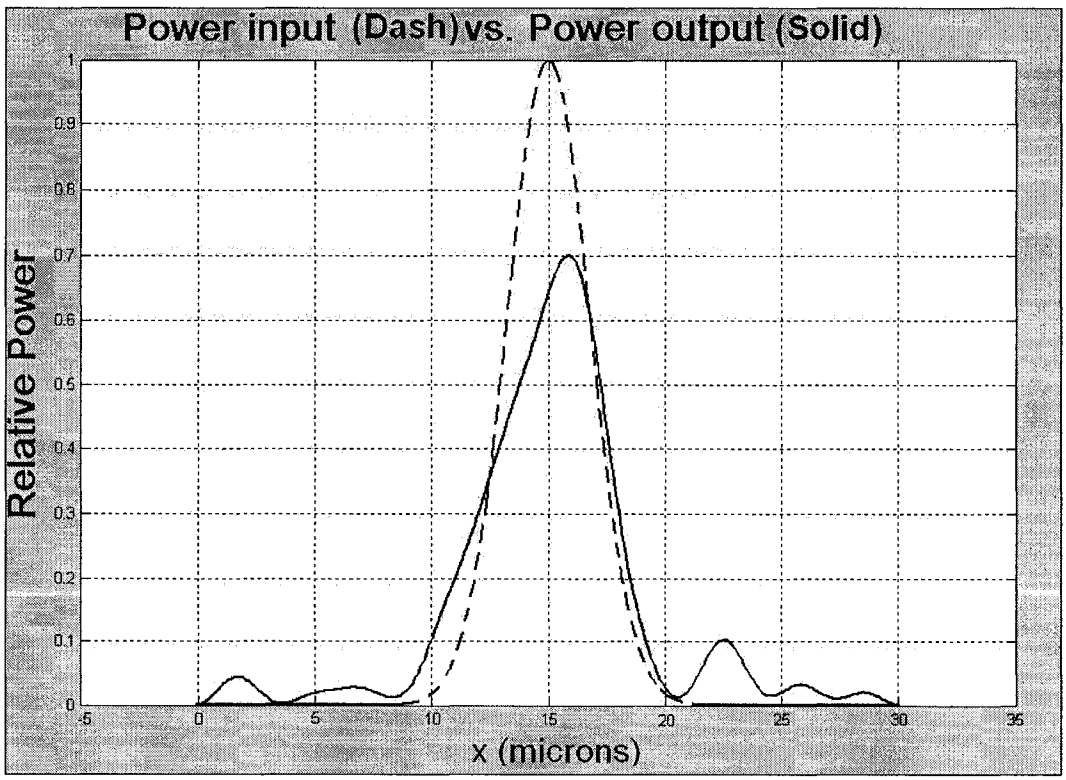

Figure 5-8: Design1 - Input Gaussian image versus MMI output image result using a Tilted LPG to couple mode #1 and mode #10 over 12 periods

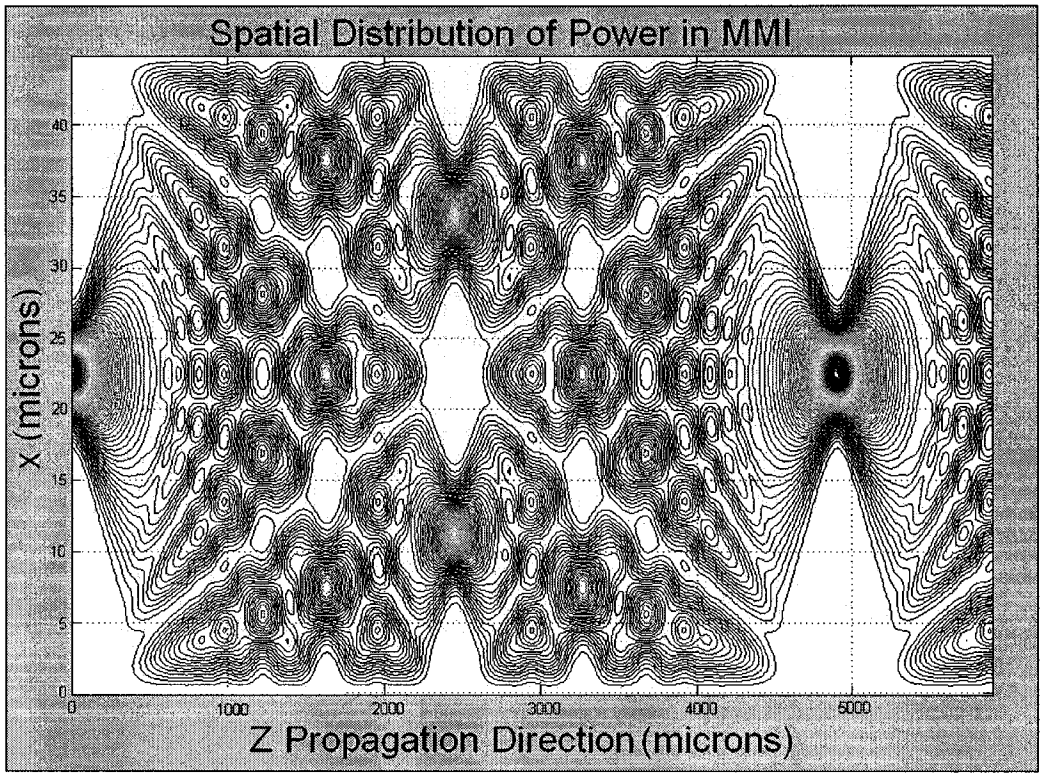

Figure 5-9: Design2 - MMI Image of a 1x5 splitter measuring 45 μm Width x 5900μm Length

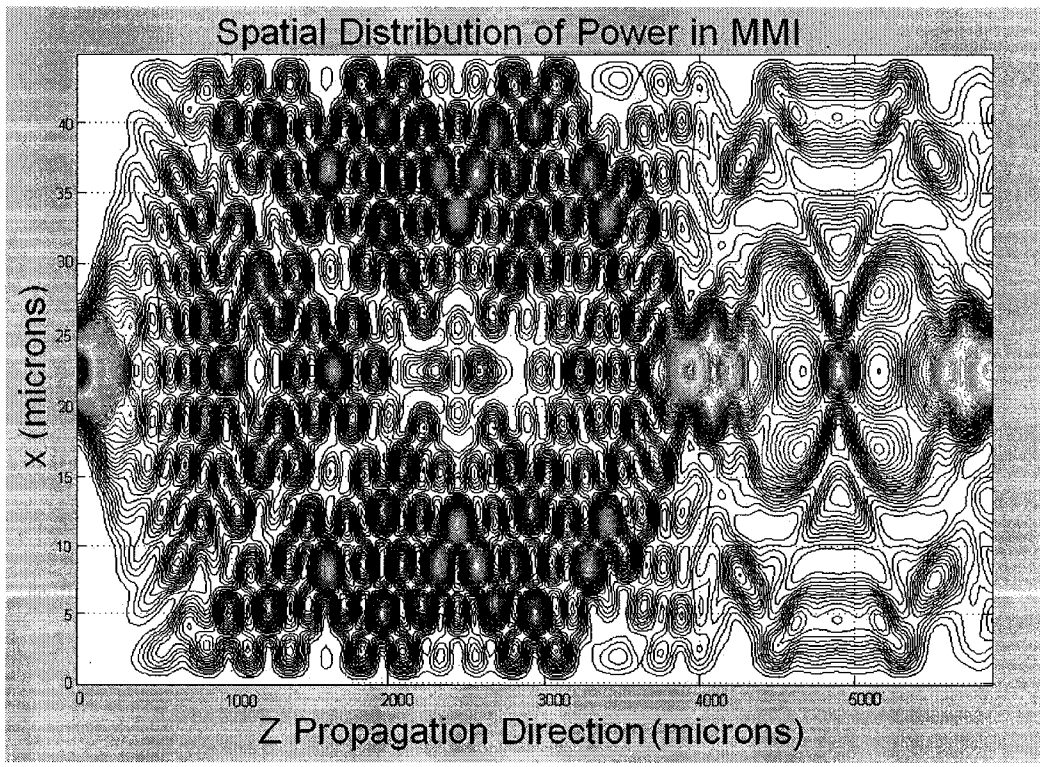

Figure 5-10: Design2 - Result of coupling mode #5 and mode #13 using a Tilted LPG over 10 periods

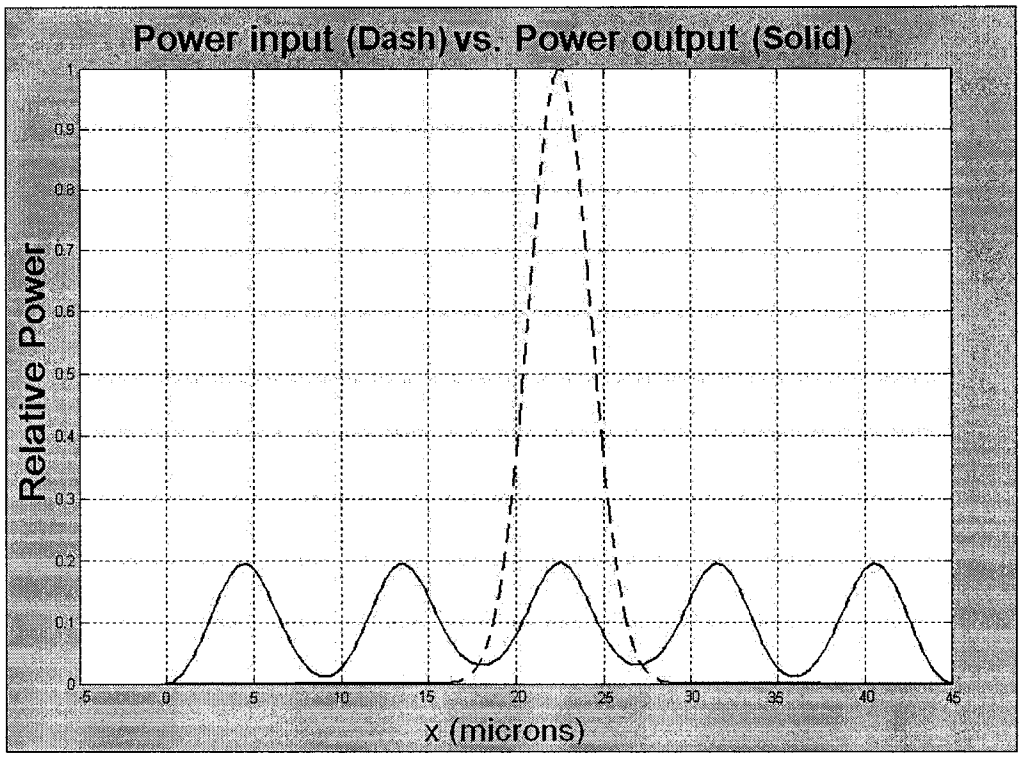

Figure 5-11: Design2 - Input Gaussian image versus MMI output image of a 1x5 splitter measuring 45 μm Width x 5900μm Length

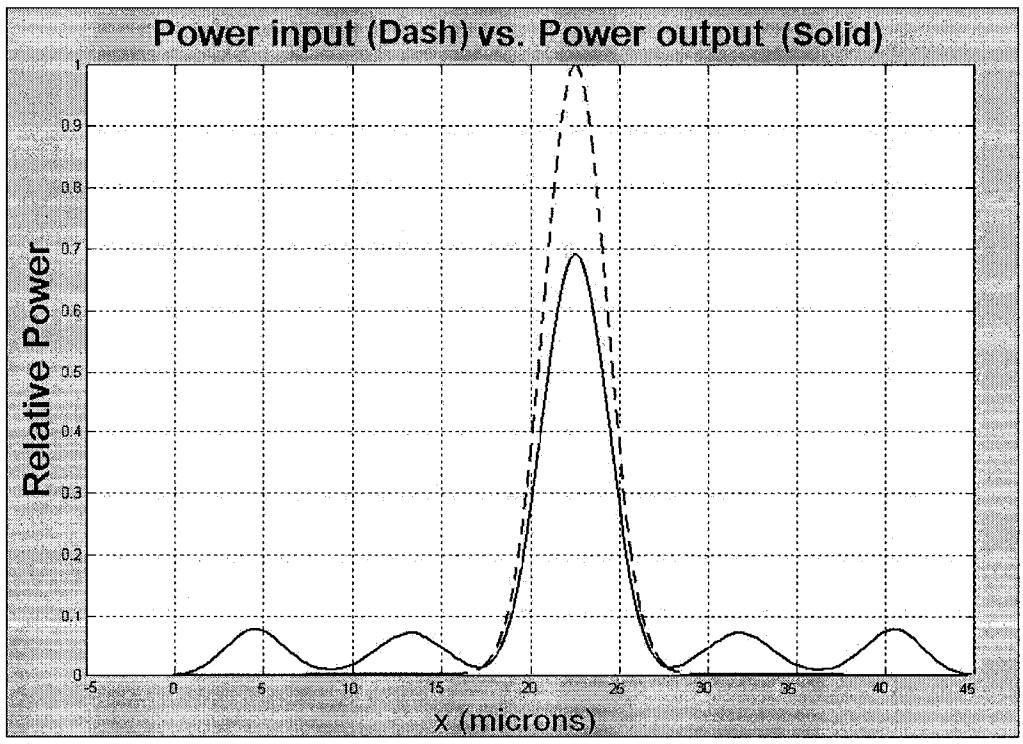

Figure 5-12: Design2 - Input Gaussian image versus MMI output image result using a Tilted LPG to couple mode #5 and mode #13 over 10 periods

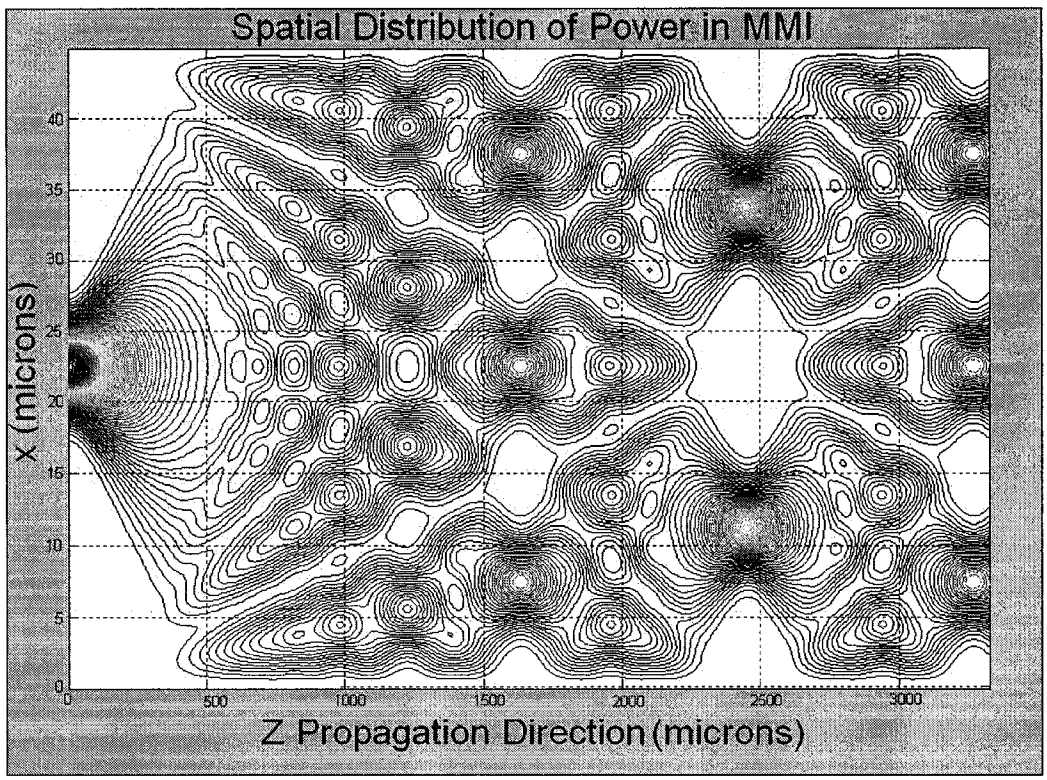

Figure 5-13: Design3 - MMI Image of a 1x3 splitter measuring 45 μm Width x 3325μm Length

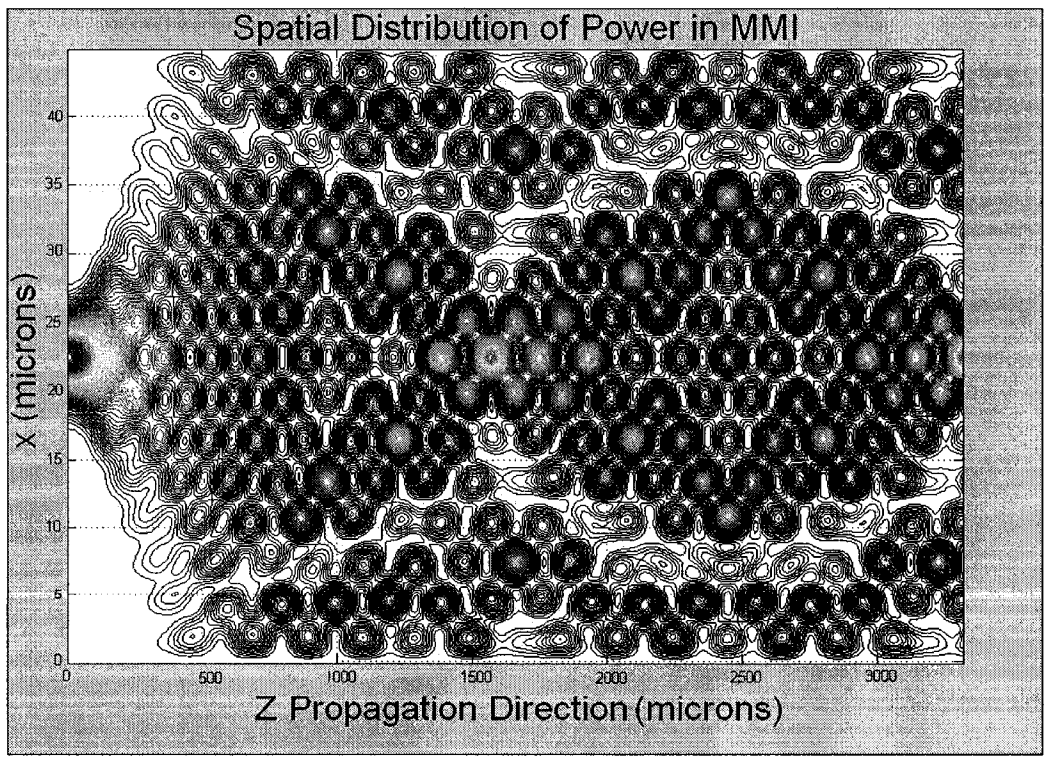

Figure 5-14: Design3 - Result of coupling mode #3 and mode #15 using a Tilted LPG over 10 periods

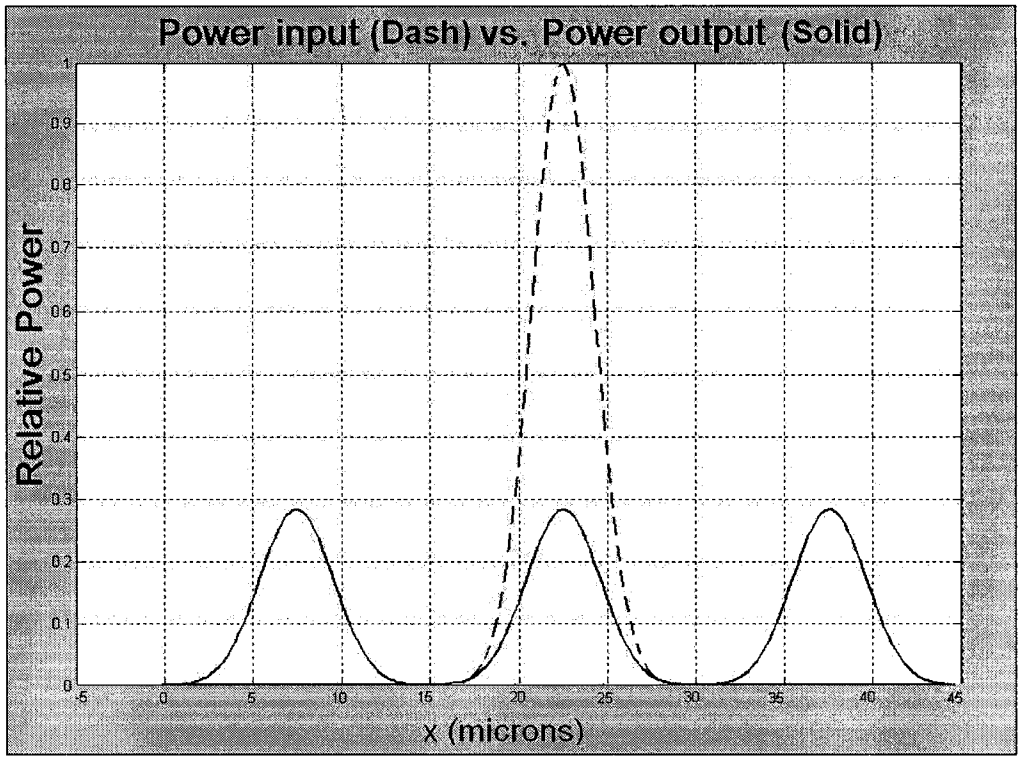

Figure 5-15: Design3 - Input Gaussian image versus MMI output image of a 1x3 splitter measuring 45 μm Width x 3325μm Length

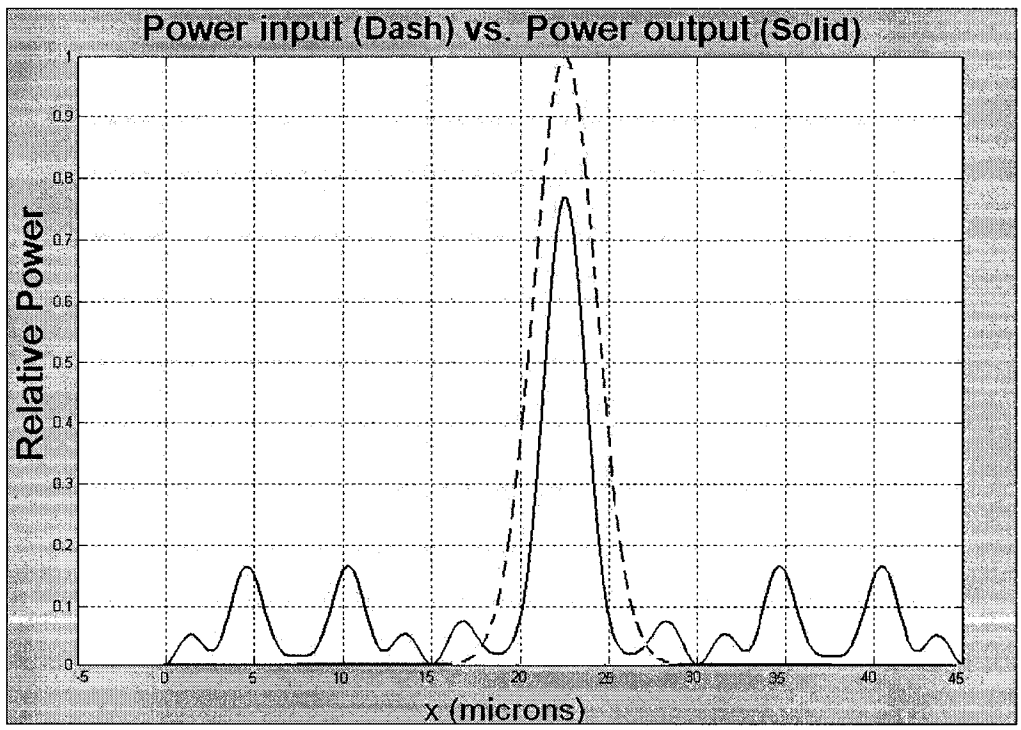

Figure 5-16: Design3 - Input Gaussian image versus MMI output image result using a Tilted LPG to couple mode #3 and mode #15 over 10 periods

As one can see from Figures 5-5 through 5-16, the tilted long period gratings cannot tailor the output images perfectly and there is always a loss of power that will be radiated out of the waveguide. Despite this loss of power the strength of this concept has finally been shown. Certainly there are uses for dynamic splitters, which can change a natural 1 x 2 splitter into a 1 x 1 through waveguide and likewise for a 1x5 splitter and a 1 x 3 splitter depicted in Designs 1-3 above.

5.3.3 Power Loss

Depending on the application, significant power losses through an integrated optical device can render it useless. Therefore, it is important to be able to estimate power losses during the design phase of the device. The total losses through an MMI device include coupling losses due to mode mismatch losses. This is due to modal mismatch between the MMI image and the output waveguides. Losses also include those seen in all waveguides, such as power loss due to absorption, scattering, and reflection losses at coupler interfaces.

For an MMI without perturbations, as independent orthogonal modes propagate along an MMI section, they interfere and self images are produced. For perfect designs these output self images are very similar in spatial characteristic as the original input signal. However, if output waveguides are not designed exactly at the maxima for the image, power will be lost due to the spreading out of the pattern. This phenomenon can be viewed by looking at the MMI examples in the previous section. Figure 5-7 depicts an MMI without perturbation for a well designed 1 x 2 splitter. This splitter, however, is not designed at the optimum z-length for a perfect 1x2 splitter. One can immediately notice that the peak power is not at 0.5 (normalized) as an ideal 1x2 splitter should be. The image has been spread out. If the output waveguide was designed with the same dimensions as the input waveguide, power will be lost. Figure 5-8 depicts an input into the MMI versus the output. One can see that the output is skewed to the right. If one designed the input waveguide of the same dimension and placed it in the middle of the MMI waveguide, power would be lost due to this spatial mismatch.

Since MMI devices typically function as splitters, coupling the output of the MMI to output waveguides is of critical importance. The coupling efficiency is calculated from an overlap integral of the field pattern of the output and the waveguide mode that can exist in the output waveguides [53]. The coupling efficiency can be given by [53]

$$\eta_{cm} = \frac{\left[\int A(x)B^*(x)dx\right]^2}{\int A(x)A^*(x)dx \int B(x)B^*(x)dx} \qquad (5\text{-}7)$$

where $A(x)$ is the amplitude distribution of the output MMI image and $B(x)$ is the amplitude distribution of the output waveguide mode.

For the three device design examples discussed in the previous section, the input waveguide to the MMI section carried a Gaussian input. Since multimode imaging is based on self-imaging effects, that is the field pattern of the input is repeated throughout the MMI waveguide, one can also model the field pattern of the MMI output as a Gaussian

$$f(x) = \exp\left[-\frac{1}{2}\left(\frac{x-x_0}{\sigma_x}\right)^2\right]. \qquad \text{(2-23 -Repeated)}$$

As a numerical example, the output of the 1x2 splitter in Figure 5-7 can be modeled as a Gaussian with a FWHM equal to 3.6 microns. The model of the output waveguide is equal to the input Gaussian characteristics, with a FWHM equal to 3 microns.

$$\eta_{cm} = \frac{\left[\int_w \exp\left[-\frac{1}{2}\left(\frac{x}{3.6e-6}\right)^2\right]\exp\left[-\frac{1}{2}\left(\frac{x}{3.0e-6}\right)^2\right]dx\right]^2}{\int_w \exp\left[-\frac{1}{2}\left(\frac{x}{3.6e-6}\right)^2\right]\exp\left[-\frac{1}{2}\left(\frac{x}{3.6e-6}\right)^2\right]dx \int_w \exp\left[-\frac{1}{2}\left(\frac{x}{3.0e-6}\right)^2\right]\exp\left[-\frac{1}{2}\left(\frac{x}{3.0e-6}\right)^2\right]dx}$$

$=.9983$

This means that 99.83% of the power contained in the output Gaussian at the end of the MMI section couples into the output waveguide.

For a strict analysis of the coupling coefficient, all modes should be analyzed separately. One can do another overlap integral between each mode at the end of the MMI, represented by a complex number, and the ideal Gaussian in the output waveguide. The electric fields, with a phase, in the output waveguide would then have to be summed, squared and integrated in order to attain the power inside. This power can be compared to the normalized input power at the z=0, the start of the MMI, and a power efficiency can be calculated.

The power maxima at the output of the MMI are not the only concern in optical systems. Unintended output power coupled to output waveguides may cause problems depending on system design. This can be illustrated by looking at Figures 5-11 and 5-12 for example #3 in the previous section.

In Figure 5-11, the output of a designed 1x5 splitter is compared to the input Gaussian. Figure 5-12 shows the output in the 'switched' state, whereby the dynamic grating is now on, a 1x1 splitter is accomplished. The 1x1 splitter has power loss, as one can see, the output field has a smaller amplitude. This power is lost in the sidelobes. These sidelobes themselves can cause problems. Since the waveguide

will be designed with 5 output waveguides, but only one of them is used in the 'switched' state, power will continue to be coupled out of the waveguide into the four unused waveguides. For example, the power coupled to the unused waveguides can result in noise accumulation in an optical telecommunications system.

5.4 Chapter 5 Summary

In this chapter, design considerations, variables and methodology were discussed. In order to simulate designs using Matlab, Runge-Kutta iterations are used to solve the coupled mode equations, which are simultaneous differential equations. A subset of designs was shown and from these, one can see the effect of tilted long period gratings on the multimode imaging. For instance, the tilted long period grating can change a natural 1x2 splitter into a 1x1 through splitter (Design 1), a natural 1x5 splitter into a 1x1 through splitter (Design 2) or a natural 1x3 splitter into a 1x1 through splitter (Design 3). Further designs are shown in Appendix I. Also discussed were power loss considerations. Depending on the application, power loss as a result of the application of a dynamic LPG may be a critically important variable.

[6] Ideas for Fabricating Dynamic Gratings

6.1 Introduction

In order to confirm the theory and simulations contained within this thesis, one must construct integrated optical devices. Simplistically, this confirmation can be accomplished by creating two MMI devices of known material and dimension; one with a long period tilted grating and one without. By coupling a laser to such a device one will be able to view the difference in imaging, and compare it to the simulation. This, however, is merely comparing two static devices. The power of writing a long period tilted grating on an MMI device lies in the ability to induce a refractive index change dynamically. Within this context, there are multiple ways to change the refractive index of a material, and thus dynamically change the power distribution out of the device. Such technologies are, but are not limited to, thermo-optic gratings, electro-optic gratings and liquid crystal gratings. These technologies will be briefly described here in order to illustrate to the reader that the theory discussed in this thesis has practical and forward-thinking uses.

6.2 Fabrication of Two Static Polymer Devices

The easiest way to compare MMI imaging with and without the effect of a long period grating is to construct two static devices, one as a simple MMI and one with an LPG written on it. A comparison of the two devices lets one see what the application of a dynamic grating could achieve. These static integrated optical devices are easiest to manufacture using polymer as a waveguide material.

Integrated optical devices using polymers are driven by the need for low cost, high yield, easy to manufacture devices. Such devices are used in the telecommunications industry for such devices as splitters, couplers, routers, filters and switches for existing telecommunications systems and new systems such as fibre-to-the-home (FTTH) [39]. Other useful properties of optical polymers, as opposed to semiconductor or glass waveguides, are its low optical losses, thermal stability, physical stability, low scattering losses and low polarization-dependent losses [39]. Polymers also have excellent thermo-optic or electro-optic properties making them suitable for high-speed electro-optic modulators or low power consumption thermo-optic devices [40]. Additionally, these polymer systems can have low absorption in the wavelength range of 400nm-1600nm, which covers the critical telecommunication windows. Furthermore, since these polymers are synthetic they may be tailored to have a refractive index over a broad range from 1.3-1.6. In essence, polymers can be tailored to meet the needs of a wide range of specific applications.

One such polymer, known as SU-8, is a cross-linkable negative tone epoxy photoresist. SU-8 also has exceptional thermal stability for temperatures below 200°C [42], is biocompatible, water impermeable, mechanically durable and chemically

resistance [41]. Furthermore, it can be used as a waveguide material due to its transparency, low loss, and smooth sidewalls after fabrication.

In order to use SU-8 as a waveguide material, cross-linking must occur. In this case, cross-linking occurs by which the reactants are transformed from a low molecular weight material into a highly cross-linked network. This is initiated by absorption of ultraviolet (UV) light generating a strong acid for cross-linking by means of a post-exposure thermal bake [49]. SU-8 is available in a number of formulations dependent on desired thickness. Since one wishes to have one mode confined in the y-axis, a thin layer is desired. As one can see from Figure 6-1, out of all the formulations of SU-8, formulation SU-8 2002 can spin down to the thinnest film thickness, roughly 3 microns. Once the device is completely fabricated, one would like to efficiently couple the SU-8 device to an optical system. For example, the input and output waveguides could couple to single mode fibres with a 9 micron diameter core. In this case, designing the SU-8 film thickness for the most efficient power coupling to the single mode fibre is desired to prevent unwanted power loss.

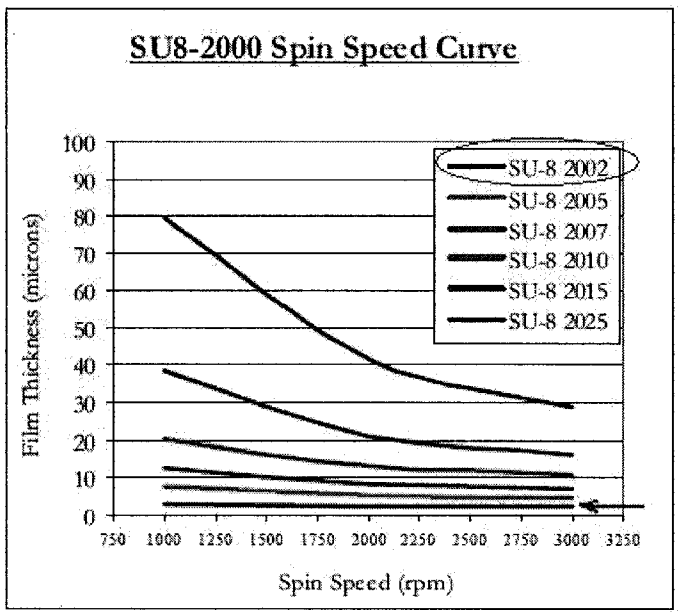

Figure 6-1: Spin speed vs. Thickness curves for selected SU-8 2000 resists [49]

To create a standard multimode splitter, without a grating, one must follow the basic fabrication steps in Figure 6-2. OMNICOAT is spun onto a cleaned wafer. OMNICOAT is used to promote adhesion between the wafer and the SU-8 and is manufactured by Microchem [70]. SU-8 2002 is then spun onto the wafer using a spin speed of 1000rpm to attain a thickness of approximately 3 microns, from Figure 6-1. The wafer is then exposed to a UV lamp through the waveguide grating mask. The UV light in the exposed area initiates a strong acid for the cross-linking to occur [49]. The SU-8 is then developed with an SU-8 developer. Since SU-8 is a negative photoresist, the exposed portion of the SU-8 stays and the unexposed portions are rinsed away. The structures left over are the multimode interference waveguides.

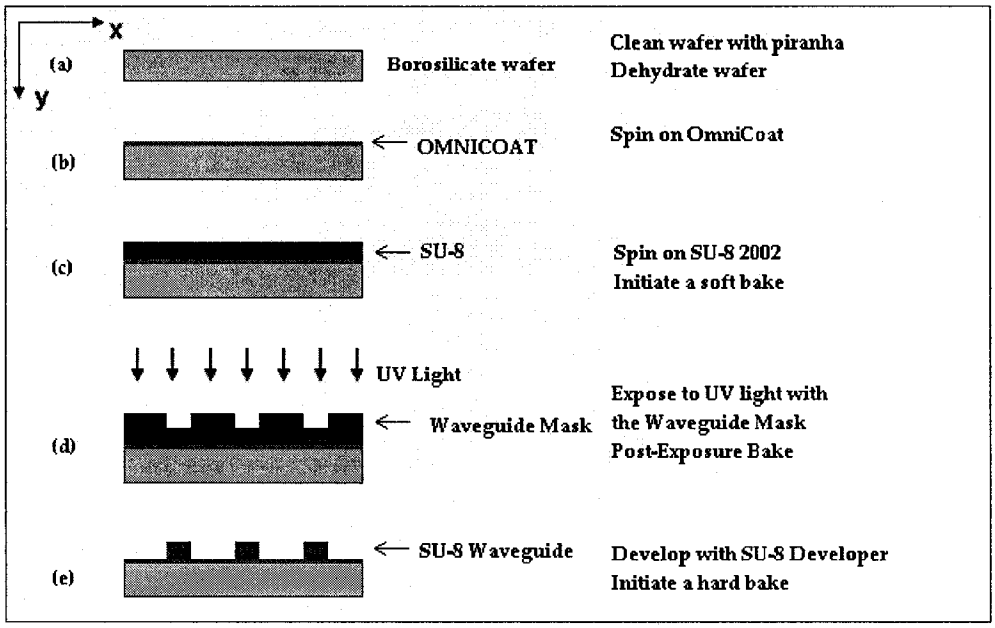

Figure 6-2: Creation of SU-8 MMI waveguides

After the SU-8 waveguides have been fabricated (Figure 6-2), a surface relief grating can be added by following the steps depicted in Figure 6-3. One can then have a multimode interference device with a tilted long period grating structure physically written on the surface.

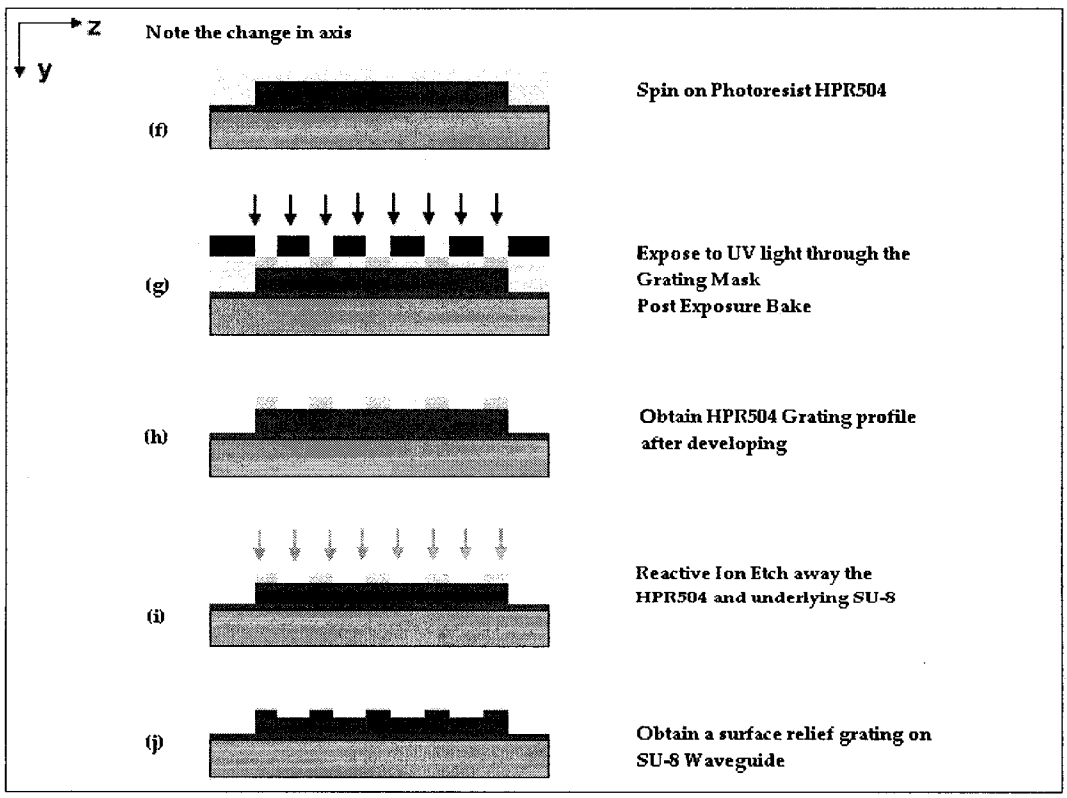

Figure 6-3: Creation of surface relief gratings on SU-8 waveguides

The first step to create a surface relief grating is depicted in Figure 6-3, which is to spin a different type of negative photoresist such as HPR504. The HPR504 layer is exposed to UV light through the grating mask. This grating mask is specifically designed to lay over the existing SU-8 waveguide and gratings are written at a specific location in the z-axis. The HPR504 photoresist is then developed using a developer. Again, the UV exposed regions of the HPR504 will stay and the rest will rinse away. This is not the final structure however, even though one has a HPR504 grating on top of an SU-8 waveguide. One must use a reactive ion etch (RIE) in order to write the gratings onto the SU-8 for a single homogenous waveguide. The RIE process uses gases O_2 and SF_6 in order to etch away both the HPR504 protective layer and the uncovered SU-8 under-layer. The two static waveguides are now complete. One need only test the unperturbed MMI versus the MMI with a surface relief grating by coupling the same laser to each and view the output images.

The surface relief grating is equivalent to perturbing the background refractive index. One would like to quantify this Δn for realistic waveguides. A surface corrugation is depicted in Figure 6-4.

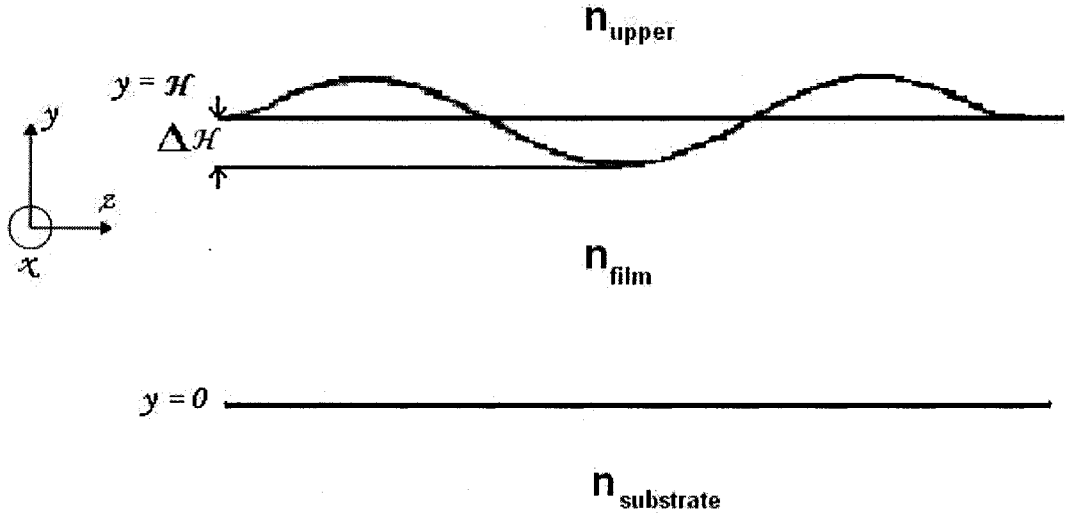

Figure 6-4: Surface relief grating

The perturbation in the effective refractive index due to the surface corrugation can be estimated as [63]

$$\Delta n_{eff} = \Delta H \frac{n_{film}^2 - n_{eff}^2}{n_{eff} H_{eff}}. \qquad (6\text{-}1)$$

For example, if $n_{filmSU-8}$=1.591, $n_{UpperAir}$=1.000, $n_{substrateBoroSilicate}$=1.476 @ 650nm light, H=3 microns, and the estimate for effective height from 2-18 (modified for height)is H_{eff}=3.3 microns, and from Equation 2-7:

$n_{eff} = \sqrt{n_{film}^2 - \frac{(\pi / H_{eff})^2}{(2\pi/\lambda)^2}} = 1.587$; then the estimation for the change in refractive index for a change of height of 20% such that ΔH =0.6 microns,

$$\Delta n_{eff} = \Delta H \frac{n_{film}^2 - n_{eff}^2}{n_{eff} H_{eff}} = (0.6e-6)\frac{1.591^2 - 1.587^2}{(1.587)(3.3e-6)} = 0.00145 .$$

6.3 Mechanisms for Dynamic Gratings

6.3.1 Introduction

Section 6.2 described one way to fabricate two structures, an unperturbed MMI, and one with a perturbation in the form of a surface relief grating. By examining these two devices, one can view the effect of the perturbation on the multimode image. However, ideally one would like to fabricate devices in order to switch the grating on and off in order to take advantage of the multimode image change. Technologies that can accomplish this are thermo-optic gratings, electro-optic gratings and liquid crystal gratings. Section 6.3, here, is devoted to discussing these technologies.

6.3.2 Thermo-optic Gratings

The operation of thermo-optic devices is based on the thermo-optic effect, which can be used to induce a dynamic grating. It consists of the variation of the refractive index of the material due to the temperature variation of the material itself. Different materials have different thermo-optic index perturbation coefficients. This adds another variable when choosing the material system. Heaters can be formed using thin-film metals, which can be heated up using external electronics. These heaters can be placed periodically on top of the multimode interference section in order to create a dynamic grating. The speed in which the grating can be turned on/off depends on how fast one can heat the material [26]. The speed is slow compared to such technologies as electro-optic devices, and the switching power is relatively high in order to heat the material. Nonetheless, it is an attractive way to induce a refractive index change due to simplicity – all dielectric materials are affected by the thermo-optic effect.

The thermo-optic effect changes the refractive index of the material, therefore it is fitting to recall the coupling coefficient stated in Equation 3-20,

$$\kappa_{\nu\mu} = \iint_{Weff} \Delta\varepsilon(x,y,z) \mathrm{E}_{\mu}(x,y) \mathrm{E}_{\nu}^{*}(x,y) dxdy \qquad \text{(Equation 3-20 –repeated)}$$

where $\Delta\varepsilon(x,y,z)$ is the permittivity perturbation. The permittivity perturbation is related to the change in refractive index by Equation 4-4: $\Delta\varepsilon(x,y,z) \approx 2\varepsilon_0 n(x,y,z)\Delta n(x,y,z)$. Since one is dealing with a tilted grating in the x-z plane, one must find an expression for $\Delta n(x,z)$ with respect to the temperature change distribution induced by the heater and represented by $\Delta T(x,z)$ [26].

The value of the thermo-optic coefficient is $\frac{dn}{d\mathrm{T}}$=-1.87e-4/°C for SU-8 over the range 20°C - 70°C (Figure 6-6). For example, in order to have Δn=0.0187, a temperature change of about 100°C would meet the requirements. For SU-8, the change in refractive index versus temperature is depicted in Figure 6-5 [40].

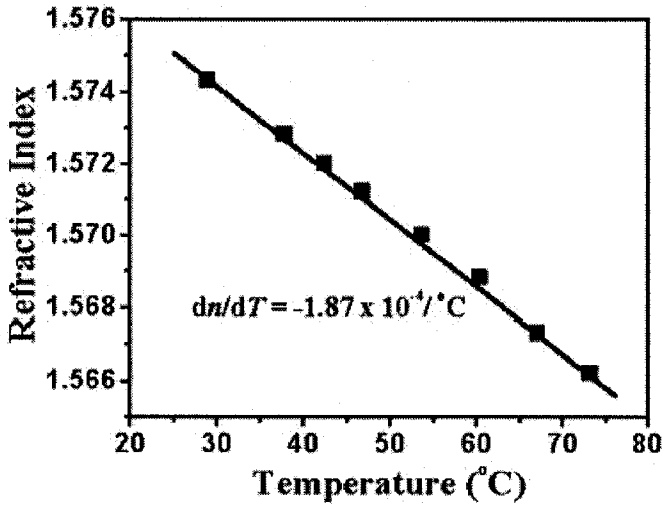

Figure 6-5: Variations in the refractive index of SU-8 as a function of temperature [40]

A mere calculation of $\frac{dn}{d\mathrm{T}}$ is not enough. In order to quantify the effect of $\Delta T(x,y,z)$ on $\Delta n(x,y,z)$, one must solve the heat equation for the structure depicted in Figure 6-6 and 6-7. One must also take into account the boundary condition set by the dimensions of the MMI device. The power generation rate per area of the heater, the thermal conductivity of the waveguide material, and the convection heat transfer coefficient of the air and material must also be taken into account. For an example of such a calculation, see Reference 26. One can then calculate the analytic expression for both the change in refractive index and the coupling coefficient with respect to the temperature-change distribution.

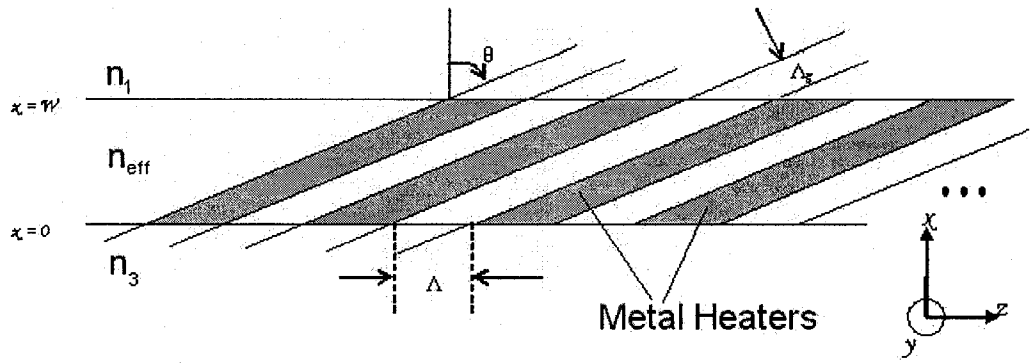

Figure 6-6: Heater placement to utilize the thermo-optic effect: x-y plane

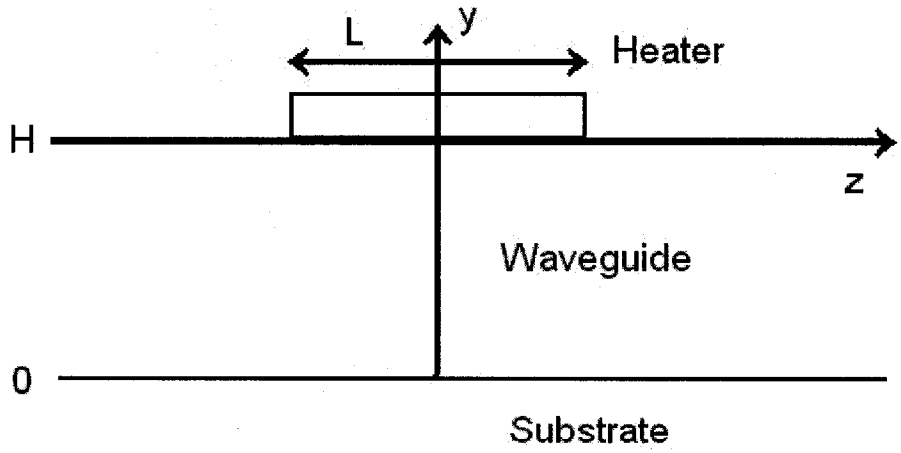

Figure 6-7: Heater placement to utilize the thermo-optic effect: y-z plane

6.3.3 Electro-optic Gratings

Certain materials will change their properties when subjected to an electric field. From the optical point of view, the refractive index n will change for an anisotropic (orientation dependent) electro-optic material. One must fabricate electrodes on an electro-optic waveguide material. An example of how an electro-optic controllable tilted grating can be induced is shown in Figure 6-8. Here electrodes are placed on both sides of the waveguide to achieve good penetration of the electric field into the waveguide. This device was fabricated and simulated in Reference 27.

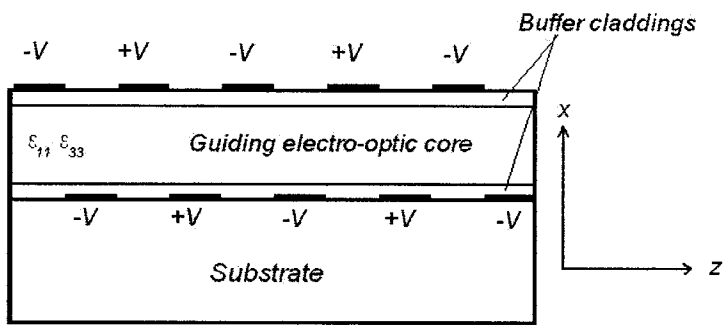

Figure 6-8: Cross-sectional view of a waveguide electro-optic grating

The change of the refractive index due to an electric field can be expressed simplistically as follows [59]

$$n(E) = n - \frac{1}{2} rn^3 \vec{E} - sn^3 \vec{E}^2 + \ldots \quad (6\text{-}2)$$

where n is the refractive index without any electric field present. Here 'r' is called the Pockels Coefficient and 's' is called the Kerr Coefficient. The dependence of the refractive index on the electric field takes on two forms, which are material dependent [59]:

1. The Kerr Effect; in centrosymmetric materials (i.e. gases, liquids, some crystals), the second term of Equation 6-2, must be zero and the equation becomes $n(E) \approx n - sn^3 \vec{E}^2$.

2. The Pockels effect, whereby the third term in Equation 6-2 is negligible and the equation becomes $n(E) \approx n - \frac{1}{2} rn^3 \vec{E}$. (6-3)

Typically integrated optics make use of the Pockels effect and thus will be discussed here in more detail.

For the Pockels effect, n(E) changes linearly with E, thus this effect is also called the linear electro-optic effect. The change in refractive index for this effect is

$$\Delta n = -\frac{1}{2} rn^3 \vec{E}. \quad (6\text{-}4)$$

If a material exhibits the Pockels effect, the change in the effective refractive index $n_{eff}(E)$ can be used to create tilted long period gratings. The phase shift is equal to the change in the propagation constant multiplied by length of the electric field, essentially the length of the electrode, the formula is

$$\phi = \Delta\beta L \quad \text{or}$$

$$\phi = \frac{2\pi L n(E)}{\lambda_0} \quad (6\text{-}5)$$

where λ_0 is the freespace wavelength of the laser going though the MMI device.

Substituting in Equation 6-3 for the Pockels effect and knowing that the Pockels effect operates when a voltage is applied across two faces of the waveguide at a distance d (E=V/d), the phase change can be written as [127]

$$\phi = \frac{2\pi nL}{\lambda_0} - \pi \frac{Lrn^3 V}{d\lambda_0}. \quad (6\text{-}6)$$

The above analysis of the electro-optic effect is a simplistic view of the change of refractive index in an unspecified material due to an electric field. When one takes

the material to be a crystal, the analysis of the electro-optical effect on a lightwave becomes significantly more complex. The reason for this is that there are three inter-related elements in the physical analysis that are occurring: the direction of wave propagation k, the direction of the applied electric field E and finally the orientation of the crystal. Furthermore, the analysis is complicated by the polarization of the lightwave: TM or TE polarization relative to the crystal axes.

In an anisotropic crystal, if an electric field is applied in any arbitrary direction say in the x-direction, the change in the refractive index, n, is not just along that x-direction but can be along the x, y and z axes. The direction and magnitude of the changes in the refractive index depends on the direction and magnitude of the applied electric field and on the material properties of the crystal. Material properties are represented by r, the Pockels coefficients. The Pockels coefficients is now represented as a tensor. New refractive indices, due to an electric field, are calculated by the index ellipsoid method [59].

The following depicts a simple example using lithium niobate as a material, which is a uniaxial negative crystal. The term uniaxial negative means that the principal refractive indices are as follows: $n_1 = n_2 = n_{Ordinary}$ and $n_3 = n_{Extraordinary}$ with $n_e < n_o$. The electro-optic coefficient r_{33} can be utilized when the guided mode is polarized along the optical axis of the crystal and an electric field also lies along the optical axis, z [27] [118]. This axis is defined by the crystal cut depicted in Figure 6-9. Literature classifies cuts of crystals by x-cut, y-cut or z-cut which means the crystals are cut with the major surface of the wafer perpendicular to the x, y, or z crystallographic axis.

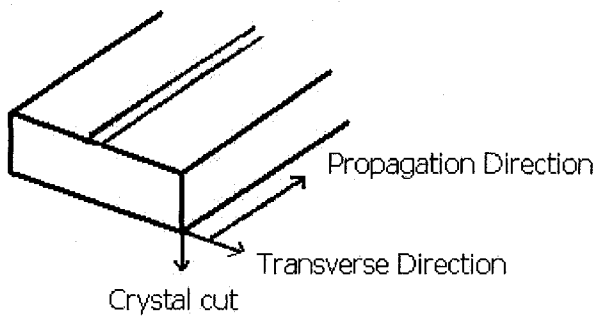

Figure 6-9: Crystal Cut Definition for crystals

The maximum electro-optic coefficient for lithium niobate is the r_{33} coefficient equal to $r_{33} = 30.8 pm/V$. In the case outlined in Reference 27, TM modes are utilized, with a z-cut waveguide and an electric field along this axis. The refractive-index perturbation is thus $\Delta n \approx \frac{1}{2} r_{33} n_e^3 \vec{E}_y$. The refractive index for lithium niobate for this extraordinary axis is 2.21 at 1550 nm of light. For an applied voltage of 5V over the height of the waveguide, 3 microns, the calculation is:

$$\Delta n \approx \frac{1}{2}(30.8e-12)(2.21)\text{^}3\left(\frac{5}{3e-6}\right) = 0.000277$$

For a more precise calculation of the electric field, the electro-optic effect, and the induced refractive index modulation, for the device depicted in Figure 6-7, an electro-static problem solver simulation is used [27].

6.3.4 Liquid Crystal Gratings

The liquid crystal state is a distinct phase of matter that exists between a crystalline solid state and the isotropic liquid state of a crystal [28]. There are many types of materials that exhibit a liquid crystal state, yet common to all are a rod-like molecular structure that has a preferred orientation; the molecules point along a common axis called the 'director'. This preferred orientation leads to the anisotropy of the material and this anisotropy causes the liquid crystal to be birefringent.

Birefringence means the liquid crystal has two indices of refraction, one for each polarization state. If the crystal is randomly oriented, a ray of light will decompose into two rays, the ordinary and extraordinary ray – the same as the lithium niobate crystal discussed in the previous section [59]. In a uniaxial crystal, there is one direction such that any light in that direction 'sees' the same refractive index, regardless of its state of polarization. This is because the electric field of the light propagating along this axis is always perpendicular to this axis. This direction is called the optic axis and for uniaxial liquid crystals is the same as the director. Thus, light polarized parallel to the director has a different index of refraction than light polarized perpendicular to the director.

Therefore, if one can change the direction of alignment of the liquid crystal, relative to the input light, one can also change the refractive index the lightwave sees. This is precisely what one seeks to accomplish when switching a grating on and off. If the waveguide is in the 'grating off' state, the light only 'sees' the refractive index of the liquid crystal in its natural state. However, if the waveguide is in the 'grating on' state, the liquid crystals can be periodically upset away from the preferred orientation and the light will 'see' a second index of refraction. This can be accomplished with an external electric field as liquid crystal molecules also exhibit strong dipoles that make them susceptible to manipulation. The liquid crystal molecules can thus be poled.

One can control the modulation of the index of the liquid crystal by changing the applied voltage as the effective refractive index is dependent according to the poling direction. The difficulty in fabrication arises because one is dealing with a liquid phase material, and the molecules move. The liquid crystal must be confined in a container. A method outlined in *Holographic PDLC for Photonic Applications* by Domash et. al, proposes to use a composite electro-optic medium, which is a mixture of polymer and nematic liquid crystal [125]. A nematic liquid crystal phase is characterized by molecules that have no positional order but tend to point along the director. The composite electro-optic medium used is called a holographic polymer-dispersed liquid crystal (H-PDLC). It can be polymerized by a laser, causing

a diffusion process whereby liquid crystal micro-droplets form preferentially in the unexposed area. After this process, alternating areas of solid polymer and liquid crystal micro-droplets form having different indices of refraction [126]. The area exposed to the laser has only polymer, and the area not exposed to the laser has a mixture of polymer and liquid crystal as depicted in Figure 6-10.

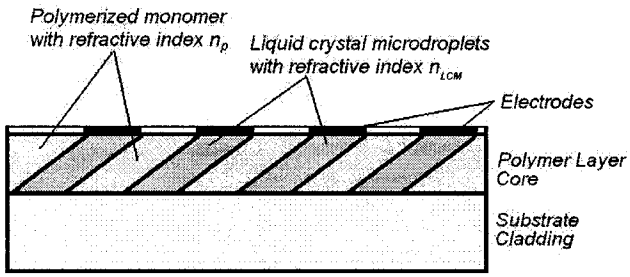

Figure 6-10: Method to create long period gratings using liquid crystals

In order to take advantage of the electro-optic properties of the liquid crystals, electrodes must be deposited on the waveguide where the liquid crystals reside. An applied voltage orients the liquid crystal molecular optical axis such that its refractive index now matches that of the polymer refractive index [126]. The period structure 'vanishes' with the application of this electric field due to index matching of the surrounding polymer as depicted in Figure 6-11. Light is transmitted through the transparent material and the multimode interference section will see no grating at all. If no voltage is applied to the electrodes, then the full influence of the long period tilted grating is in effect as depicted in Figure 6-12. Core modes will couple with core modes and the MMI imaging will change.

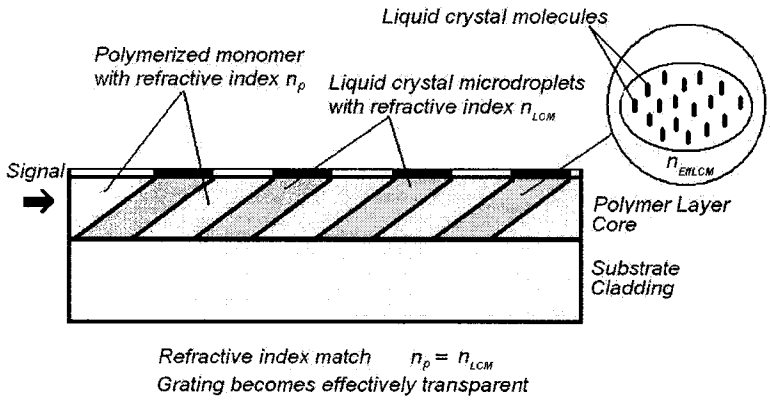

Figure 6-11: Electric field applied: liquid crystals rearrange to index match the surrounding polymer

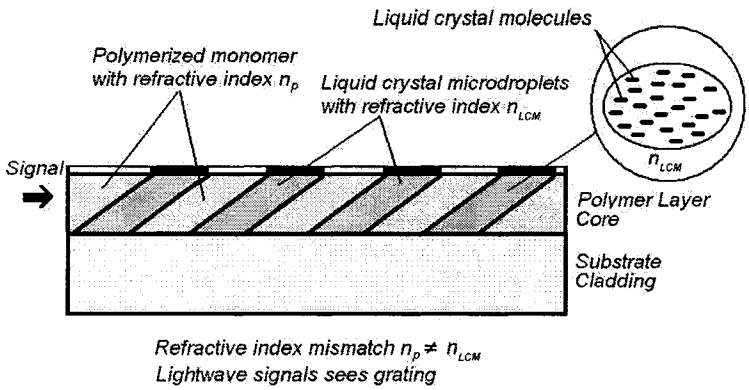

Figure 6-12: Electric field is turned off: refractive index perturbation exists

A numerical example of the change of refractive index is accomplished using methods similar to that of electro-optic crystals in the previous section. The refractive index changes dependent on the applied voltage and subsequent reorientation, by angle, of the liquid crystal molecules. This change is several orders of magnitude higher than conventional dielectrics such as Lithium Niobate and index modulations can be as large as large as 0.05 [128].

6.3 Chapter 6 Summary

This chapter discussed possible technologies one can use in order to create a dynamic long period grating. In order to see the effect of a tilted long period grating on the multimode images, one can construct two static devices, one with a tilted long period grating and one without and compare the outputs. Dynamic gratings can conceivably be accomplished using many technologies. This chapter specifically discussed thermo-optic gratings, electro-optic gratings and liquid crystal gratings. Each technology has its own considerations and advantages. The thermo-optic grating and liquid crystal grating can produce a higher change in refractive index; however they are slower devices than an electro-optic grating. Depending on the application, it may be more practical to induce a dynamic grating using one technology rather than another.

[7] Summary and Future Endeavors

7.1 Summary of Project

The goal of this thesis is to analyze the effect of perturbations on guided mode coupling and subsequent multimode imaging within a planar multimode waveguide. The perturbations are tilted long period gratings, as the perturbation needs an x (or y) dependency in order to efficiently couple core modes to other core modes. The perturbations can both change the phase and power of modes. The combined effect of the two changes the MMI images. A background on MMIs and General Coupled Mode equations was presented in Chapter 2 and Chapter 3 respectively. Coupled mode theory specific to tilted long period gratings was developed in Chapter 4. A simulation using MATLAB was based on these coupled mode equations and designs were considered in Chapter 5. Finally, ideas for fabricating the tilted long period gratings dynamically was presented in Chapter 6.

The concept of coupling core modes to other core modes via a long period grating within an MMI device is a novel concept not seen before, to the knowledge of the writer. This was an exploratory project asking the question whether it was realistic and possible to change the multimode images in this manner. Once an analytic analysis was performed, it was found that theoretically it is possible to couple core modes to core modes and change multimode images. Furthermore, with the help of a simulation, this change can be quantified.

Using MATLAB, designs were produced in order to illustrate 'image switching', assuming a dynamic grating that can be switched on and off. Chapter 5 results illustrated a 1x2 optical splitter can change into a 1x1 splitter by inducing a change of refractive index to couple modes #1 to #10. The second design showed a 1x5 splitter can change into a 1x1 splitter by inducing coupling between mode #5 and #13. The third design shows a 1x3 splitter can change into a 1x1 splitter by inducing coupling between mode #3 and #15. Chapter 5 also discusses the power loss that can occur. MMIs devices without perturbations can be designed without a loss of significant power. Once a perturbation is in place, however, significant power loss is observed due the multimode image changes.

The simulation depends on a large number of input variables, as does the actual perturbed MMI device. A change in any one of these variables can drastically change the MMI imaging and concurrently the vitally important output image. The input lightwave has variables: wavelength of laser light, polarization and full-width half maximum of the input beam which is dependent on the width of the input waveguide. The input waveguide has variables: width and placement along the x-axis. As discussed in sections 2.3.2 and 2.3.3 the placement of the input waveguides along the x-axis dictates the excitation of core modes and also dictates the type of interference: general interference, paired interference or symmetric interference. For the entire waveguide, a key variable is the material system and thickness of the core. The

simulation must know the wavelength dependent refractive index of the substrate, core and cladding as well as the thicknesses of each. The simulation assumes the substrate and cladding go to infinity in the y-dimension from the point of view of guided modes. It is important to try to design the waveguide such that only one mode is allowed to propagate in the y-dimension. Therefore, the core is designed to be thin, on the order of a few microns, which is possible using thin film methods. Using the restriction of one mode in the y-dimension allows easy calculation of the effective refractive index from the x-z plane point of view. The width of the MMI section in the x-dimension dictates how many modes can exist in the waveguide given the material system. The placement and dimensions of the output waveguides is critical in order to couple light out of the MMI device for use in other parts of the optical system. As discussed in section 5.3.4, depending on the application, the high power loss through the devices may render the device useless.

So far, variables discussed are for all MMI devices – with or without perturbations. There are of course a large number of perturbation variables as well. For the long period tilted grating, the variables are the tilt angle, periodicity of the gratings along the z-axis and number of periods. If one wishes to induce the perturbations by a surface relief grating, the variables are the grating topology – is the surface relief grating imprinted as a sine wave or square wave in the y-z axis? Other variables are the depth of the corrugation and resulting change of refractive index. Furthermore, where one places the gratings along the z-axis can change the MMI imaging as shown in Figure 5-4. Is there a portion of the unperturbed waveguide before or after the tilted grating section? All these variables give the designer a wide range of parameters for design, which is good, as one could conceive a near infinite number of waveguides. However, as a drawback, a high number of variables may lead to difficulties with fabrication, characterization and troubleshooting.

7.2 Future Endeavors

The variables discussed in section 7.1 were all considered within the MATLAB program used as a basis for simulation. However, these are not the only variables that can affect the MMI images. For example, modeled in this thesis was one grating per MMI section. Of course, one could have multiple gratings on the MMI section, sequentially placed. Theoretically, one could design the first grating to couple mode #1 to mode #12, then a second grating to couple mode #3 to mode #15 or any combination, then view the MMI imaging. Also for example, the perturbation does not need to be modeled as a tilted long period grating. This is a simplistic structure and allows for the analytical examination of the coupled mode equations. The perturbation can be of an unusual shape. The definition of the change of refractive index can be x,y, and z dependent. An example of an unusually shaped perturbation is to induce a refractive index perturbation by a surface corrugation, and then induce another permanent perturbation by photoinducing a refractive index change on top of this using a photo-sensitive material system. As a future endeavor, the investigation of multiple gratings, and unusual perturbation structures should be explored for an MMI device. In addition, perturbations such as gratings or unusual structures can be

induced using technologies such as thermo-optic, electro-optic or liquid crystal materials as discussed in Chapter 6 or other technologies such as systematic strained waveguides or even microfluidic gratings. Such technologies should be investigated and fabricated.

The simulation written in MATLAB uses the coupled mode equations and Runge-Kutta iterations in order to solve the change of phase and power of the individual modes. It can output a plot of the multimode imaging, and the power output at the end of the MMI section. What the program lacks, however, is the ability to predict where the MMI images form in the z-length dimension or the x-dimension. In section 2.3.2 and 2.3.3, for an MMI without perturbations, the z-length for a given number of images can be predicted. Also, in section 2.3.4, where these images appear in the x-axis can also be predicted. However, once a perturbation is in place, one can no longer analytically predict where these images form. The designs were thus carried out in a logical guess and test methodology. Since there are a large number of variables, the designer has a wealth of parameters to change in order to fine-tune the images. However, if it is mathematically impossible to predict the image placements in the x-z axis, as a future endeavor, one can write a program that has the ability to optimize designs. This optimization can be in the form of a genetic algorithm. In a perfect program, one would design an MMI of a certain dimension and material system. Then one would input the desired spatial distribution of power at the output of the waveguide and the program would output the perturbation characteristics such as the change of refractive index, dependent on x, y and z, and the placement of perturbation.

The technology of 'image switching' by virtue of a dynamic perturbation can have a number of uses. One of these uses can be in the realm of telecommunications. Splitters are used in telecommunication systems in order to route wavelengths to different optical devices or system nodes. If one can switch the MMI device such that it goes from say a 1x1 splitter to a 1x2 splitter, one can use it for protection switching. Wavelength protection in telecommunication systems is used to provide redundancy in case of failure such as a severed fibre between nodes. In this case, fast switching is desired. Therefore, one might seek to investigate electro-optic dynamic gratings as the materials used are known for responding to an applied electric field with a quick change in refractive index. Another application can be tunable splitters. The majority of MMI splitters cannot change their splitting characteristics. By virtue of a switchable refractive index perturbation, theoretically, one may be able to change a splitter from a 1x2 splitter to a 1x3 or a 1x4 splitter. This could reduce capital costs for an organization.

In conclusion, it has been theoretically shown that multimode images can change by virtue of core mode to core mode coupling using dynamic long period gratings. It has also been shown that this change can be quantized by simulating devices in MATLAB. These devices have a multitude of variables the designer can change. Such devices can also have a number of uses, for example in telecommunications. Since these MMI devices are naturally all optical devices, they concur with the industry move towards all optical systems.

References

[1] V. Rastogi and K. S. Chiang, "Long-period gratings in planar optical waveguides," *Appl. Opt.,* vol. 41, no. 30, pp. 6351-6355, Oct. 2002.

[2] K. S. Chiang, K. P. Lor, Q. Liu, C. K. Chow, Y. M. Chu and H.P. Chan, "Long-Period Waveguide Gratings," *Jpn. J. Appl. Phys.*, vol. 43, no. 8B, pp. 5690-5696, 2004.

[3] K. S. Lee, "Mode coupling in tilted planar waveguide gratings," *Appl. Opt.*, vol. 39, no. 33, pp. 6144-6149, Nov. 2000.

[4] A. M. Vengsarkar, P. J. Lemaire, J. B. Judkins, V. Bhatia, T. Erdogan and J. E. Sipe, "Long-Period Fiber Gratings as Band-Rejection Filters," *J. Lightwave Technol.*, vol. 14, no. 1, pp. 58-65, Jan. 1996.

[5] M. Bachmann, P. A. Besse, and H. Melchior, "General self-imaging properties in N x N multimode interference couplers including phase relations," *Appl. Opt.*, vol. 33, no. 18, pp. 3905-3911, Jun. 1994.

[6] K. S. Lee and T. Erdogan, "Fiber mode coupling in transmissive and reflective tilted fiber gratings," *Appl. Opt.*, vol. 39, no. 9, 1394-1404, Mar. 2000.

[7] L. B. Soldano and E. C. M Pennings, "Optical Multi-Mode Interference Devices Based on Self-Imaging: Principles and Applications," *J. Lightwave Technol.*, vol. 13, no. 4, pp. 615-627, Apr. 1995.

[8] L. B. Soldano, F. B. Veerman, M. K. Smit, B. H. Verbeek, A. H. Dubost, and E. C. M. Pennings, "Planar Monomode Optical Couplers Based on Interference Effects," *J. Lightwave Technol.*, vol. 10, no. 12, pp. 1843-1850, Dec. 1992.

[9] M. Bachmann, P. A. Besse, and H. Melchior, "Overlapping-image multimode interference couplers with a reduced number of self-images for uniform and nonuniform power splitting," *Appl. Opt.*, vol. 34, no. 30, pp. 6898-6910, 1995.

[10] T. Erdogan, "Fiber Grating Spectra," *J. Lightwave Technol.*, vol. 15, no. 8, pp. 1277-1294, Aug. 1997.

[11] E. C. M Pennings, R. van Roijen, M. J. N. van Stralen, P. J. de Waard, R. G. M. P. Koumans, and B. H. Verbeek, "Reflection properties of multimode interference devices," *IEEE Photon. Technol. Lett.*, vol. 6, no. 6, pp. 715-718, Jun. 1994.

[12] P. A. Besse, M. Bachmann, H. Melchior, L. B Soldano, and M. K. Smit, "Optical Bandwidth and Fabrication Tolerances of Multimode Interference Couplers," *J. Lightwave Technol.*, vol. 12, no. 6, pp. 1004-1009, Jun. 1994.

[13] A. Yariv, "Coupled-Mode Theory for Guided Wave Optics," *IEEE J. Quantum Electron.*, vol. QE-9, no. 9, pp. 919-933, Sep. 1973.

[14] K. O. Hill and G. Meltz, "Fiber Bragg Grating Technology Fundamentals and Overview," *J. Lightwave Technol.*, vol. 15, no. 8, pp. 1263-1276, Aug. 1997.

[15] T. Erdogan and J. E. Sipe, "Tilted fiber phase gratings," *J. Opt. Soc. Am. A.*, vol. 13, no. 2, pp. 296-313, Feb. 1996.

[16] E. Peral and A. Yariv, "Supermodes of Grating-Coupled Multimode Waveguides and Application to Mode Conversion Between Copropagating Modes Mediated by Backward Bragg Scattering," *J. Lightwave Technol.*, vol. 17, no. 5, pp. 942-947, May 1999.

[17] J. B. D. Soole, M. R. Amersfoort, H. P. LeBlanc, N. C. Andreadakis, A. Rajhel, C. Caneau, R. Bhat, M. A. Koza, C. Youtsey, and I. Adesida, "Use of Multimode Interference Couplers to Broaden the Passband of Wavelength-Dispersive Integrated WDM Filters," *IEEE Photon. Technol. Lett.*, vol. 8, no. 10, pp. 1340-1342, Oct. 1996.

[18] A. L. Y. Low, Y. S. Yong, A. H. You, S. F. Chien, and C. F. Teo, "A Five-Order Mode Converter for Multimode Waveguide," *IEEE Photon. Technol. Lett.*, vol. 16, no. 7, pp. 1673-1675, Jul. 2004.

[19] W-C. Chuang, C-Y. Chang, C-C. Lai, and K-C. Lin, "Integrated-Optics Multimode-Interference Wavelength Division Multiplexer for Optical Communication," *Fiber and Integrated Optics*, vol. 18, pp. 93-104, 1999.

[20] J. Leuthold, "Multimode Interference Couplers with Tunable Power Splitting Ratios," *J. Lightwave Technol.*, vol. 19, no. 5, pp. 700-707, May 2001.

[21] J. Leuthold, J. Eckner, E. Gamper, P. A. Besse, and H. Melchior, "Multimode Interference Couplers for the Conversion and Combining of Zero- and First-Order Modes," *J. Lightwave Technol.*, vol. 16, no. 7, pp. 1228-1239, Jul. 1998.

[22] S-L. Tsao, H-C. Guo, and C-W. Tsai, "A novel 1 x 2 sing-mode 1300/1550 nm wavelength division multiplexer with output facet-tilted MMI waveguide," *Opt. Comm.*, vol. 232, pp. 371-379, 2004.

[23] M. Aslund, L. Poladian, J. Canning and C. Martijn de Sterke, "Add-Drop Multiplexing by Grating-Induced Dispersion in Multimode Interference Device," *IEEE Photon. Technol. Lett.*, vol. 13, no. 9, pp. 969-971, Sep. 2001.

[24] T. Agustsson, "Bragg Grating-Assisted MMI-Coupler for Add-Drop Multiplexing," *J. Lightwave Technol.*, vol. 16, no. 8, pp. 1517-1522, Aug. 1998.

[25] S. Nagai, G. Morishima, H. Inayoshi, and K. Utaka, "Multimode Interference Photonic Switches (MIPS)," *J. Lightwave Tech.*, vol. 20, no.4 , pp. 675-681, Apr. Apr. 2002.

[26] M-S. Kwon and S-Y. Shin, "Tunable Notch Filter Using a Thermooptic Long-Period Grating," *J. Lightwave Technol.*, vol. 22, no. 8, pp. 1968-1975, Aug. 2004.

[27] M. Kulishov, P. Cheben, X. Daxhelet, and S. Delprat, "Electro-optically induced tilted phase gratings in waveguides," J. *Opt. Soc. Am. B.*, vol. 18, no. 4, pp. 457-464, Apr. 2001.

[28] Y. Jeong, B. Yang, B. Lee, H. S. Seo, S. Choi and K. Oh, "Electrically Controllable Long-Period Liquid Crystal Fiber Gratings," *IEEE Photon. Technol. Lett.*, vol. 12, no. 5, pp. 519-521, May 2000.

[29] Y. Yamamoto, T. Kamiya, and H. Yanai, "Improved Coupled Mode Analysis of Corrugated Waveguides and Lasers," *IEEE J. Quantum Electron.*, vol. QE-14, no. 4, pp. 245-258, Apr. 1978.

[30] Y. Zhu, B. M. Lacquet, P. L. Swart, S. J. Spammer, P. Shum, and C. Lu, "Device for concatenation of phase-shifted long-period grating and its application as gain-flattening fiber filter," *Opt. Eng.*, vol. 42, no. 5, pp. 1445-1450, May 2003.

[31] D. B. Stegall and T. Erdogan, "Dispersion control with use of long-period fiber gratings," *J. Opt. Soc. Am. A.*, vol. 17, no. 2, pp. 304-312, Feb. 2000.

[32] H. Jeong and K. Oh, "Theoretical Analysis of Cladding-Mode Waveguide Dispersion and Its Effects on the Spectra of Long-Period Fiber Grating," *J. Lightwave Technol.*, vol. 21, no. 8, pp. 1838-1845, Aug. 2003.

[33] S. W. James and R. P. Tatam, "Optical fibre long-period grating sensors: characteristics and application," *Meas. Sci. Technol.* Vol. 14, pp. R49-R61, 2003.

[34] S. T. Lee, R. D. Kumar, P. S. Kumar, P. Radhakrishnan, C. P. G. Vallabhan, and V. P. N. Nampoori, "Long period gratings in multimode optical fibers: application in chemical sensing," *Opt. Comm.*, vol. 224, pp. 237-241, 2003.

[35] K. W. Gaff, F. Ladouceur and J. D. Love, "Two-wavelength planar add/drop WDM filter employing a three-mode coupling Bragg grating," *Electron. Lett.*, vol. 36, no. 13, pp. 1142-1144, Jun. 2000.

[36] X. Daxhelet and M. Kulishov, "Theory and practice of long-period gratings: when a loss becomes a gain," *Opt. Lett.*, vol. 28, no. 9, pp.686-688, May 2003.

[37] K. S. Lee and T. Erdogan, "Fiber mode conversion with tilted gratings in an optical fiber," *J. Opt. Soc. Am. A.*, vol. 18, no. 5, pp. 1176-1185, May 2001.

[38] T. Erdogan, "Cladding-mode resonance in short- and long-period fiber grating filters," *J. Opt. Soc. Am. A.*, vol. 14, no. 8, pp. 1760-1773, Aug. 1997.

[39] L. Eldada, and L W. Shacklette, "Advances in polymer integrated optics," *IEEE J. Sel. Top. Qun. Elect. Lett.*, vol. 6, no. 1, pp. 54-78, Jan./Feb. 2000.

[40] K. K. Tung, W. H. Wong and E. Y. B. Pun, "Polymeric optical waveguides using direct ultraviolet photolithography process," *Appl. Phys. A.*, 2003.

[41] G. Hong, A. S. Holmes and M. E. Heaton, "SU8 resist plasma etching and its optimization," *DTIP 2003 Mandelieu – La Napoule, France*, pp.268-271, May 2003.

[42] A. Borreman, S. Musa, A. A. M. Kok, M. B. J. Diemeer and A. Driessen, "Fabrication of Polymeric Multimode Waveguides and Devices in SU-8 Photoresist Using Selective Polymerization," *Proc. Symp. IEEE/LEOS Benelux Chapter*, pp. 83-86. 2002.

[43] M. Shaw, D. Nawrocki, R. Hurditch, and D. Johnson, "Improving the process capability of SU-8," MicroChem Corp., Website: https://www.microchem.com/resources/su8_process_capability_paper_1.pdf.

[44] D. W. Johnson, A. Jeffries, D. W. Minsek, and R. J. Hurditch, "Improving the process capability of SU-8, part II," MicroChem Corp., Website: https://www.microchem.com/resources/su8_process_capability_paper_2.pdf.

[45] J. S. Kim, J. W. Kang, and J. J. Kim, "Simple and low cost fabrication of thermally stable polymeric multimode waveguides using a UV-curable epoxy," *Jpn. J. Appl. Phys.*, vol. 42, pp. 1277-1279, 2003.

[46] J-S. Kim, J-W. Kang and J-J. Kim, "Fabrication of multimode polymeric waveguides and micromirrors using UV and X-ray lithography," *SPIE Proc.*, vol. 4991, pp. 398-405, 2003.

[47] L. Pang, W. Nakagawa, and Y. Fainman, "Fabrication of optical structures using Su-8 photoresist and chemically assisted ion beam etching," *Opt. Eng.*, vol. 42, no. 10, pp. 2912-2917, Oct. 2003.

[48] Omnicoat Adhesion Promoter/Release Layer, MicroChem Corp., Website: http://www.microchem.com/products/pdf/OMNICOAT.pdf.

[49] NANO^{TM} SU-8 2002-2025, MicroChem Corp., Website: http://www.microchem.com/products/pdf/SU8_2002-2025.pdf

[50] C.Vassallo, *Optical Waveguide Concepts*, Elsevier, Amsterdam, The Netherlands, 1991.

[51] S. Martellucci and A.N. Chester, *Integrated optics – Physics and Applications*, Plenum Press, New York, 1983.

[52] T. Tamir et al., *Guided Wave Optoelectronics,* Springer-Verlag, Germany, 1990.

[53] R.G. Hunsperger, *Integrated Optics – Theory and Technology,* Springer, Germany, 2002.

[54] K. Chandrasekharan, *Introduction to Analytic Number Theory*, Springer-Verlag, Germany, 1969.

[55] F. T. S. Yu and S. Yin, *Fiber Optic Sensors*, Marcel Dekker Inc., New York, 2002.

[56] S. Kawai, *Handbook of Optical Interconnects*, Taylor & Francis, Florida, 2005.

[57] G. P. Agrawal, *Fiber-Optic Communication Systems 2nd Edition*, John Wiley & Sons Inc., New York, 1997.

[58] M. Ohring, Material *Science of Thin Films 2nd Edition*, Academic Press, San Diego, 2002.

[59] B.E.A Saleh and M.C. Teich, *Fundamental of Photonics*, 1st Edition, New York, John Wiley & Sons, Inc., 1991.

[60] J.D. Rancourt, *Optical Thin Films Users' Handbook*, 1st Edition, New York, Macmillan Publishing Company, 1987.

[61] D. K. Ferry, *Quantum Mechanics*, 2nd Edition, Bristol UK, IOP Publishing Ltd, 2001.

[62] K.M. Sivalingam and S. Subramaniam, *Optical WDM Networks: Principles and Practice*, 1st Edition, Norwell, Massachusetts, Kluwer Academic Publishers, 2000.

[63] R. R. A. Syms and J.R. Cozens, *Optical Guided Waves and Devices*, London, Mcgraw-Hill, 1992.

[64] P. Yeh, *Optical Waves in Layered Media*, New York, John Wiley & Sons, 1998.

[65] A. W. Snyder, *Optical Waveguide Theory*, London, Chapman & Hall, 1983.

[66] F. Sporleder, *Waveguide tapers, transitions and couplers*, London, P. Peregrinus, 1979.

[67] K. Okamoto, *Fundamentals of Optical Waveguides*, San Diego, California, Academic Press, 2000.

[68] C. R. Pollock and M. Lipson, *Integrated Photonics*, Norwell Massachusetts, Kluwer Academic Publishers, 2003.

[69] R. J. Schilling, *Applied numerical methods for engineers using MATLAB and C*, Pacific Grove, California, Thomson-Engineering, 2000.

[70] N. S. Lagali, *The Generalized Mach-Zehnder Interferometer using Multimode Interference Couplers for Optical Communication Networks*, Ph. D. Thesis, 2000.

[71] N. H. Gopaluni, *Pump-Signal combiners for optical amplifier arrays based on multimode interference,* MSc. Thesis, 2003.

[72] N. Xie, *3DMMI For Optical Layer Routing*, MSc. Thesis, 2006

[73] R. DeCorby, *Course content from ECE 685: Photonic Devices for Communication*, 2003.

[74] Q. Liu, K. S. Chiang, and V. Rastogi, "Analysis of Corrugated Long-Period Gratings in Slab Waveguides and Their Polarization Dependence," *J. Lightwave Technol.*, vol. 21, no. 12, 3399-3405, Dec. 2003.

[75] Y. Zhao and J. C. Palais, "Simulation and Characteristics of Long-Period Fiber Bragg Grating Coherence Spectrum," *J. Lightwave Technol.*, vol. 16, no. 4, pp. 554-561, Apr. 1998.

[76] G. W. Chern and L. A. Wang, "Transfer matrix method based on perturbation expansion for periodic and quasi-periodic binary long-period gratings," *J. Opt. Soc. Am. A.*, vol. 16, no. 11, pp. 2675-2689, Nov. 1999.

[77] Y. Jeong and B. Lee, "Nonlinear Property Analysis of Long-Period Fiber Gratings Using Discretized Coupled-Mode Theory," *IEEE J. Quantum Electron.*, vol. 35, no. 9, pp. 1284-1292, Sep. 1999.

[78] M. Florjanczyk and R. Tremblay, "A remark about mode coupling in guided wave optics," *Am. J. Phys.*, vol. 60, no. 5, pp. 462-465, May 1992.

[79] J. E. Sipe, C. Martijn De Sterke, and B. J. Eggleton, "Rigorous derivation of coupled mode equations for short, high-intensity grating-coupled, co-propagating pulses," *Journal of Modern Optics*, vol. 49, no. 9, pp. 1437-1452, 2002.

[80] A. Yariv and M. Nakamura, "Periodic Structures for Integrated Optics," *IEEE J. Quantum Electron.*, vol. QE-13, no. 4, pp. 233-251, Apr. 1977.

[81] B-G. Kim and E. Garmire, "Comparison between the matrix method and the coupled-wave method in the analysis of Bragg reflector structures," *J. Opt. Soc. Am. A.*, vol. 9, no. 1, pp. 132-136, Jan. 1992.

[82] Y. Silberberg and G. I. Stegeman, "Nonlinear coupling of waveguide modes," *Appl. Phys. Lett.*, vol. 50, no. 13, pp. 801-803, Jan. 1987.

[83] S. Trillo, S. Wabnitz and G. I. Stegeman, "Nonlinear Codirectional Guided Wave Mode Conversion in Grating Structures," *J. Lightwave Technol.*, vol. 6, no. 6, pp. 971-976, Jun. 1988.

[84] M-S. Kwon and S-Y. Shin, "Simple and fast numerical analysis of multilayer waveguide modes," *Opt. Comm.*, vol. 233, pp. 119-126, Jan. 2004.

[85] G-W. Chern, L. A. Wang, and C-Y. Lin, "Transfer-matrix approach based on modal analysis for modeling corrugated long-period fiber gratings," *Appl. Opt.*, vol. 40, no. 25, pp. 4476-4486, Sep. 2001.

[86] W-P. Huang, "Coupled-mode theory for optical waveguides: an overview," *J. Opt. Soc. Am. A.*, vol. 11, no. 3, pp. 963-983, 1994.

[87] K. S. Chiang, K. M. Lo, and K. S. Kwok, "Effective Index Method with Built-In Perturbation Correction for Integrated Optical Waveguides," *J. Lightwave Technol.*, vol. 14, no. 2, pp. 223-228, Feb. 1996.

[88] J. M. Heaton and R. M. Jenkins, "General Matrix Theory of Self-Imaging in Multimode Interference (MMI) Couplers," *IEEE Photon. Technol. Lett.*, vol. 11, no. 2, pp. 212-214, Feb. 1999.

[89] www.microchem.com

[90] http://gratings.fo.gpi.ru/index.php?page=11

[91] hyperphysics.phy-astr.gsu.edu/hbase/phyopt/totint.html

[92] www.corning.com

[93] www.lightreading.com

[94] http://www.crc.ca/

[95] www.sabeusphotonics.com/technology/tech_gratings.html

[96] http://www.cranfield.ac.uk/soe/cpoe/cpoebrag3.htm

[97] http://www.mellesgriot.com/products/optics/mp_3_4.htm (borosilicate glass)

[98] http://www.pgo-online.com/intl/katalog/borosilicate_glass_wafers.html (borosilicate glass)

[99] F. Y. M. Chan and K. S. Chiang, "Analysis of apodized phase-shifted long-period fiber gratings," *Opt. Comm.*, vol. 244, pp. 233-243, 2005.

[100] K-W. Chung and S. Yin, "Analysis of widely tunable long-period grating by use of an ultrathin cladding layer and higher-order cladding mode coupling," *Opt. Lett.*, vol. 29, no. 8, pp. 812-813, Apr. 2004.

[101] M-S. Kwon, K-H. Kim, Y-H. Oh, and S-Y. Shin, "Fabrication of an integrated optical filter using a large-core multimode waveguide vertically coupled to a single mode waveguide," *Opt. Exp.*, vol. 11, no. 18, pp. 2211-2216, Sept. 2003.

[102] T. Mizunami, T. V. Djambova, T. Niiho, and S. Gupta, "Bragg Gratings in Multimode and Few-Mode Optical Fibers," *J. Lightwave Technol.*, vol. 18, no. 2, pp. 230-235, Feb. 2000.

[103] H. Kogelnik and C. V. Shank, "Coupled-Wave Theory of Distributed Feedback Lasers," *J. Appl. Phys.*, vol. 43, no. 5, pp. 2327-2355, May 1972.

[104] W-F. Liu, I-M. Liu, L-W. Chung, D-W. Huang, and C. C. Yang, "Acoustic-induced switching of the reflection wavelength in a fiber Bragg grating," *Opt. Lett.*, vol. 25, no. 18, pp. 1319-1321, Sep. 2000.

[105] J. A. Rogers, P. Kuo, A. Ahuja, B. J. Eggleton and R. J. Jackman, "Characteristics of heat flow in optical fiber devices that use integrated thin-film heaters," *Appl. Opt.*, vol. 39., no. 28, pp. 5109-5116, Oct. 2000.

[106] Y. Koyamada, "Analysis of Core-Mode to Radiation-Mode Coupling in Fiber Bragg Gratings with Finite Cladding Radius," *J. Lightwave Technol.*, vol. 18, no. 9, pp. 1220-1225, Sep. 2000.

[107] K. S. Chiang, Y. Liu, M. N. Ng, and S. Li, "Coupling between two parallel long-period fiber gratings," *Electron. Lett.*, vol. 36, no. 16, pp. 1408-1409, Aug. 2000.

[108] H. Furuta, H. Noda, and A. Ihaya, "Novel Optical Waveguide for Integrated Optics," *Appl. Opt.*, vol. 13, no. 2, pp. 322-326, Feb. 1974.

[109] A. Ferreras, F. Rodriguez, E. Gomez-Salas, J. L. de Miguel, and F. Hernandez-Gil, "Useful Formulas for Multimode Interference Power-Splitter/Combiner Design," *IEEE Photon. Technol. Lett.*, vol. 5, no. 10, pp. 1224-1227, Oct. 1993.

[110] M. Rajarajan, B. M. A. Rahman, and K. T. V. Grattan, "A Rigorous Comparison of the Performance of Directional Couplers with Multimode Interference Devices," *J. Lightwave Technol.*, vol. 17, no. 2, pp. 243-248, Feb. 1999.

[111] Z. S. Liu and R. Magnusson, "Concept of Multiorder Multimode Resonant Optical Filters," *IEEE Photon. Technol. Lett.*, vol. 14, no. 8, pp. 1091-1093, Aug. 2002.

[112] F. Bilodeau, K. O. Hill, B. Malo, D. C. Johnson, and I. M. Skinner, "Efficient, Narrowband $LP_{01} \leftrightarrow L_{02}$ Mode Converters Fabricated in Photosensitive Fibre: Spectral Response," *Electron. Lett.*, vol. 27, no. 8, pp. 682-684, Apr. 1991.

[113] K. O. Hill, B. Malo, K. A. Vineberg, F. Bilodeau, D. C. Johnson, and I. Skinner, "Efficient Mode Conversion in Telecommunication Fibre Using Externally Written Gratings," *Electron. Lett.*, vol. 26, no. 16, pp. 1270-1272, Aug. 1990.

[114] P. Munoz, D. Pastor, and J. Capmany, "Analysis and design of arrayed waveguide gratings with MMI couplers," *Opt. Exp.*, vol. 9, no. 7, pp. 328-338, Sep. 2001.

[115] T. Szkopek, V. Pasupathy, J. E. Sipe, and P. W. E. Smith, "Novel Multimode Fiber for Narrow-Band Bragg Gratings," *IEEE J. Select. Topics Quantum Electron.*, vol. 7, no. 3, pp. 425-433, May/Jun. 2001.

[116] S. He, X. Ao, and V. Romanov, "General properties of N x M self-images in a strongly confined rectangular waveguide," *Appl. Opt.*, vol. 42, no. 24, pp. 4855-4859, Aug. 2003.

[117] K. S. Lee and T. Erdogan, "Transmissive Tilted Gratings for LP_{01} – to – LP_{02} Mode Coupling," *IEEE Photon. Technol. Lett.*, vol. 11, no. 10, pp. 1286-1288, Oct. 1999.

[118] M. Kulishov, X. Daxhelet, M. Gaidi and M. Chaker, "Electronically reconfigurable superimposed waveguide long-period gratings," *J. Opt. Soc. Am. A.*, vol. 19, no. 8, pp. 1632-1648, Aug. 2002.

[119] W. Huang and J. Hong, "A Transfer Matrix Approach Based on Local Normal Modes for Coupled Waveguides with Periodic Perturbations," *J. Lightwave Technol.,* vol. 10, no. 10, pp. 1367-1375, Oct. 1992.

[120] R. Hou, Z. Ghassemlooy, A. Hassan, C. Lu, and K. P. Dowker, "Modeling of long-period fibre grating response to refractive index higher than that of cladding," *Meas. Sci. Technol.* Vol. 12, pp. 1-5, 2001.

[121] R. Ulrich and T. Kamiya, "Resolution of self-images in planar optical waveguides, "*J. Opt. Soc. Am.*, vol. 68, no. 5, pp. 583-592, 1978.

[122] F. Wang, J. Yan, L. Chen, X. Jiang, and M. Wang, "Optical Switch Based on Multimode Interference Coupler," *IEEE Photon. Technol. Lett.*, vol. 18, no. 2, pp. 420-423, Jan. 2006.

[123] Micro-etch RIE General Operating Procedure, from the University of Alberta Nanofab website: http://www.nanofab.ualberta.ca/equipment_process.php

[124] S E. Miller "Integrated optics: an introduction,"*Bell Syst. Tech. J.* vol. 48, pp.2059-69, 1969.

[125] L. Domash, G . Crawford, A. Ashmead, R. Smith, M. Popovich, J. Storey "Holographic PDLC for Photonic Applications," *Liquid Crystals IV, Proceedings of SPIE,* vol. 4107, 2000.

[126] A. Ashmead "Electronically switchable Bragg gratings provide versatility," *Lightwave: Passive and Active Components – Special Report.*

[127] A.A. Berezhnoi, "Anisotropy of Electrooptical Interaction in $LiNbO_3$ Crystals," *Optics and Spectroscopy*, vol. 92, no. 3, 2002.

[128] A. Fratalocchi, R. Asquini, G. Assanto, "Integrated electro-optic switch in liquid crystals," *Optics Express*, vol. 13, no. 1, 2005.

Appendix I: Device Designs

All designs were carried out with $\Delta n = 0.02$

Design #1) Originally a 1 x 2 splitter, convert to a through waveguide with loss≈30%.

Effective Refractive Index	MMI Dimensions (Microns)		INPUT WAVEGUIDES (microns)		OUTPUT WAVEGUIDES (microns)		Wavelength nm	Spatial Width microns	Comments
	X	Z	Placement in X	Dimensions X (Width)	Placement in X	Dimensions X (Width)			
1.5312	30	3150	15	3.5	22.5	3.5	650.3	3.5 waveguide width, 2.5 modeled	106 Possible Modes in x dimension
					7.5	3.5			

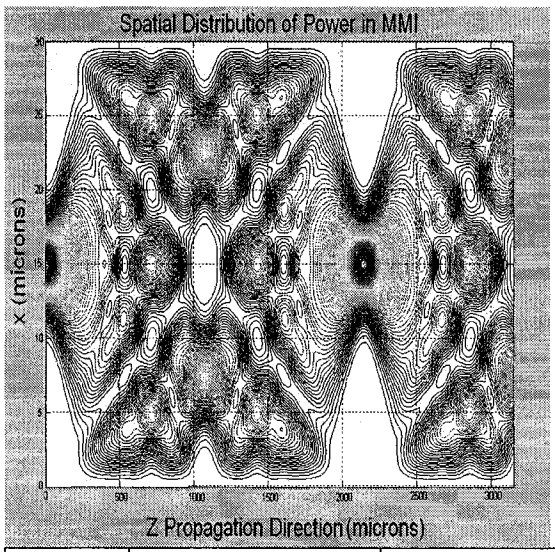

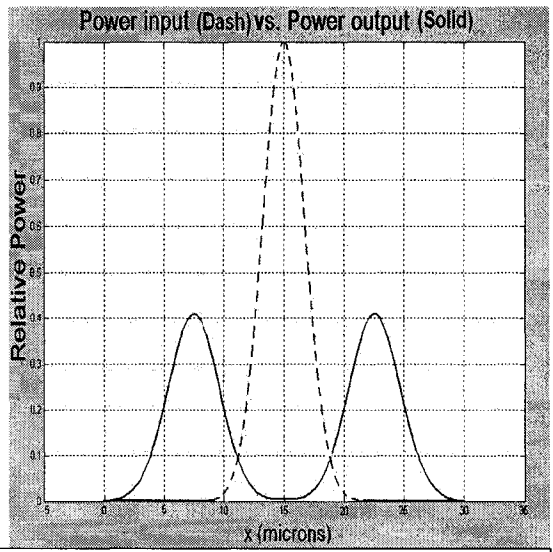

Design: Choose Modes Coupled		Extra Output Waveguides for new images (microns)		GRATING					
		Placement in X	Dimensions in X	Where Grating starts in z	Number of Periods	Period Length in Z (microns)	Period Length in Z'	Grating Angle	Grating Intensity peak-to-peak (delta ref. Index)
First	Second								
1	10	15	3.5	0	12	173.0774	6.0321	88.0027	0.02

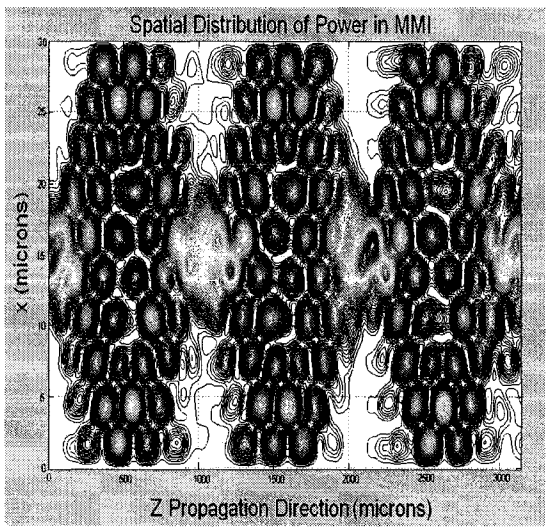

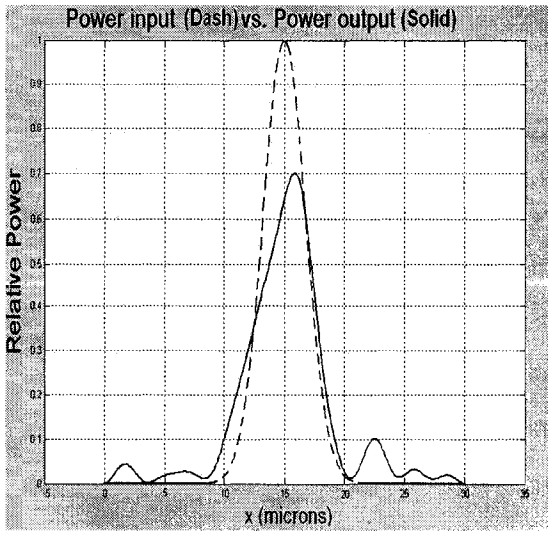

Design #2) Originally a 1 x 5 splitter, convert to a through waveguide with loss ≈30%.

Effective Refractive Index	MMI Dimensions (Microns)		INPUT WAVEGUIDES (microns)		OUTPUT WAVEGUIDES (microns)		Wavelength nm	Spatial Width microns	Comments
	X	Z	Placement in X	Dimensions X (Width)	Placement in X	Dimensions X (Width)			
1.5631	45	5900	22.5	3.5	4.5	3.5	650.3	3.5 waveguide width, 2.5 modeled	165 Possible Modes in x dimension
					13.5	3.5			
					22.5	3.5			
					31.5	3.5			
					40.5	3.5			

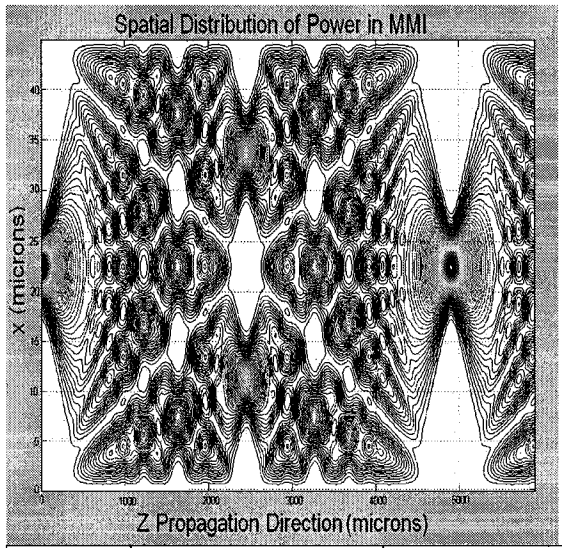

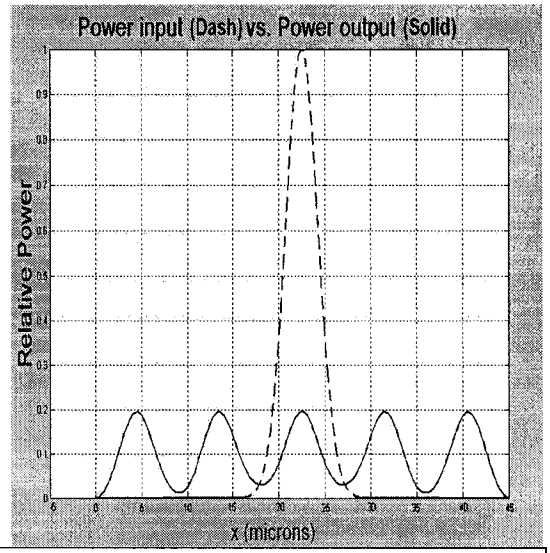

Design: Choose Modes Coupled		Extra Output Waveguides for new images (microns)		GRATING					
		Placement in X	Dimensions in X	Where Grating starts in z	Number of Periods	Period Length in Z (microns)	Period Length in Z'	Grating Angle	Grating Intensity peak-to-peak (delta ref. Index)
First	Second								
5	13	None	None	0	10	272.2059	6.9473	88.5375	0.02

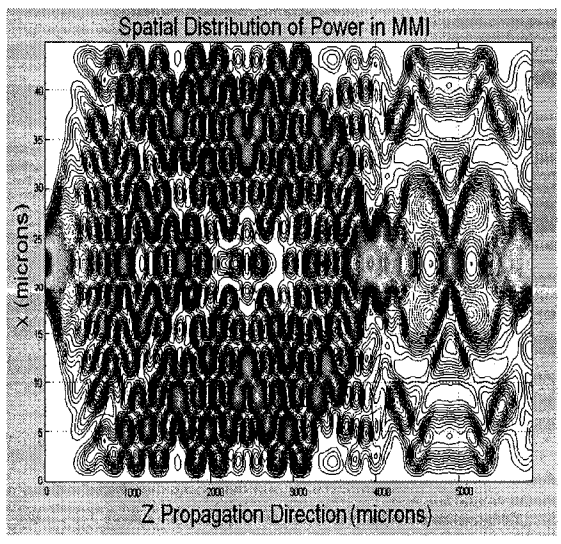

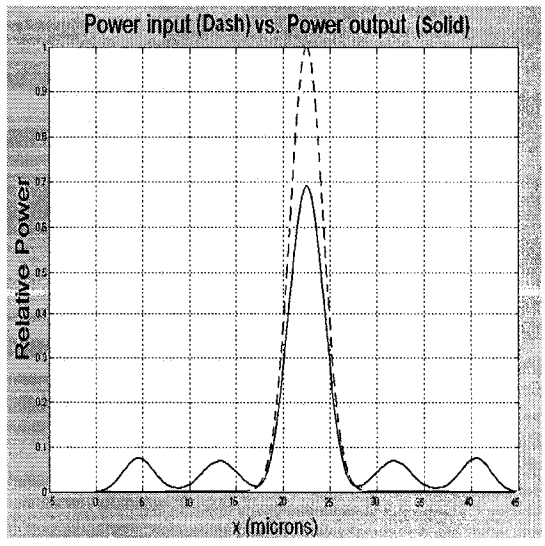

Design #3) Originally a 1 x 3 splitter, convert to a through waveguide with loss ≈25%.

Effective Refractive Index	MMI Dimensions (Microns)		INPUT WAVEGUIDES (microns)		OUTPUT WAVEGUIDES (microns)		Wavelength nm	Spatial Width microns	Comments
	X	Z	Placement in X	Dimensions X (Width)	Placement in X	Dimensions X (Width)			
1.5631	45	3260	22.5	3.5	22.5	3.5	650.3	3.5 waveguide width, 2.5 modeled	165 Possible Modes in x dimension
					37.5	3.5			
					7.5	3.5			

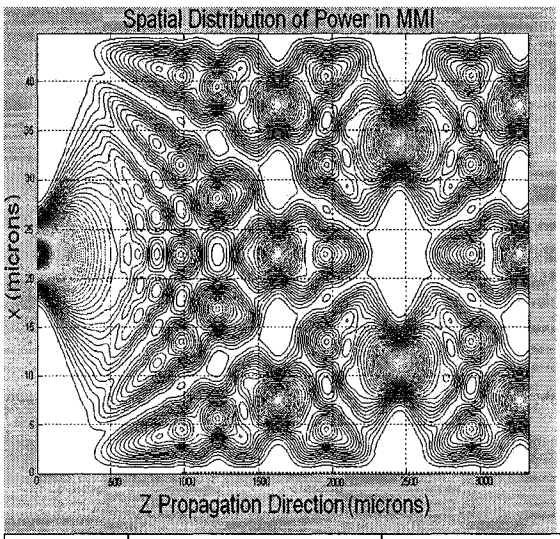

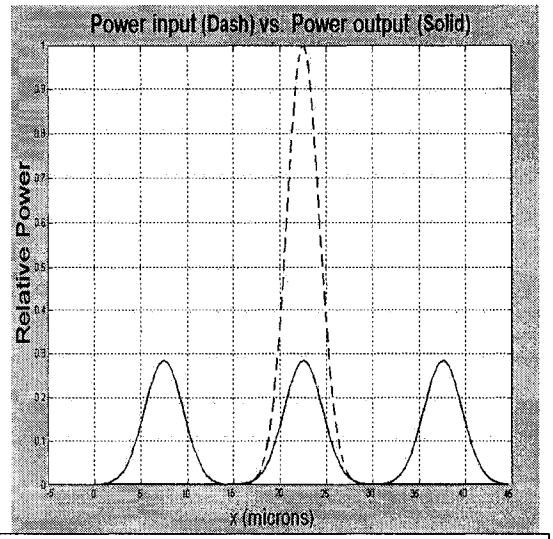

Design: Choose Modes Coupled		Extra Output Waveguides for new images (microns)		GRATING					
		Placement in X	Dimensions in X	Where Grating starts in z	Number of Periods	Period Length in Z (microns)	Period Length in Z'	Grating Angle	Grating Intensity peak-to-peak (delta ref. Index)
First	Second								
3	15	None	None	0	10	181.4322	6.0197	88.0987	0.02

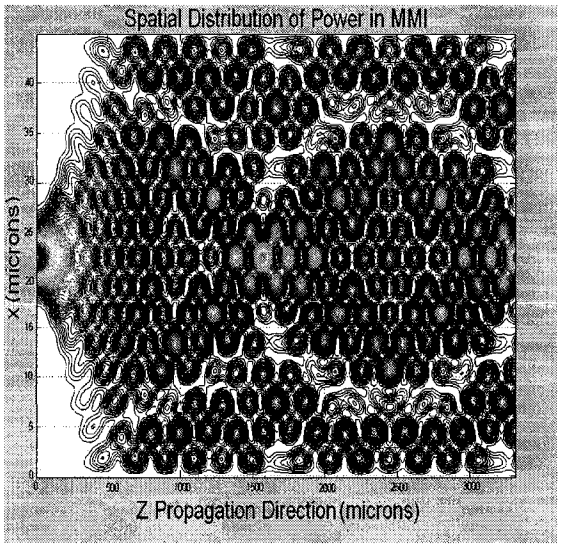

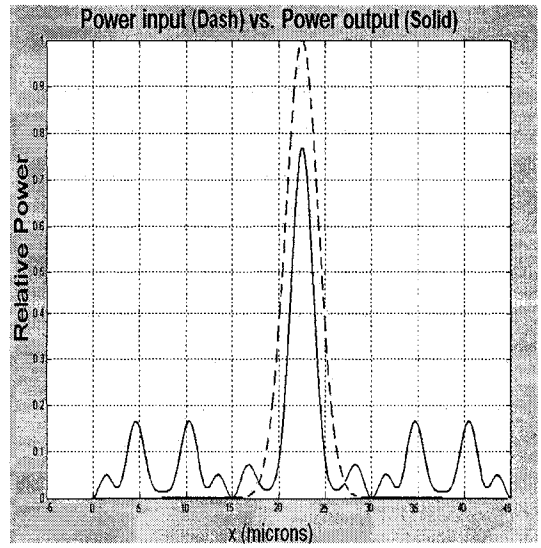

Design #4) Originally a 1 x 5 splitter, convert to a 1 x 2 splitter with ≈30% at each output and the rest of the power lost.

Effective Refractive Index	MMI Dimensions (Microns)		INPUT WAVEGUIDES (microns)		OUTPUT WAVEGUIDES (microns)		Wavelength nm	Spatial Width microns	Comments
	X	Z	Placement in X	Dimensions X (Width)	Placement in X	Dimensions X (Width)			
1.5741	60	7000	30	3.5	6	3.5	650.3	3.5 waveguide width, 2.5 modeled	222 Possible Modes in x dimension
					18	3.5			
					30	3.5			
					42	3.5			
					54	3.5			

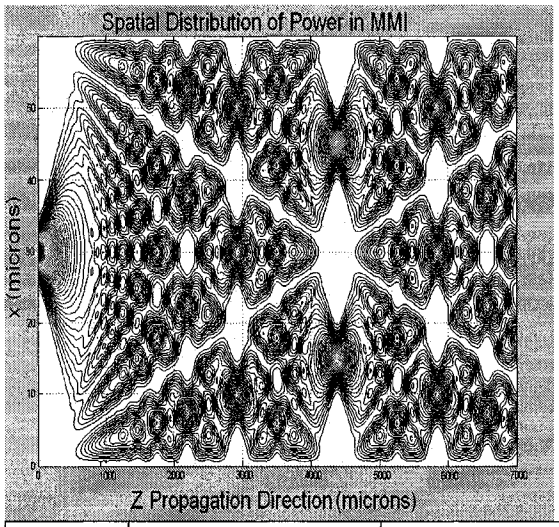

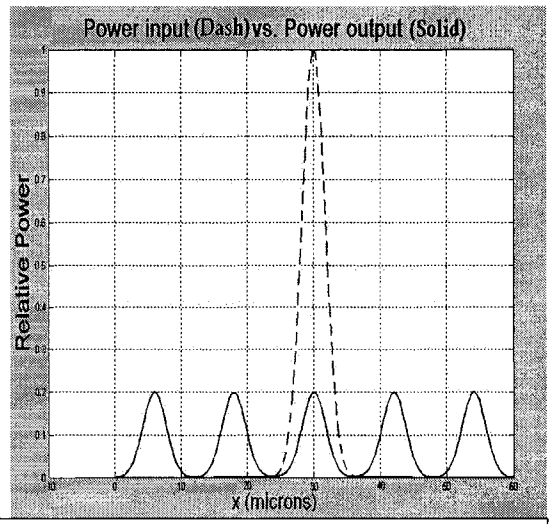

Design: Choose Modes Coupled		Extra Output Waveguides for new images (microns)		GRATING					
		Placement in X	Dimensions in X	Where Grating starts in z	Number of Periods	Period Length in Z (microns)	Period Length in Z'	Grating Angle	Grating Intensity peak-to-peak (delta ref. Index)
First	Second								
1	13	None	None	0	10	417.1075	9.2547	88.7286	0.02

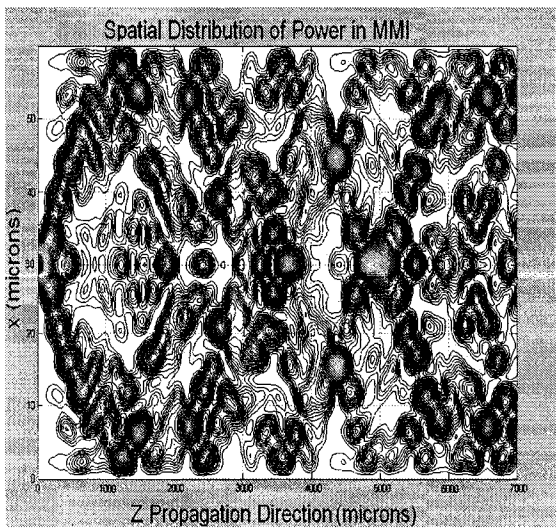

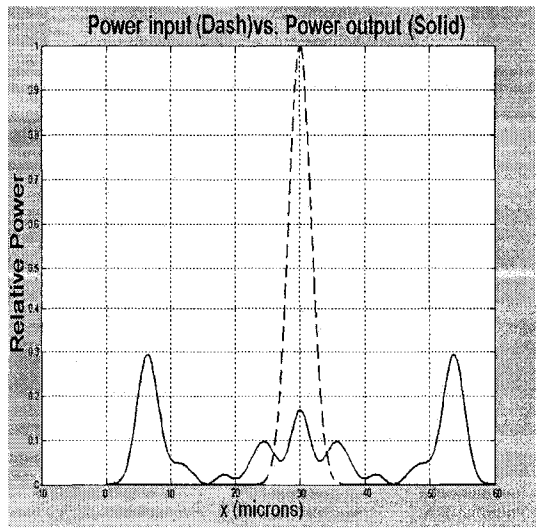

Design #5) Originally a 1 x 3 splitter, convert to a through waveguide with unacceptable loss – may be able to refine design with fabrication

Effective Refractive Index	MMI Dimensions (Microns)		INPUT WAVEGUIDES (microns)		OUTPUT WAVEGUIDES (microns)		Wavelength nm	Spatial Width microns	Comments
	X	Z	Placement in X	Dimensions X (Width)	Placement in X	Dimensions X (Width)			
1.5792	75	9100	37.5	3.5	62.5	3.5	650.3	3.5 waveguide width, 2.5 modeled	279 Possible Modes in x dimension
					37.5	3.5			
					12.5	3.5			

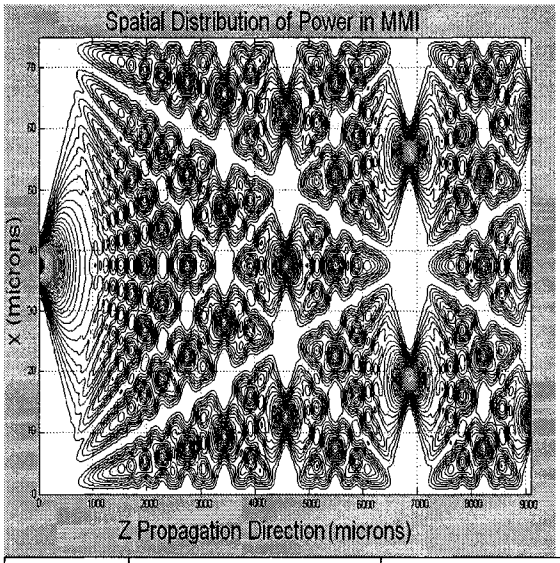

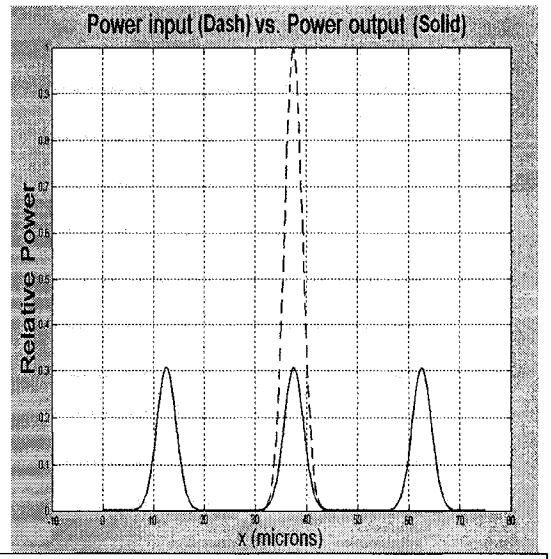

Design: Choose Modes Coupled		Extra Output Waveguides for new images (microns)		GRATING					
		Placement in X	Dimensions in X	Where Grating starts in z	Number of Periods	Period Length in Z (microns)	Period Length in Z'	Grating Angle	Grating Intensity peak-to-peak (delta ref. Index)
First	Second								
1	15	None	None	0	10	489.8456	10.0205	88.8279	0.02

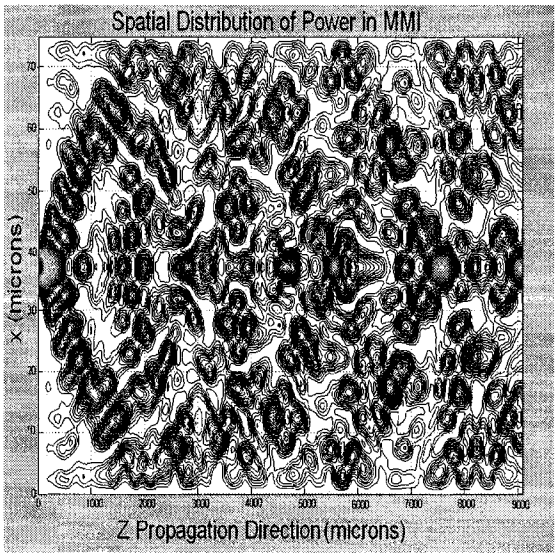

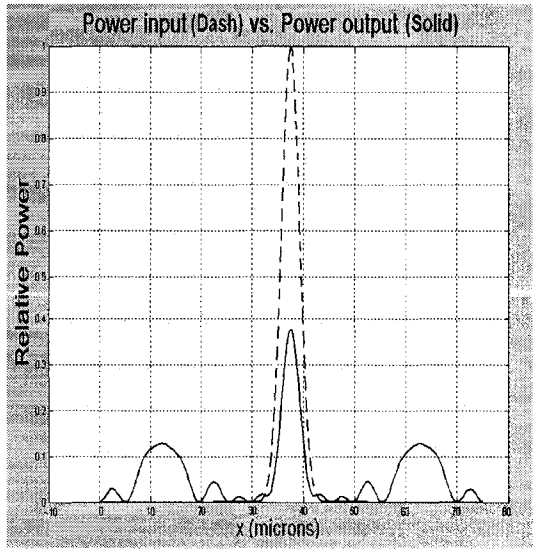

Design #6) Originally a 1 x 5 splitter, convert to a 1 x 2 splitter with ≈40% at each output and the rest of the power lost.

Effective Refractive Index	MMI Dimensions (Microns)		INPUT WAVEGUIDES (microns)		OUTPUT WAVEGUIDES (microns)		Wavelength nm	Spatial Width microns	Comments
	X	Z	Placement in X	Dimensions X (Width)	Placement in X	Dimensions X (Width)			
1.5631	45	5900	22.5	3.5	4.5	3.5	650.3	3.5 waveguide width, 2.5 modeled	165 Possible Modes in x dimension
					13.5	3.5			
					22.5	3.5			
					31.5	3.5			
					40.5	3.5			

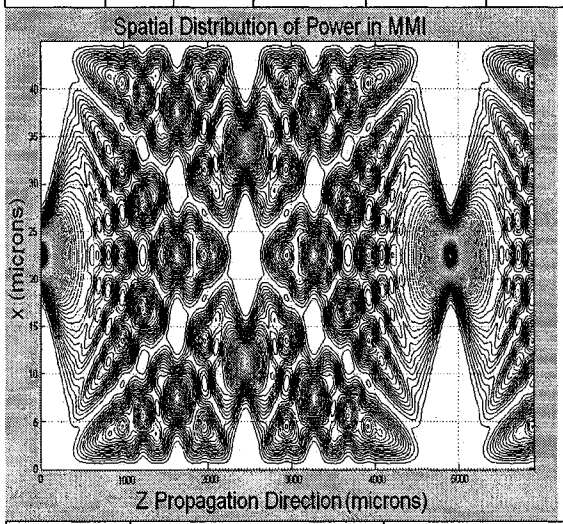

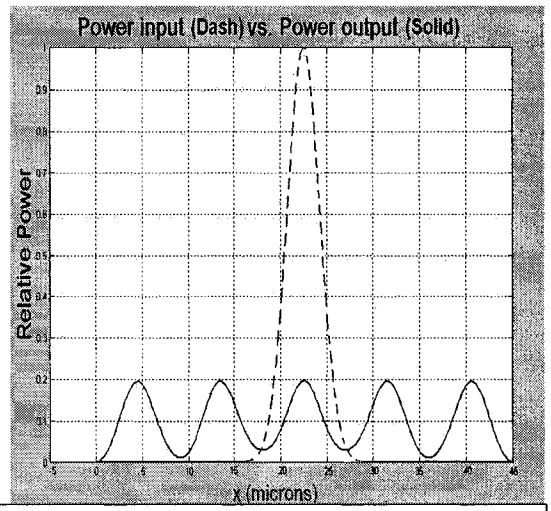

Design: Choose Modes Coupled		Extra Output Waveguides for new images (microns)		GRATING					
		Placement in X	Dimensions in X	Where Grating starts in z	Number of Periods	Period Length in Z (microns)	Period Length in Z'	Grating Angle	Grating Intensity peak-to-peak (delta ref. Index)
First	Second								
1	9	42	3.5	0	7	490.2597	10.0362	88.8270	0.02
		3	3.5						

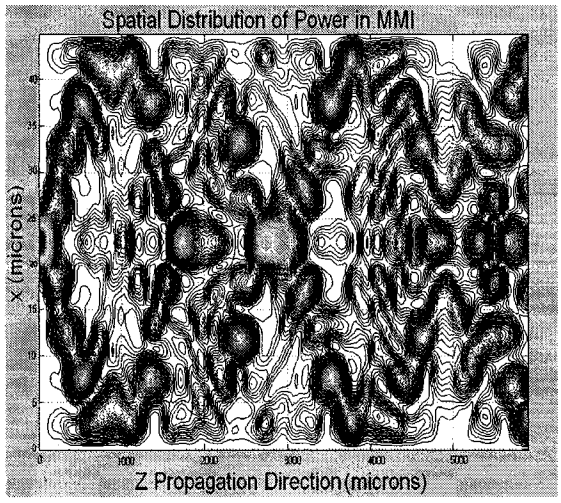

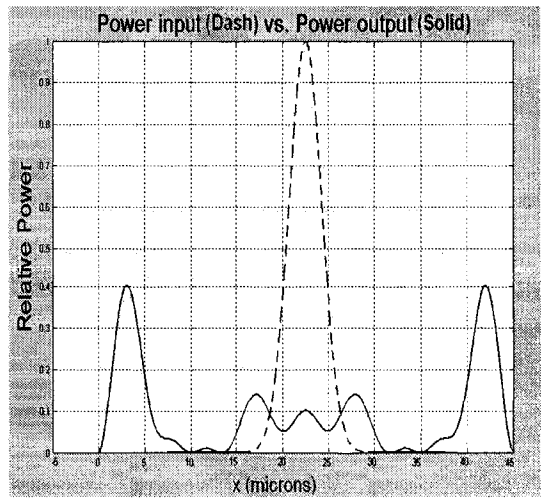

Appendix II: Matlab Program Flowchart

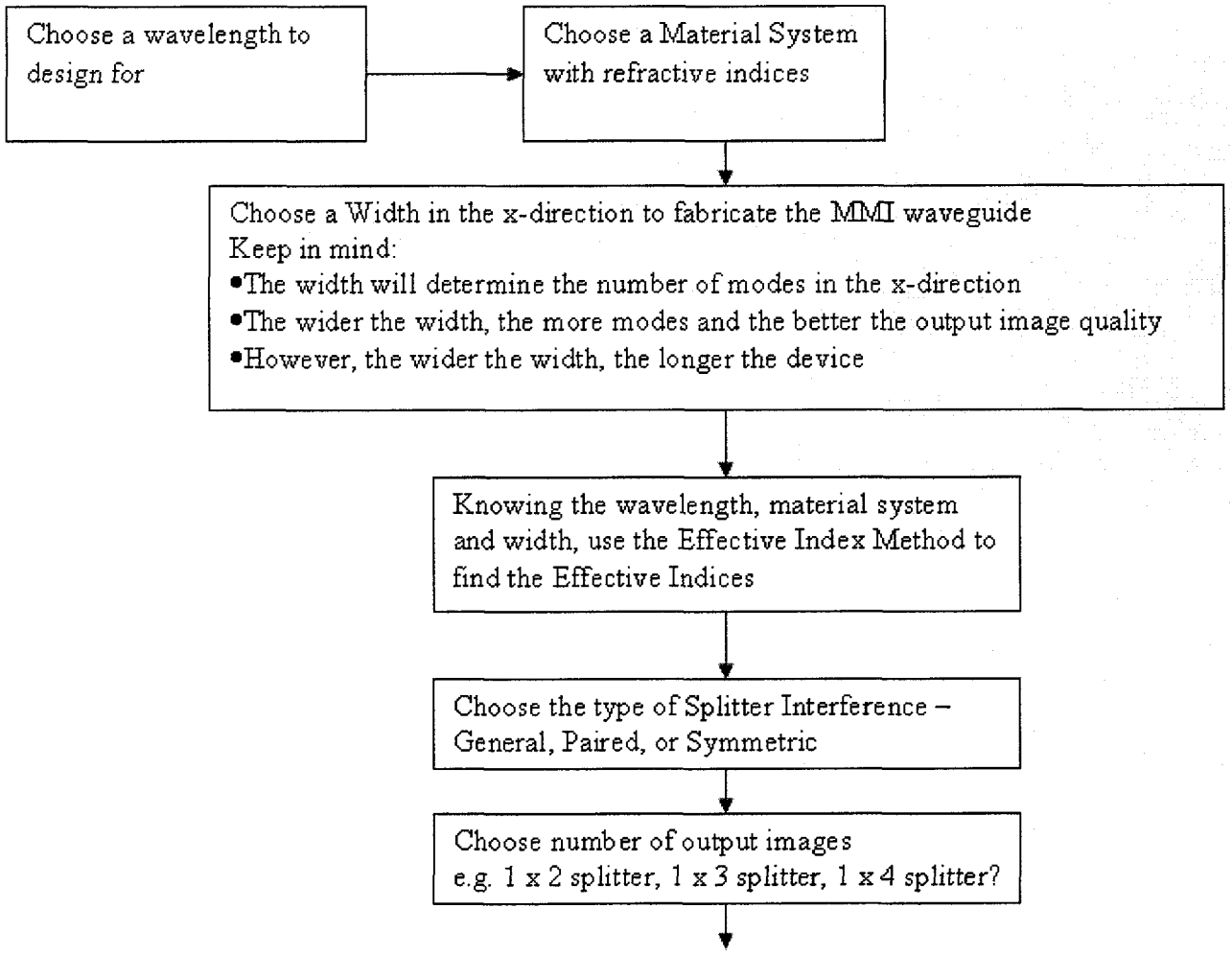

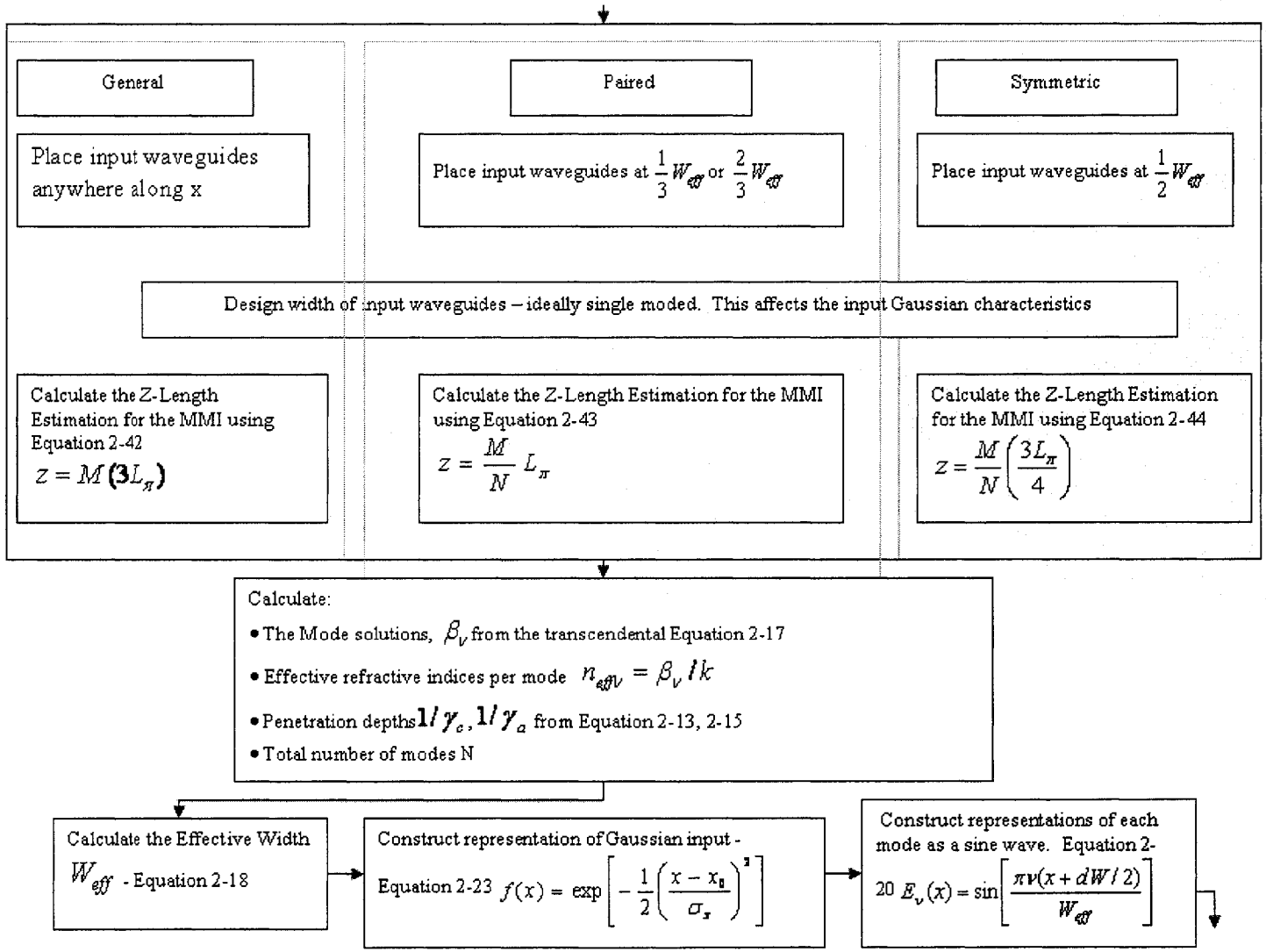

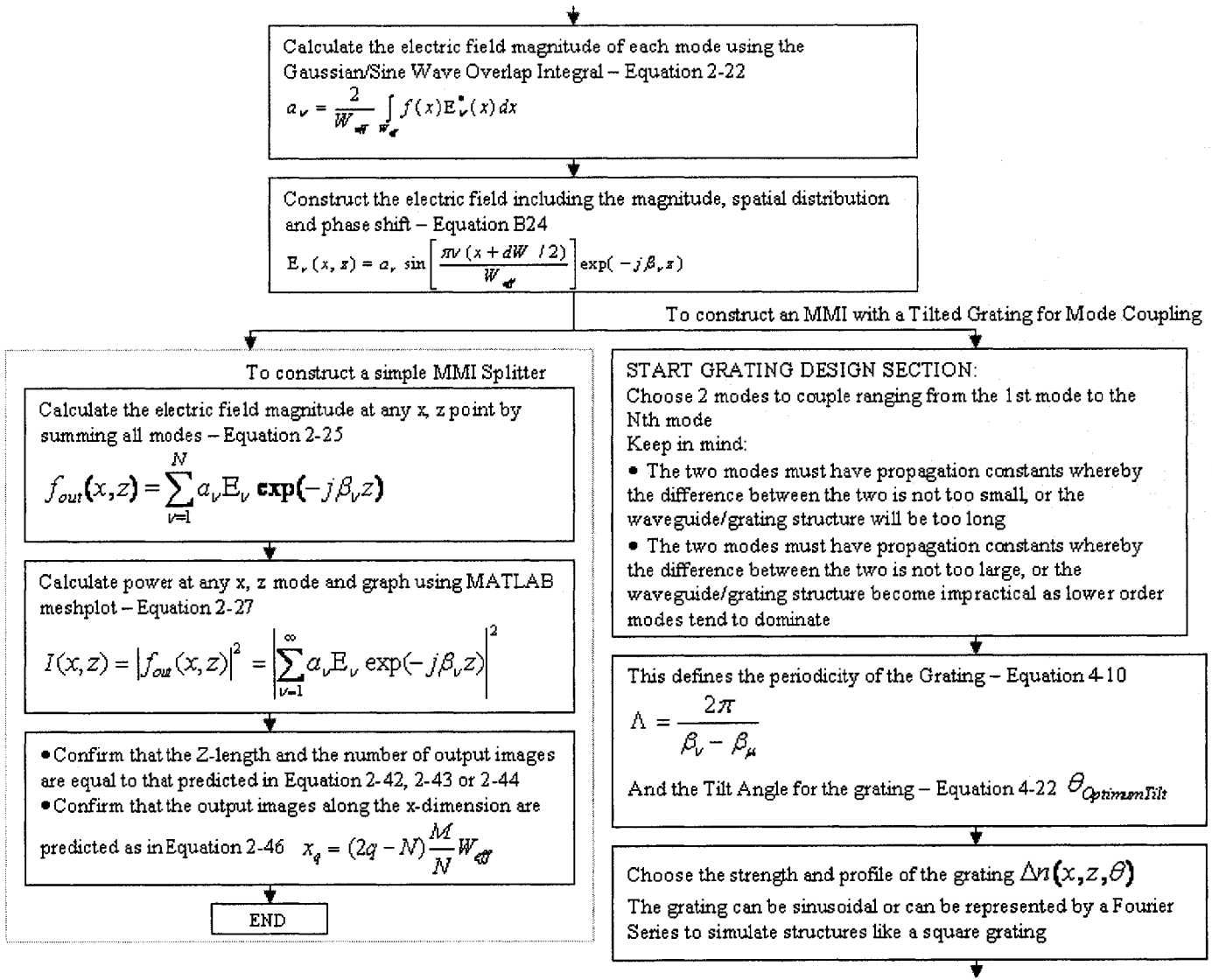

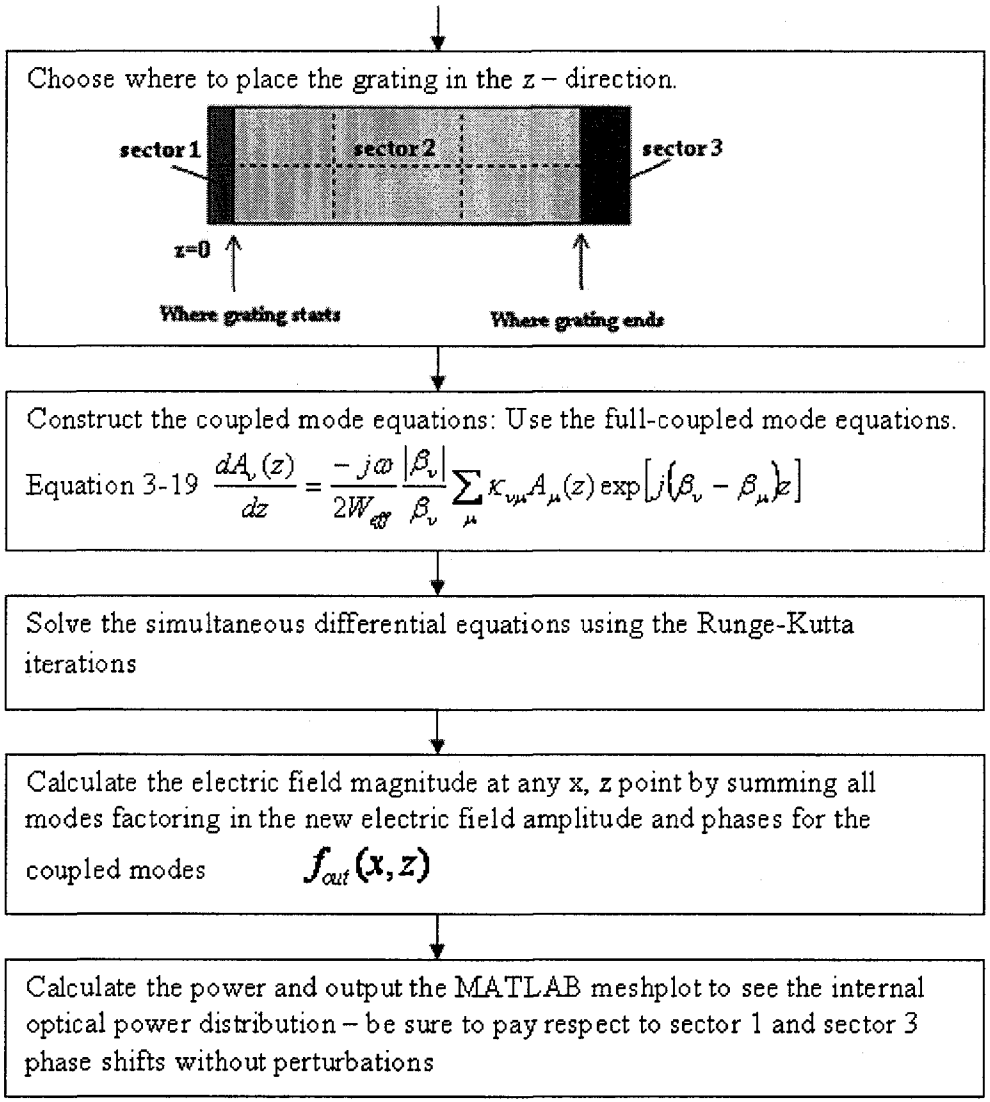

Appendix III: Bragg Grating Theory

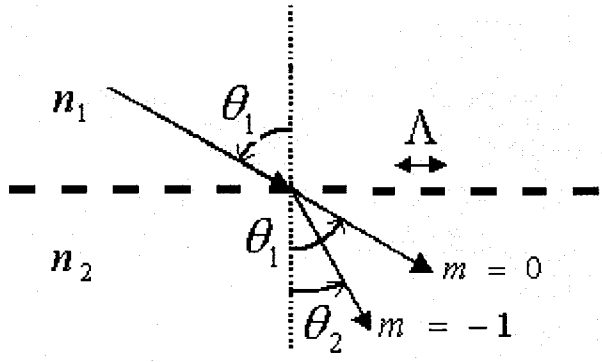

Figure A1: Diffraction of a lightwave by a grating

Since a grating can be modeled as an optical diffraction grating as shown in Figure A1, knowing the incident lightwave angle θ_1, one can predict the direction θ_2 into where constructive interference occurs using the following equation [10]:

$$n\sin\theta_2 = n\sin\theta_1 + m\frac{\lambda}{\Lambda} \tag{A1}$$

In Equation A1, m is an integer, Λ is the grating period and λ is the wavelength at which the grating most efficiently couples. This equation is identical to Bragg's Law for the diffraction of x-rays off crystal surfaces at certain angles. Since the mode propagation constant is $\beta = (2\pi/\lambda)n\sin\theta$ and $m = -1$ for first order diffraction, Equation A1 can be written for Bragg theory:

$$\beta_\mu = \beta_\nu - \frac{2\pi}{\Lambda} \tag{A2}$$

Equation A2 is obviously equivalent to Equation 4-10 in Chapter 4. The phase matching condition directly falls out of Bragg diffraction theory.